TriDurLE

National Center for Transportation Infrastructure Durability & Life-Extension

Project ID: 2022-WSU-01

Protective Performance of Externally-Bonded, Nano-Modified FRP for Concrete in Chloride Environments

Final Report

by

Amir Ali Shahmansouri
Zhen Lei
Xianming Shi
University of Miami

for

National University Transportation Center TriDurLE
Department of Civil & Environmental Engineering
405 Spokane Street PO Box 642910
Washington State University Pullman, WA 99164-2910

December 2025

Acknowledgements

Disclaimer

Table of Contents

Contents

List of Figures

List of Tables

Executive Summary

Concrete infrastructure in cold regions is highly vulnerable to combined freeze-thaw (F/T) cycling and chloride exposure, which accelerates deterioration through cracking, scaling, and loss of mechanical capacity. Externally bonded carbon fiber-reinforced polymer (CFRP) systems are widely used to strengthen and protect deteriorated concrete; however, the long-term durability of the CFRP-concrete interface, particularly the epoxy adhesive layer, remains a critical concern under aggressive environmental conditions. This study evaluated the feasibility of using montmorillonite nanoclay (nC)-modified epoxy adhesives to enhance the durability and mechanical performance of CFRP-wrapped concrete in cold, chloride-laden environments.

A comprehensive laboratory experimental program was conducted to investigate bond durability, transport properties, compressive performance, and microstructural and molecular-level mechanisms of CFRP-wrapped concrete systems. Both normal and pre-aged concrete substrates were examined to represent intact and deteriorated field conditions. Nano-modification strategies involving nanosilica (nS), graphene oxide (GO), and montmorillonite nC were first screened based on bond durability under control and hydrothermal aging (HTA) conditions, followed by detailed mechanical and durability evaluation of the most effective system.

The results demonstrated that bond durability governs the long-term performance of nano-modified CFRP-concrete systems. All nano-modifiers exhibited dosage-dependent behavior, with bond-strength enhancement occurring only within narrow optimal ranges. Among the materials evaluated, montmorillonite nC-modified epoxy exhibited the most robust and consistent bond-durability performance, maintaining superior bond strength under both room-temperature and elevated-temperature HTA. Based on this outcome, nC was selected as the sole nano-modification strategy for subsequent compressive performance evaluation.

CFRP confinement significantly enhanced the compressive strength of concrete prior to environmental exposure, increasing strength by approximately 99% for normal concrete and 82% for pre-aged concrete. Under prolonged F/T cycling in a 3 wt% NaCl solution, nC-modified CFRP systems exhibited improved strength retention, reduced stiffness degradation, and delayed failure, with the most pronounced benefits observed for pre-aged concrete. Transport testing further revealed that nC modification substantially reduced gas permeability and water absorption, particularly during the initial sorptivity stage associated with microcrack-controlled transport. Strong correlations were identified between transport properties and mechanical degradation, highlighting the critical role of moisture and gas ingress in driving damage progression.

Microscopic and physicochemical analyses provided mechanistic validation for these findings. nC-modified epoxy exhibited reduced microcrack density, lower surface hydrophilicity, chemical interaction with the epoxy matrix, and increased glass transition temperature and thermal stability. These microstructural and molecular-level modifications underpin the observed improvements in bond durability, transport resistance, and mechanical performance.

Overall, this study demonstrates that montmorillonite nC is an effective nano-modifier for enhancing the durability, transport resistance, and mechanical performance of CFRP-wrapped concrete in cold, chloride-exposed environments, particularly for deteriorated substrates. The findings establish bond durability as a critical screening metric for selecting nano-modification strategies prior to structural performance evaluation and provide practical guidance for improving the long-term effectiveness of CFRP strengthening systems in cold-region infrastructure.

Future research will extend this work to include additional environmental stressors such as sulfate attack, acid exposure, ultraviolet aging, microbial activity, and wet-dry cycling, as well as field validation. Further exploration of alternative nanomaterials, non-epoxy polymer matrices, and multi-nanomaterial hybrid systems is also recommended to advance the development of durable, high-performance FRP-concrete systems for infrastructure protection and rehabilitation.

Chapter 1. Introduction

1.1. Problem Statement

Concrete infrastructure plays a critical role in transportation systems and is routinely exposed to aggressive environmental conditions that accelerate deterioration and reduce service life. In cold and coastal regions, repeated freeze-thaw (F/T) cycling, moisture ingress, temperature variation, and exposure to chemical agents such as chlorides or sulfates contribute to progressive damage in concrete elements. These mechanisms promote microcracking, surface scaling, and loss of mechanical integrity, ultimately compromising structural safety and increasing maintenance demands (Rusnak, 2025).

Externally bonded fiber-reinforced polymer (FRP) systems, particularly carbon fiber-reinforced polymer (CFRP), have been widely adopted as an effective technique for strengthening, retrofitting, and protecting concrete structures. CFRP systems offer advantages such as high strength-to-weight ratio, corrosion resistance, and ease of installation, making them attractive for extending the service life of existing infrastructure. However, the long-term effectiveness of externally bonded CFRP systems is fundamentally governed by the durability of the CFRP-epoxy-concrete interface, which is responsible for stress transfer between the concrete substrate and the reinforcement (Brandtner-Hafner, 2024).

Field experience and laboratory studies have shown that premature degradation of the bonded interface, rather than failure of the CFRP itself, often controls performance under environmental exposure. Moisture, elevated temperature, F/T cycling, and chemical attack can degrade epoxy adhesives, weaken the near-surface concrete, and alter interfacial failure modes. These processes may significantly reduce bond strength and limit the ability of CFRP systems to mobilize their full strengthening potential. The problem is further exacerbated when CFRP is applied to pre-aged or environmentally deteriorated concrete, where substrate integrity is already compromised (Gholami et al., 2013).

Conventional epoxy adhesives used in CFRP applications are not specifically engineered for long-term durability under coupled environmental actions. As a result, there is a critical need to develop and evaluate strategies that enhance interfacial durability and mitigate environmentally induced bond degradation. Among the proposed solutions, nano-modification of epoxy adhesives has emerged as a promising approach to improve mechanical properties, transport resistance, and durability of the CFRP-concrete interface. Nevertheless, systematic, durability-driven investigations linking nano-modified adhesives to interfacial bond performance under realistic exposure conditions remain limited (Lei et al., 2025).

1.2. Objectives

The primary objective of this study is to evaluate the durability of externally bonded CFRP systems by explicitly quantifying CFRP-concrete interfacial performance and its retention under aggressive environmental exposures, with particular emphasis on the effectiveness of nano-modified epoxy adhesives in mitigating bond degradation and improving composite performance. The specific objectives of this research are to:

1. Quantify CFRP-concrete bond strength and interfacial failure behavior using pull-off testing and failure mode assessment, considering key installation variables including CFRP fabric type and resin saturation condition.

2. Determine the sensitivity of interfacial bond durability to hydrothermal aging (HTA) by comparing

bond strength retention and failure characteristics under room-temperature wet exposure and elevated-temperature hot-wet exposure.

3. Screen and optimize nano-modification strategies for epoxy adhesives by evaluating nanosilica (nS), graphene oxide (GO) (acidic and neutral), and sodium montmorillonite nanoclays (nCs) across dosage ranges and saturation states, and identifying the most effective modifiers for durability evaluation.

4. Assess the influence of concrete substrate condition on CFRP system performance, by comparing intact and pre-aged substrates and examining how substrate deterioration alters interfacial durability, confinement response, and dominant failure mechanisms.

5. Quantify the impact of CFRP confinement and nano-modified epoxy on mechanical degradation under coupled F/T and chloride exposure, including compressive strength retention, modulus of elasticity (MoE) evolution, scaling-related mass/dimensional changes, and failure modes.

6. Link interfacial and material-level mechanisms to macroscopic durability performance, by correlating transport indicators (water absorption and gas permeability) and physicochemical/microstructural observations (contact angle, microscopy, FTIR, DSC/TGA) with the observed bond and mechanical performance trends.

1.3. Expected Contributions

This study contributes to the understanding and practical application of externally bonded CFRP systems for concrete infrastructure through the following key outcomes:

1. Provide an interface-centered durability assessment of CFRP systems, demonstrating that long-term performance is governed primarily by CFRP-concrete bond degradation rather than initial strength enhancement alone, particularly under moisture- and temperature-driven environmental exposure.

2. Quantify the effects of HTA, F/T cycling, and chloride exposure on CFRP bond retention, showing how elevated temperature and coupled F/T-salt environments accelerate interfacial deterioration and alter dominant failure mechanisms.

3. Deliver a systematic experimental screening of nano-modified epoxy adhesives, comparing nS, GO (acidic and neutral), and sodium montmorillonite nCs across dosage, saturation state, and CFRP fabric type, and identifying optimal nano-modification windows and performance trade-offs.

4. Demonstrate the critical influence of concrete substrate condition on CFRP durability, showing that pre-aged concrete exhibits greater sensitivity to interfacial degradation, stiffness loss, and transport-related damage, and that nano-modification is particularly beneficial for mitigating deterioration in damaged substrates.

5. Establish quantitative relationships between interfacial transport behavior and mechanical degradation, linking water absorption and gas permeability to reductions in bond strength, compressive strength, and MoE, and highlighting transport properties as early indicators of durability loss.

6. Provide mechanistic evidence connecting nano-scale epoxy modification to macroscopic performance, integrating bond testing, transport measurements, microstructural observations, surface wettability, and thermal analysis to explain the improved durability of nano-modified CFRP-concrete systems.

7. Generate durability-oriented experimental evidence to support material selection and strengthening strategies, offering practical insight into the selection of epoxy formulations and nano-modification approaches for CFRP applications in cold-region and chemically aggressive service environments.

1.4. Report Overview

This report is organized into five chapters. **Chapter 1** introduces the research problem, objectives, expected contributions, and overall structure of the study. **Chapter 2** presents a comprehensive literature review on externally bonded FRP systems, CFRP-concrete interface durability, environmental degradation mechanisms, and nano-modified epoxy adhesives, culminating in the identification of key research gaps. **Chapter 3** describes the materials, specimen preparation, exposure protocols, and experimental methods employed in the study. **Chapter 4** presents and discusses the experimental results, with emphasis on CFRP-concrete bond durability, hydrothermal and F/T degradation, and the relationships among interfacial performance, transport behavior, microstructural characteristics, and mechanical response. Finally, **Chapter 5** summarizes the main findings, presents the conclusions, and provides recommendations for future research and practical application.

Chapter 2. Literature Review

2.1. Externally Bonded FRP Systems

Externally bonded FRP systems have been widely adopted over the past several decades for the strengthening, repair, and rehabilitation of reinforced concrete infrastructure. The technique involves bonding prefabricated or wet lay-up FRP laminates to the surface of existing concrete members using polymeric adhesives, most commonly epoxy resins. Owing to their high strength-to-weight ratio, corrosion resistance, and ease of installation, FRP systems, particularly CFRP, offer an efficient means of enhancing structural performance without significantly increasing member size or self-weight (Zaman et al., 2013).

Externally bonded FRP systems have been successfully applied to improve the flexural capacity, shear resistance, and confinement performance of concrete elements. In flexural strengthening, CFRP sheets or plates bonded to the tension face of beams increase tensile capacity and delay steel yielding. In shear strengthening, CFRP strips or wraps oriented perpendicular or inclined to the member axis enhance shear resistance and mitigate brittle failure. For columns, circumferential CFRP wrapping provides passive confinement, improving axial strength, ductility, and deformation capacity by restraining lateral expansion of the concrete core (Mhanna et al., 2019). Design guidelines, such as ACI PRC-440.2 (ACI Committee 440, 2023), provide analytical frameworks for these applications and have facilitated the widespread implementation of FRP retrofitting technologies in practice.

Despite their demonstrated effectiveness, the performance of externally bonded FRP systems is fundamentally governed by the behavior of the FRP-adhesive-concrete interface. Because load transfer between the concrete substrate and the FRP reinforcement occurs through the adhesive layer, inadequate bonding can lead to premature failure modes such as debonding, concrete cover peeling, or interfacial shear failure. In many cases, these interface-controlled failures occur before full utilization of the tensile capacity of the FRP, thereby limiting strengthening efficiency. Experimental studies consistently show that the weakest plane within the bonded system often lies either within the near-surface concrete layer or at the adhesive-concrete interface, rather than within the FRP itself (Al-Saadi et al., 2019).

The susceptibility of externally bonded FRP systems to interface-related failure is further exacerbated by environmental exposure and substrate condition. Factors such as moisture ingress, temperature variation, F/T cycling, chloride or sulfate attack, and pre-existing damage in the concrete substrate can progressively degrade bond integrity. These degradation mechanisms may alter adhesive properties, weaken chemical and mechanical adhesion at the interface, and promote microcracking within the concrete surface layer. As a result, long-term durability, rather than initial strength gain, has emerged as a critical concern for externally bonded FRP retrofits, particularly in aggressive service environments (Ortiz et al., 2023).

Consequently, increasing attention has been directed toward strategies that improve bond reliability and durability rather than simply enhancing FRP material properties. Approaches such as surface preparation techniques, mechanical anchorage systems, and modification of the adhesive layer have been investigated to mitigate debonding and enhance stress transfer. Among these, engineering the adhesive, through material selection or modification, has been recognized as a particularly effective intervention point, since

the adhesive layer directly governs the interaction between the FRP reinforcement and the concrete substrate (Ueda & Dai, 2005).

In this context, externally bonded FRP systems provide a highly effective strengthening solution when adequate bond performance is achieved and maintained. However, their long-term effectiveness is intrinsically linked to the durability of the bonded interface. This recognition motivates the detailed examination of interfacial degradation mechanisms, environmental effects, and adhesive modification strategies discussed in the subsequent sections of this literature review.

2.2. CFRP-Concrete Interface Durability

Although externally bonded CFRP systems provide substantial improvements in strength and ductility of concrete members, their long-term performance is frequently limited by the durability of the CFRP-concrete interface. Unlike internal reinforcement, externally bonded FRP relies entirely on the integrity of a relatively thin adhesive layer and the near-surface concrete zone to transfer stresses. As a result, degradation processes that affect either the adhesive or the concrete surface can significantly compromise load transfer and trigger premature failure (Sen, 2015).

The CFRP-concrete interface is a heterogeneous, multi-phase region consisting of the concrete substrate, the polymeric adhesive, and the FRP laminate. Each constituent responds differently to environmental and mechanical actions. Concrete is porous and moisture-sensitive, epoxy adhesives are susceptible to physical and chemical aging, and CFRP laminates exhibit anisotropic behavior with limited through-thickness strength. This mismatch in material properties creates stress concentrations at the interface and makes the bonded region particularly vulnerable to deterioration over time (Evans et al., 1999).

One of the most critical durability challenges arises from moisture ingress. Epoxy adhesives commonly used in FRP strengthening are prone to water absorption, which can lead to plasticization, reduction in stiffness and strength, and changes in fracture behavior. Moisture uptake may also disrupt chemical bonding at the adhesive-concrete interface, weakening adhesion and promoting interfacial debonding. In the concrete substrate, moisture transport facilitates leaching of calcium hydroxide, swelling of hydration products, and development of microcracks in the near-surface zone, further reducing bond reliability (Shrestha et al., 2015).

Temperature effects and coupled moisture-temperature exposure present additional challenges. Elevated temperatures accelerate diffusion processes and polymer chain mobility, increasing the rate of adhesive degradation (Viana et al., 2016). Under hydrothermal conditions, reductions in glass transition temperature and mechanical properties of epoxy adhesives have been reported, which can significantly alter stress transfer behavior. Repeated thermal cycling may also induce differential thermal strains between CFRP, adhesive, and concrete, promoting microcracking and progressive interfacial damage (Carbas et al., 2014).

In cold regions, F/T cycling, often combined with deicing salts, represents a particularly aggressive durability environment. Repeated freezing and thawing can induce internal cracking, scaling, and surface deterioration in concrete, reducing the cohesive strength of the substrate adjacent to the adhesive layer (Subash & Subash, 2024). When salts such as chlorides or sulfates are present, transport processes are further intensified, leading to chemical attack, crystallization pressures, and accelerated degradation (Luo et al., 2024). These mechanisms not only weaken the concrete but also exacerbate moisture penetration at the CFRP-concrete interface, increasing the likelihood of debonding or mixed-mode failure (Shrestha et al., 2016).

The condition of the concrete substrate prior to strengthening also plays a critical role in interface durability. Pre-existing damage, such as microcracking, scaling, or loss of surface integrity due to environmental exposure, can significantly reduce bond strength and alter failure modes. In such cases, failure may initiate within the deteriorated concrete layer rather than at the adhesive interface, limiting the effectiveness of CFRP confinement or reinforcement even when high-strength adhesives are used (Li et al., 2023).

Collectively, these durability challenges highlight that the performance of externally bonded CFRP systems is governed not only by the intrinsic properties of the FRP material but also, and more critically, by the long-term stability of the bonded interface. Conventional strengthening designs that assume intact bonding conditions may therefore overestimate service-life performance when environmental degradation is not adequately considered. This recognition has driven increasing research interest toward understanding interfacial degradation mechanisms and developing strategies to enhance the durability of the CFRP-concrete interface, which form the basis for the discussions in the following sections.

2.3. Moisture and Temperature Effects on FRP Bond

Moisture and temperature are among the most influential environmental factors affecting the durability of externally bonded FRP systems. Because the CFRP-concrete interface relies on a polymeric adhesive to transfer stresses, environmental exposure that alters the physical or chemical properties of the adhesive can significantly degrade bond performance. When moisture and elevated temperature act simultaneously, degradation mechanisms are often accelerated, leading to pronounced reductions in interfacial strength and changes in failure mode (Shrestha et al., 2015; Viana et al., 2016).

Moisture exposure primarily affects FRP bond performance through water absorption by epoxy adhesives and transport processes within the concrete substrate (Dai et al., 2010; Shrestha et al., 2015). Epoxy resins are hygroscopic to varying degrees, and absorbed water can act as a plasticizer, reducing MoE, tensile strength, and fracture resistance. Moisture uptake may also weaken adhesive-concrete adhesion by disrupting hydrogen bonding and other physicochemical interactions at the interface. Experimental studies have consistently shown that prolonged water immersion leads to measurable reductions in pull-off or shear bond strength, even in the absence of mechanical loading (Fazli et al., 2018).

Temperature further amplifies moisture-related degradation. Elevated temperatures increase diffusion rates of water molecules into the adhesive layer and enhance polymer chain mobility, accelerating physical aging and chemical degradation. Under hot-wet conditions, epoxy adhesives may experience reductions in glass transition temperature, softening of the polymer network, and increased susceptibility to crack initiation and propagation. These effects compromise the adhesive's ability to effectively transfer stresses from the concrete substrate to the CFRP laminate (Korkees, 2023).

HTA, which combines moisture exposure with elevated temperature, is therefore widely used as an accelerated conditioning method to simulate long-term service environments. Hydrothermal conditioning has been shown to induce more severe degradation than either moisture or temperature acting alone (Karbhari, 2022). Typical observations include reduced interfacial stiffness, decreased bond strength, and a shift in failure mode from cohesive failure in concrete toward adhesive or interfacial failure. Such transitions indicate that the adhesive layer becomes the weakest link in the bonded system following hydrothermal exposure (Mariam et al., 2019).

The influence of HTA is also closely tied to the adhesive chemistry and formulation. Epoxies with lower crosslink density or poor resistance to moisture diffusion tend to degrade more rapidly, while systems

with improved network structure or enhanced barrier properties exhibit better bond retention (Han et al., 2018). In addition, the thickness and uniformity of the adhesive layer can affect moisture transport paths and stress distribution, further influencing bond durability under hydrothermal conditions (Mariam et al., 2019).

From a structural perspective, degradation of the CFRP-concrete bond under hydrothermal exposure can significantly reduce the effectiveness of FRP strengthening (Xie et al., 2018). Even modest reductions in interfacial strength may limit load transfer efficiency and prevent full mobilization of the CFRP reinforcement, particularly in systems where debonding governs failure (Goda et al., 2024). Consequently, assessments of FRP performance based solely on initial bond strength may substantially overestimate long-term capacity if hydrothermal effects are not considered (Harle, 2024).

These findings underscore the importance of explicitly evaluating the effects of moisture, temperature, and their combined action on FRP bond behavior. HTA protocols provide a practical means of accelerating degradation processes and revealing interfacial weaknesses that may not be apparent under short-term testing. This understanding forms a critical basis for investigating strategies aimed at enhancing bond durability, such as modification of the adhesive layer, which are discussed in subsequent sections of this literature review.

2.4. Freeze-Thaw and Chloride Effects

In cold and temperate regions, concrete infrastructure is frequently exposed to repeated F/T cycling, often in the presence of deicing salts (Ghazy & Bassuoni, 2018). These coupled actions represent one of the most aggressive durability environments for both unprotected concrete and externally bonded FRP strengthening systems. Freeze-thaw damage and chloride ingress not only deteriorate the concrete substrate but also compromise the integrity of the CFRP-concrete interface, which governs load transfer and long-term performance (Zhang et al., 2022).

Freeze-thaw cycling induces internal stresses in concrete due to the volumetric expansion of water upon freezing. When the tensile stresses generated by ice formation exceed the tensile capacity of the cementitious matrix, microcracks develop and progressively coalesce (Guo et al., 2022). Repeated cycles lead to scaling, surface peeling, loss of mass, and reductions in mechanical properties. The damage is most pronounced in the near-surface zone of concrete, which is the same region relied upon for anchoring externally bonded FRP systems. As a result, F/T deterioration directly weakens the cohesive strength of the concrete layer adjacent to the adhesive interface (Sun & Dang, 2025).

The presence of chlorides, typically from deicing salts such as sodium chloride, further exacerbates F/T damage. Chloride solutions lower the freezing point of pore water, increase saturation levels, and intensify osmotic and crystallization pressures during thermal cycling (Wang et al., 2006). In addition, chloride ingress accelerates transport processes within concrete, increasing moisture availability at the interface and promoting chemical interactions that can destabilize hydration products. These combined effects often lead to more rapid surface deterioration and deeper penetration of damage compared to F/T exposure in water alone (Rajani & Kleiner, 2001).

For externally bonded CFRP systems, F/T and chloride exposure introduce coupled degradation mechanisms affecting both the concrete substrate and the adhesive layer. Deterioration of the concrete surface reduces the effective bond area and promotes failure within the weakened substrate rather than in the adhesive or FRP (Zhou et al., 2015). Simultaneously, repeated moisture movement and salt exposure can degrade epoxy adhesives through physical aging, hydrolysis, and microcracking. Differential thermal

strains between CFRP, adhesive, and concrete during F/T cycling may also generate interfacial stresses that contribute to progressive debonding (Liu et al., 2019).

Experimental studies on FRP-strengthened concrete subjected to F/T and chloride environments consistently report reductions in bond strength, changes in failure mode, and diminished strengthening efficiency over time. In many cases, initial exposure stages are characterized by modest strength retention or even slight increases due to continued cement hydration or pore filling by salt crystallization. However, with increasing numbers of cycles, accelerated degradation occurs, marked by surface scaling, rapid loss of concrete integrity, and sharp declines in residual mechanical performance. For FRP-confined elements, deterioration of the interface can limit the confinement effect, preventing full mobilization of the FRP jacket and leading to premature failure (Hao et al., 2024; Zhou et al., 2015).

The influence of F/T and chloride exposure is particularly critical when CFRP systems are applied to pre-aged or environmentally damaged concrete. Pre-existing microcracking, scaling, or surface weakening significantly increases susceptibility to interfacial degradation, as the adhesive must bond to an already compromised substrate. In such cases, the durability of the CFRP-concrete interface, rather than the strength of the FRP reinforcement, becomes the controlling factor in long-term performance (Bai et al., 2024).

These observations highlight that evaluating FRP strengthening systems under F/T and chloride exposure requires consideration of both substrate deterioration and interfacial durability. Conditioning protocols that combine cyclic freezing and thawing with salt exposure provide a realistic and accelerated means of assessing performance in cold-region environments. Understanding the mechanisms by which F/T and chlorides affect concrete and bonded FRP systems is therefore essential for developing effective strategies to enhance interface durability, particularly through improvements in adhesive formulation and transport resistance, as discussed in the following sections.

2.5. Nano-modified Epoxy Adhesives

The durability challenges associated with externally bonded CFRP systems have motivated increasing interest in engineering the adhesive layer rather than modifying the FRP reinforcement or the concrete substrate alone (Frigione & Lettieri, 2018). Because the adhesive governs stress transfer, moisture transport, and failure initiation at the CFRP-concrete interface, targeted modification of epoxy adhesives has been recognized as a highly effective strategy for improving bond performance and long-term durability (Zhang et al., 2021). Among the approaches investigated, incorporation of nanoscale fillers into epoxy matrices has emerged as a promising method to enhance mechanical properties, transport resistance, and interfacial stability (Gonçalves et al., 2022).

Nano-modified epoxy adhesives typically incorporate low dosages of nanoparticles to alter the polymer network at the micro- and nano-scale without compromising workability or constructability (Shadlou et al., 2015). When properly dispersed, nanomaterials can improve stiffness, fracture toughness, and crack resistance, while simultaneously increasing diffusion path tortuosity for moisture and aggressive ions (Hoque & Yao, 2025). These improvements are particularly relevant for FRP strengthening applications exposed to moisture, temperature variation, F/T cycling, and chemical attack.

2.5.1. nS-modified epoxy adhesives

Nanosilica has been widely studied as a reinforcing filler for epoxy systems due to its high surface area, chemical stability, and compatibility with polymer matrices (Uniyal et al., 2025). In epoxy adhesives, nS

particles can enhance stiffness and tensile strength by acting as rigid fillers and promoting stress redistribution within the polymer network (Yang et al., 2014). In addition, nS has been shown to increase fracture toughness through mechanisms such as crack deflection, crack pinning, and energy dissipation around particle–matrix interfaces (Raja Othman et al., 2025).

From a durability perspective, nS can reduce permeability and moisture diffusion by refining the microstructure of the cured epoxy and increasing the tortuosity of transport pathways. However, the effectiveness of nS is strongly dependent on dosage and dispersion quality (Pang et al., 2018; Uniyal et al., 2025). Excessive nS content may lead to particle agglomeration, increased viscosity, and impaired fiber wet-out, which can negatively affect bond performance. Consequently, reported benefits are often limited to narrow dosage ranges, underscoring the need for careful optimization in FRP adhesive applications.

2.5.2. GO-modified epoxy adhesives

Graphene oxide has attracted significant attention as a nano-modifier for epoxy adhesives due to its high aspect ratio and abundance of oxygen-containing functional groups (Dalfi et al., 2025). These functional groups promote strong interactions with polymer chains and mineral surfaces, enhancing interfacial adhesion at the CFRP-concrete interface (Jiang et al., 2021). Even at very low dosages, GO has been shown to improve tensile strength, fracture toughness, and bond performance of epoxy adhesives (Guo et al., 2023).

In addition to mechanical enhancement, GO can influence moisture resistance and interfacial chemistry. The layered structure of GO nanoplatelets increases diffusion path length, reducing water and ion transport through the adhesive layer (Karimi et al., 2023). However, the performance of GO-modified epoxies is highly sensitive to surface chemistry, oxidation state, and dispersion. Poorly dispersed or overly reduced GO may diminish interfacial benefits or introduce defects that compromise durability (Wu et al., 2025). These sensitivities have contributed to variability in reported results across studies.

2.5.3. nC-modified epoxy adhesives

Montmorillonite nC has emerged as one of the most effective nano-modifiers for epoxy adhesives in FRP applications. Nanoclays consist of layered silicate platelets with high aspect ratios, which can intercalate or exfoliate within the epoxy matrix. When properly dispersed, nC platelets enhance stiffness, fracture resistance, and thermal stability, while significantly reducing permeability to moisture and aggressive ions (Shelly et al., 2024).

A key advantage of nC-modified epoxy adhesives is their ability to improve durability under aggressive environmental conditions (Lei et al., 2021). The layered structure of nC increases diffusion path tortuosity and acts as a physical barrier to moisture ingress, slowing hydrolytic degradation and transport-induced damage. Microstructural studies frequently report a transition from a few wide cracks in neat epoxy to multiple finer cracks in nC-modified systems, indicating improved crack control and energy dissipation. Compared with other nanomaterials, nC has also been shown to tolerate relatively higher loadings without severe agglomeration, making it attractive for field-applied FRP systems (Taheri, 2020).

2.5.4. Limitations and research needs

Despite the demonstrated potential of nano-modified epoxy adhesives, several limitations remain in the existing literature. Many studies focus on short-term mechanical properties under controlled laboratory

conditions, with limited attention to coupled environmental exposure and long-term durability. Comparative evaluations among different classes of nanomaterials using consistent test methods are scarce, making it difficult to establish clear performance hierarchies. In addition, bond durability is often inferred indirectly from global mechanical response rather than measured explicitly through interface-focused tests.

Another limitation is the frequent use of intact concrete substrates, whereas many real-world applications involve pre-aged or environmentally damaged concrete. The interaction between nano-modified adhesives and deteriorated substrates remains insufficiently understood. Furthermore, optimal dosage ranges and dispersion strategies are highly system-dependent, and excessive nano-content can negatively affect workability and bond performance.

Overall, nano-modified epoxy adhesives represent a promising pathway for enhancing the durability and reliability of externally bonded FRP systems. However, systematic, durability-driven studies that link nano-scale modification of epoxy adhesives to interfacial bond performance under realistic environmental exposures are still limited. Addressing these gaps is essential for advancing the practical application of nano-engineered adhesives in FRP strengthening of concrete infrastructure.

2.6. Research Gaps

Despite extensive research on externally bonded CFRP systems and increasing interest in nano-modified epoxy adhesives, several critical limitations remain in the existing literature that restrict the reliable assessment and long-term implementation of FRP strengthening technologies. These limitations span experimental scope, durability assessment, interfacial characterization, and integration of material-scale mechanisms with structural performance. These gaps are synthesized from the literature reviewed in Sections 2.1-2.5.

First, many studies on CFRP-strengthened concrete continue to emphasize short-term mechanical performance, such as strength enhancement under monotonic loading, while providing limited evaluation of long-term durability. Although improvements in flexural capacity, shear resistance, and confinement efficiency are well documented, the persistence of these gains under realistic environmental exposure is often assumed rather than experimentally verified. As a result, structural performance predictions may significantly overestimate service-life behavior when interfacial degradation governs failure.

Second, durability investigations are frequently conducted under isolated environmental actions, such as moisture exposure, elevated temperature, or F/T cycling in water. In practice, FRP-strengthened concrete is commonly subjected to coupled deterioration mechanisms, including moisture, temperature variation, F/T cycling, and chemical attack from chlorides or sulfates. The combined effects of these actions on CFRP-concrete bond behavior remain insufficiently understood, particularly with respect to damage accumulation and failure mode transition.

Third, although nano-modified epoxy adhesives have shown promise in enhancing mechanical and transport properties, comparative and systematic evaluations across different nanomaterial types are limited. Many studies focus on a single nano-modifier and a narrow dosage range, making it difficult to establish generalizable conclusions or performance hierarchies among nS, GO, and nC systems. Moreover, differences in specimen geometry, curing conditions, exposure protocols, and test methods further complicate cross-study comparisons.

Fourth, interfacial bond behavior is often inferred indirectly from global structural response rather than measured explicitly. While confinement efficiency or flexural strength improvements provide useful

insight, they do not directly quantify degradation of the CFRP-concrete interface. Interface-focused tests, such as pull-off or shear bond measurements, are still underutilized in durability studies, despite their relevance to debonding-controlled failure modes. This gap limits mechanistic understanding of how adhesive degradation translates into loss of strengthening effectiveness.

Fifth, the majority of experimental studies evaluate FRP systems bonded to intact, laboratory-cured concrete substrates, whereas many real-world applications involve pre-aged or environmentally deteriorated concrete. The interaction between nano-modified adhesives and damaged concrete surfaces, including the influence of microcracking, scaling, and weakened surface layers, remains poorly characterized. As a result, the effectiveness of adhesive modification strategies under realistic substrate conditions is uncertain.

Finally, there is a lack of integrated frameworks that link nano-scale modification of epoxy adhesives to interfacial transport behavior, bond durability, and macroscopic mechanical performance under environmental exposure. While microstructural and chemical characterization techniques have been applied in isolation, their results are rarely correlated quantitatively with bond strength retention and structural response.

Collectively, these limitations highlight the need for a systematic, durability-driven evaluation of nano-modified CFRP-concrete systems. Such an approach should incorporate controlled environmental conditioning, explicit measurement of interfacial bond performance, comparative assessment of multiple nano-modifiers, and consideration of both intact and pre-aged concrete substrates. Addressing these gaps forms the basis of the experimental program presented in this study.

Chapter 3. Methodology

3.1. Materials

This section describes the constituent materials used in the preparation of concrete substrates, externally bonded CFRP systems, and nano-modified epoxy adhesives investigated in this study. All materials were selected to ensure compliance with relevant ASTM standards, compatibility between cementitious and polymeric components, and relevance to durable strengthening and protective applications in chloride- and F/T-exposed concrete infrastructure. Particular emphasis was placed on (i) the use of Portland limestone cement (PLC) and supplementary cementitious materials to achieve high-performance yet lower-clinker concrete, (ii) commercially available CFRP fabrics and epoxy resins representative of field-applied strengthening systems, and (iii) a range of nanomaterials incorporated into the epoxy matrix to modify interfacial behavior at the CFRP-concrete interface. The chemical composition, physical properties, and relevant performance characteristics of each material are summarized below to provide a clear basis for interpreting the mechanical, transport, and durability results presented in subsequent sections.

3.1.1. Portland limestone cement

The PLC employed in this study conforms to ASTM C595 Type IL specifications and was produced by intergrinding portland cement clinker with approximately 5–15% finely ground limestone. Its oxide composition (Table 1) is dominated by calcium oxide (≈61%) and silica (≈19%), accompanied by smaller but significant contributions from alumina, ferric oxide, magnesia, and sulfate, which together ensure the formation of the primary clinker phases and appropriate levels of sulfate balance. Loss on ignition values (~5.6%) reflect the carbonate contribution from limestone addition. The minor oxides (Na_2O, K_2O, TiO_2, P_2O_5, ZnO, Mn_2O_3, and trace sulfide) are present only in low amounts, consistent with the requirements of ASTM C595 for blended hydraulic cements.

Table 1. Chemical composition of PLC determined by XRF.

SiO_2	Al_2O_3	Fe_2O_3	CaO	MgO	SO_3	LOI	Na_2O	K_2O	TiO_2	P_2O_5	ZnO	Mn_2O_3	S^{2-}	IR
18.95	3.60	2.80	60.55	2.90	2.35	5.60	0.20	0.50	0.25	0.10	0.03	0.05	≤ 0.05	≤ 1.0

In terms of physical properties (Table 2), the PLC exhibited a relative density in the range of 2.8–3.1 and a strongly alkaline pH (12-13) when in slurry form, typical of hydraulic cements. Its fineness is notably higher than that of ordinary portland cement, with a Blaine surface area of approximately 470 m^2/kg and over 97% of particles passing the 45 μm sieve. This enhanced fineness improves early hydration kinetics and helps compensate for the reduced clinker fraction associated with limestone substitution. Setting times determined in accordance with ASTM C191 fell within standard limits, with initial and final sets of approximately 117 and 218 minutes, respectively, reflecting balanced hydration behavior suitable for both workability and construction scheduling. The cement also displayed excellent soundness, with autoclave expansion averaging only 0.031%, well below the allowable ASTM limit.

Table 2. Physical properties of PLC.

Relative density (specific gravity)	pH (wet slurry)	Limestone content	Blaine fineness (surface area)	% passing 45 µm sieve (No. 325)	Initial setting time	Final setting time	Autoclave expansion	Air content of mortar	Mortar compressive strength (ASTM C109)
2.8 – 3.1	12 – 13	5 – 15 %	470 m²/kg	97.4 %	117 min	218 min	0.031 %	6.9 %	28.9 MPa @ 3 d 34.8 MPa @ 7 d 42.9 MPa @ 28 d

Fresh mortar prepared with this PLC demonstrated an air content of about 6.9%, which is compatible with typical workability expectations. Strength development was satisfactory and in fact exceeded ASTM C595 minimum requirements, with compressive strengths of 28.9 MPa at 3 days, 34.8 MPa at 7 days, and 42.9 MPa at 28 days. These results confirm that the limestone addition did not compromise early or long-term strength. The particle size distribution, illustrated in Figure 1, highlights the predominance of fine particles, with limestone grains generally finer than the clinker phases, contributing to the filler effect, improved packing, and nucleation sites that support hydration. Collectively, these chemical and physical characteristics demonstrate that the PLC used in this study possesses reliable performance attributes while providing a reduction in clinker factor consistent with sustainability objectives.

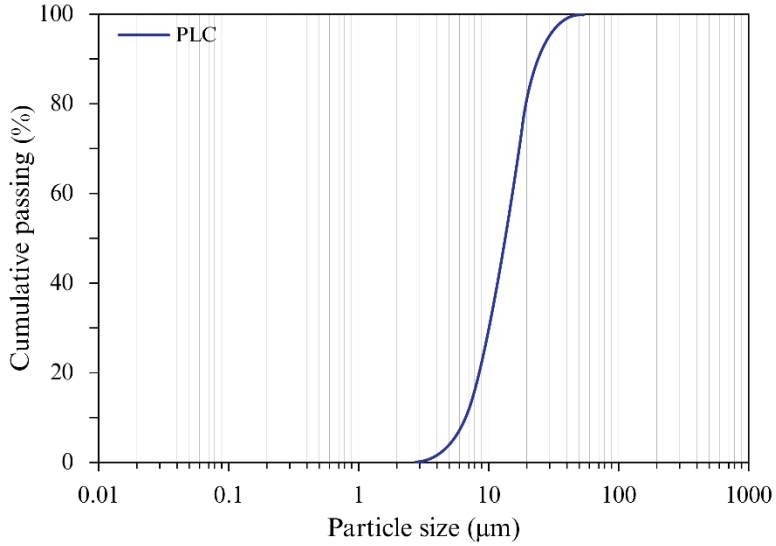

Figure 1. Particle size distribution of PLC.

3.1.2. Silica fume

The supplementary cementitious material used in this study was densified silica fume (SF) (MasterLife® SF 100, Master Builders Solutions), a by-product of the silicon metal industry consisting primarily of amorphous silicon dioxide. According to the manufacturer's Technical and Safety Data Sheets, the product has a specific gravity of about 2.2, a bulk density of 2100–2300 kg/m³, and a neutral pH (6-8), and appears as a fine gray powder. In compliance with ASTM C1240, the SF meets the specification limits of ≥ 85% SiO_2, ≤ 6% loss on ignition, ≤ 3% moisture content, and specific surface area ≥ 15 m²/g, with less than 10% retained on the 45 µm sieve and a strength activity index ≥ 105% at 7 days. Typical dosages recommended in the TDS range from 5–15% by mass of cementitious material, with the material supplied

in densified form to facilitate handling and mixing. Beyond its compliance with ASTM requirements, the product is recognized for its ability to improve concrete performance by filling voids between cement grains, refining pore structure, and reacting pozzolanically with calcium hydroxide to form additional C–S–H, thereby enhancing strength and durability while reducing permeability and chemical ingress.

3.1.3. Fina aggregate (sand)

The fine aggregate used in this study was Sakrete® Multi-Purpose Sand, a graded and washed natural sand composed predominantly of quartz (crystalline silica, CAS No. 14808-60-7). It met the requirements of ASTM C33 for fine aggregates in concrete. The particle-size distribution was verified by ASTM C136, and the specific gravity and absorption were determined according to ASTM C128. Appropriate dust-control and handling measures were observed due to the presence of respirable crystalline silica.

3.1.4. Coarse aggregate (gravel)

The coarse aggregate used in this study was Sakrete® All Purpose Gravel, a graded and washed gravel commonly applied in custom concrete mixes, drainage bases, and exposed aggregate finishes. The material consists primarily of quartz (crystalline silica, CAS No. 14808-60-7), which may represent 60-100% of the composition. It met the requirements of ASTM C33 for coarse aggregates in concrete. The particle-size distribution was confirmed by ASTM C136, and the specific gravity and absorption were determined according to ASTM C127. As with fine aggregate, handling precautions were taken due to the presence of respirable crystalline silica and its long-term health risks.

3.1.5. Water

The water used in this study complied with the requirements of ASTM C1602. Potable tap water was employed, which is acceptable without further testing under the standard. In accordance with ASTM C1602, the use of potable water ensures compliance with the performance requirements for compressive strength and setting time, and it minimizes the risk of deleterious chemical constituents such as chlorides, sulfates, or alkalis. The water quality was therefore considered suitable for mixing and curing concrete specimens without the need for additional qualification testing.

3.1.6. High-range water-reducer

High-range water-reducing admixture (HRWR). A polycarboxylate ether-based high-range water-reducing admixture, MasterGlenium® 7500 (BASF Master Builders Solutions), was used in this study. The admixture conforms to the requirements of ASTM C494 as both a Type A (water-reducing) and Type F (high-range water-reducing) admixture. According to the manufacturer's technical data, it provides a wide dosage range (2-15 fl oz/100 lb of cementitious material), enabling both moderate and high water reduction while maintaining slump retention and controlled setting characteristics. The product is free of added chlorides and is non-corrosive, making it suitable for reinforced and prestressed concrete applications. In this study, MasterGlenium® 7500 was used to reduce the water-to-cementitious materials ratio (w/cm) while achieving the required workability, ensuring consistency with high-performance concrete production practices.

3.1.7. Concrete

Concrete was proportioned per Table 3 using PLC with 5% SF replacement of cement mass, potable mixing water (ASTM C1602), natural aggregates conforming to ASTM C33, and a polycarboxylate ether-based HRWR (MasterGlenium® 7500; ASTM C494 Type A/F). Specimens were mixed, consolidated, molded, and cured in accordance with ASTM C192. The fresh slump was 80 mm, measured per ASTM C143; density and yield were determined per ASTM C138. The mixture had a total w/cm of 0.33 and was designed to achieve a target 28-day compressive strength of 60 MPa, consistent with high-performance structural concrete requirements.

Table 3. Mix proportions of concrete.

Water	PLC	SF	FA	CA	SP	Slump
		kg/m^3				*mm*
180	513	27	810	1120	1.2	80

3.1.8. Mortar

For FRP-wrapped pre-aged concrete specimens, surface preparation was performed by removing loose paste and aggregates using a steel brush and compressed air. A thin leveling layer of cement mortar, mixed at a sand : cement : water ratio of 2 : 2 : 1 by weight, was then applied to fill pits and irregularities on the substrate surface. The sand employed in the preparation of the surface mortar was a high-purity silica sand supplied by U.S. Silica Company. According to the manufacturer's safety data sheet, the product consists of 95–99.9% crystalline silica (quartz), is chemically stable, insoluble in water, and has a specific gravity of approximately 2.65. It is widely used in mortars, grouts, and cement-based products. The sand complies with ASTM C33 requirements for fine aggregates in mortar applications, and its use in the present study ensured compatibility with the PLC-based mortar system. The mortar layer was allowed to harden for 24 h before the epoxy adhesive and carbon fiber fabric were applied. The FRP-wrapped, pre-aged specimens were then cured under laboratory conditions for 14 days prior to testing.

3.1.9. Carbon fiber reinforced polymer

Externally bonded CFRP reinforcement was applied using Simpson Strong-Tie® CSS-CUCF11 and CSS-CUCF22, which are unidirectional, high-strength, non-corrosive carbon fabrics designed to be field laminated with the companion CSS-ES saturating resin to form a structural CFRP composite. Both fabrics are ICC-ES evaluated (ESR-3403) in accordance with AC125 for concrete and unreinforced masonry strengthening applications using externally bonded FRP systems, and are NSF-listed as safe for potable-water contact. They are also part of the UL-tested assembly (Design No. N861) that achieved a four-hour fire rating when tested under ASTM E119 full-scale fire exposure, and both meet Class A flame-spread and smoke-developed index requirements when coated with FX-207.

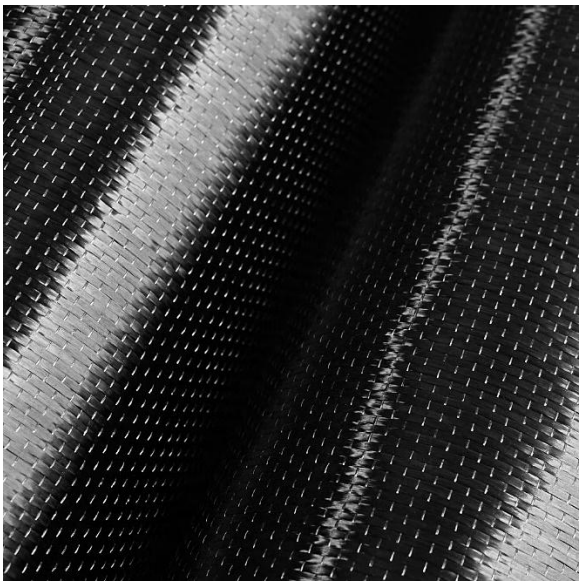

Figure 2. Unidirectional carbon fabric.

The CSS-CUCF11 fabric has an areal weight of 370 g/m² and a nominal dry thickness of 0.21 mm. The dry fiber exhibits a tensile strength of 4,600 MPa, a tensile modulus of 260 GPa, and an elongation at break of 1.9 %. When laminated with the CSS-ES saturating resin and post-cured for 48 h at 60 °C in accordance with ASTM D3039, the resulting cured composite achieves a tensile strength of 880 MPa, a tensile modulus of 98 GPa, an elongation at break of 0.9 %, and a cured layer thickness of 0.5 mm. In contrast, the CSS-CUCF22 fabric is approximately twice as heavy, with an areal weight of 740 g/m² and a dry thickness of 0.42 mm, while maintaining the same dry-fiber tensile strength (4,600 MPa), modulus (260 GPa), and elongation (1.9 %). The cured composite from CUCF22 develops a tensile strength of 880 MPa, a modulus of 98 GPa, an elongation of 0.9 %, and a thickness per layer of 1.0 mm.
Both CFRP fabrics are characterized by high tensile strength-to-weight ratio, ambient-temperature curing capability, non-corrosive behavior, and compatibility with a wide range of finish coatings. They are suitable for use in seismic retrofit, load-rating upgrades, defect remediation, and blast-mitigation applications involving concrete or masonry substrates. In this study, the CFRP sheets were cut to the required dimensions, saturated with the waterborne amine epoxy resin, and applied to the prepared concrete surfaces using the wet-layup method, following the manufacturer's technical instructions and the procedures recommended in ACI PRC-440.2 (ACI Committee 440, 2023) for externally bonded FRP strengthening systems.

3.1.10. Epoxy

A two-component waterborne amine epoxy system (Corotech® V440, Benjamin Moore) was employed as the saturating resin for the CFRP application. The resin is formulated to provide strong adhesion, abrasion resistance, and chemical durability on concrete and other substrates. The product consists of a 3:1 mix ratio (by volume) of resin (Part A) to curing agent (Part B), with a pot life of 2–4 h at 25 °C and an induction time of 30 min. The cured coating achieves a gloss finish with a volume solids content of approximately 43%, a dry film thickness of 1.5–1.9 mils per coat, and a full cure time of 3–5 days under laboratory conditions. Performance evaluations indicate high durability: adhesion (ASTM D3359) rating of 5B, pencil hardness of HB after 1 week cure, impact resistance up to 160 in-lb, abrasion resistance

(ASTM D4060) of 90 mg loss per 1,000 cycles, and excellent resistance to fresh water, salt water, and wastewater exposure. The system is low-VOC (< 250 g/L), water-cleanable, and suitable for use in USDA-inspected facilities. In this study, the epoxy was mixed, applied, and cured in accordance with the manufacturer's instructions and ACI PRC-440.2 (ACI Committee 440, 2023) guidelines for CFRP strengthening systems.

Figure 3. Waterborne epoxy adhesive.

3.1.11. Nanosilica

A high-purity silicon dioxide (SiO_2, CAS 7631-86-9) nanopowder (Sigma-Aldrich 718483) was used as the nS modifier. The powder is white and odorless, supplied as nanoparticles with a BET surface area of 175–225 m^2/g and a slurry pH of 3.7–4.7; residual moisture is <1.5% by mass. The material has a density of ~2.56 g/cm^3, is slightly water-soluble (≈0.076 g/L at 37 °C), and is classified in the SDS as not a hazardous substance/mixture under GHS when handled with appropriate dust control. These attributes make it suitable for use as a nano-scale rheology and interface modifier in cementitious and epoxy systems.

Figure 4. Nanosilica.

3.1.12. Graphene oxide

Two GO-based nanomaterials supplied by JMC Fine Chemicals (Korea) were used: a high-oxygen graphite oxide (JGO/JGTO series) and a partially reduced GO (JPRGO series). According to the manufacturer's TDS, both materials contain >90% single-layer sheets with controlled lateral size in the 5–15 μm range, produced through JMC's scalable sulfuric-acid oxidation process. The acidic GO (GO^a) contains 40–50% oxygen, exhibits the characteristic lamellar morphology shown in the TDS SEM images, and is supplied as either a solid powder or a 0.5–1.5 wt% aqueous dispersion. In contrast, the neutral, partially reduced GO (GO^n) contains 10–15% oxygen, has improved conductivity (<30 S/cm), and shows a more collapsed sheet morphology due to partial restoration of the sp^2 carbon network.

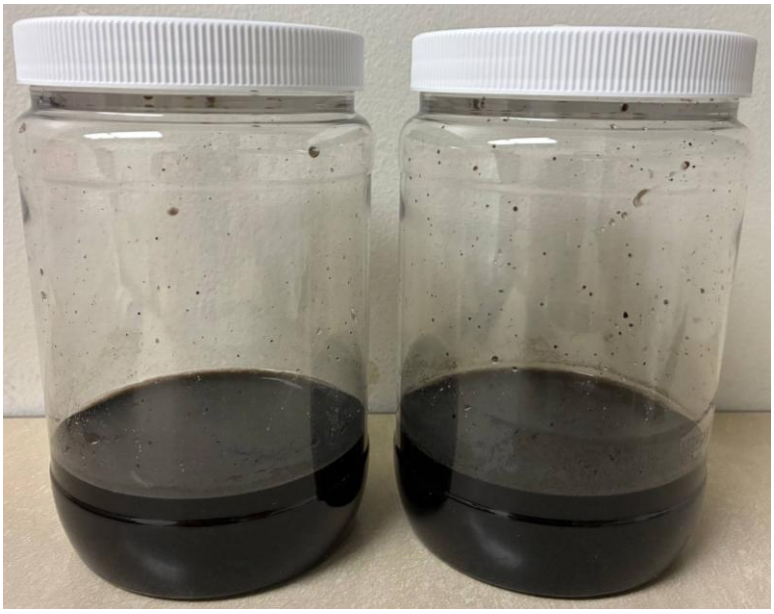

Figure 5. Graphene oxide.

To quantify their surface chemistry in our system, the pH of both GO types was experimentally measured after dispersing the powders in deionized water at identical solid concentrations. The GO^a exhibited a pH of 4.7, reflecting its high density of oxygenated functional groups (carboxyl, hydroxyl, epoxy), while the GO^n showed a pH of approximately 7, consistent with its partially reduced nature and lower surface oxygen content. These measured pH differences provide an important indication of each material's protonation state, dispersion behavior, and potential interactions with cementitious phases and epoxy functional groups in the CFRP-concrete interface.

3.1.13. Nanoclay

Three grades of sodium montmorillonite nC were employed to evaluate their influence on the FRP-concrete system: Bentobrite® 770 (nC^B), Polargel® NF (nC^F), and Polargel® T (nC^T) (American Colloid Company). Bentobrite® 770 is a white, micronized sodium bentonite consisting primarily of dioctahedral smectite with a surface area exceeding 750 m^2/g when dispersed; it has a pH of 8.5–10.5, specific gravity of 2.6, and viscosity of 300-600 cP at 5% solids. Polargel® NF is a hydroclassified, water-washed sodium montmorillonite supplied as a white, microfine powder; it exhibits high purity, brightness ≥80, pH of 9.0–10.0, specific gravity of 2.6, and viscosity of 40–200 cP at 5% solids. Polargel® T is also a hydroclassified

sodium montmorillonite, with enhanced thixotropic efficiency; it has brightness ≥80, pH of 8.5–10.5, specific gravity of 2.6, free swell ≥24 mL, and viscosity of 200–800 cP at 5% solids. All three nCs are insoluble in water and alcohol, but disperse to create very high surface areas, functioning effectively as suspending agents, binders, and thixotropic modifiers. Their incorporation in this study was intended to enhance interfacial properties through nanoscale modification of the epoxy matrix.

Figure 6. Montmorillonite nC.

3.2. Specimens

A comprehensive set of specimen configurations was prepared to systematically evaluate the bond performance, mechanical response, and durability of externally bonded CFRP systems applied to concrete substrates under varying material conditions and degrees of pre-existing damage. The specimen matrix included prismatic specimens for pull-off bond testing, as well as cylindrical concrete specimens representing unwrapped, pre-aged, CFRP-wrapped, and nano-modified CFRP-wrapped conditions. Both normal and pre-aged concrete substrates were considered to capture the influence of substrate deterioration on CFRP-concrete interfacial behavior and confinement effectiveness. Controlled variations in epoxy modification, curing duration, and surface preparation were implemented to isolate the effects of nanomaterial incorporation and environmental degradation. The specimen geometries, preparation procedures, and curing protocols described in the following subsections were selected to ensure consistency with relevant ASTM standards and to provide a robust basis for comparative evaluation of bond durability, transport properties, and compressive performance.

3.2.1. Pull-off specimens

Bond strength between the externally bonded CFRP laminate and the concrete substrate was evaluated using prismatic concrete specimens prepared and tested in accordance with ASTM D7522, which specifies the pull-off test method for FRP laminate systems bonded to concrete substrates. Each specimen consisted of a rectangular concrete prism with nominal dimensions of 406 mm × 102 mm × 102 mm. The CFRP laminate was externally bonded to one of the 406 mm × 102 mm faces using the wet lay-up method with the designated epoxy adhesive. After curing and any prescribed pre-aging or environmental conditioning, the bonded CFRP surface was prepared for pull-off testing in accordance with ASTM D7522. Circular

steel loading fixtures (dollies) with a diameter of 50 mm were adhesively bonded to the CFRP surface using a high-strength epoxy adhesive. For each prism specimen, five individual pull-off test locations were prepared, resulting in five replicate measurements per specimen. The spacing between adjacent dollies was selected to avoid overlap of stress fields and to ensure independent measurements, consistent with ASTM D7522 recommendations.

(a) sandblasted concrete substrate

(b) CFRP-bonded concrete surface

(c) installation of steel dolly

(d) pull-off bond testing setup

Figure 7. Preparation and testing sequence for CFRP-concrete pull-off bond specimens.

Following dolly installation and adhesive curing, the CFRP laminate and adhesive were scored using a diamond core drill with an internal diameter equal to the dolly diameter. The scoring extended through the CFRP laminate and adhesive and into the concrete substrate to a depth between 6 and 12 mm, ensuring isolation of the test area without intersecting internal reinforcement. Pull-off loading was applied normal to the laminate surface using a fixed-alignment adhesion tester at a controlled stress rate not exceeding 1 MPa/min, as specified by ASTM D7522, until failure occurred. For each pull-off test, the maximum tensile force and corresponding failure mode were recorded and classified according to ASTM D7522 (e.g., cohesive failure in substrate, adhesive failure at the interface, or mixed-mode failure). For each specimen, the average pull-off bond strength from the five dolly tests was calculated and reported as the representative bond strength value. These averaged results were used in subsequent analysis and comparison of CFRP and nano-modified CFRP systems, ensuring improved statistical reliability and reduced influence of local surface heterogeneity.

3.2.2. Reference concrete

Reference specimens (REF) were plain concrete cylinders (Ø 50.8 mm × 101.6 mm) cast with the mix proportions given in Table 3. After demolding, they were moist-cured for 28 days in accordance with ASTM C192. These unwrapped cylinders served as the baseline reference for all comparisons.

3.2.3. Pre-aged concrete

Pre-aged specimens were concrete cylinders identical in geometry and mix design to the control specimens, but subjected to an accelerated deterioration protocol based on F/T cycling in a chloride solution to simulate environmental aging representative of cold-region exposure. The pre-aging process was designed to reduce the compressive strength of the concrete to approximately 85% of its 28-day reference value, thereby representing a moderately deteriorated substrate condition prior to surface treatment or CFRP application.

3.2.4. FRP-wrapped concrete

For wrapped specimens (FRP), oven-dried concrete cylinders were coated with a uniform layer of epoxy adhesive and wrapped with one layer of unidirectional CFRP fabric (CSS-CUCF11). The resin application rate was ~420 g/m², as recommended by the manufacturer. Wrapped specimens were cured under laboratory conditions for 7 days before testing.

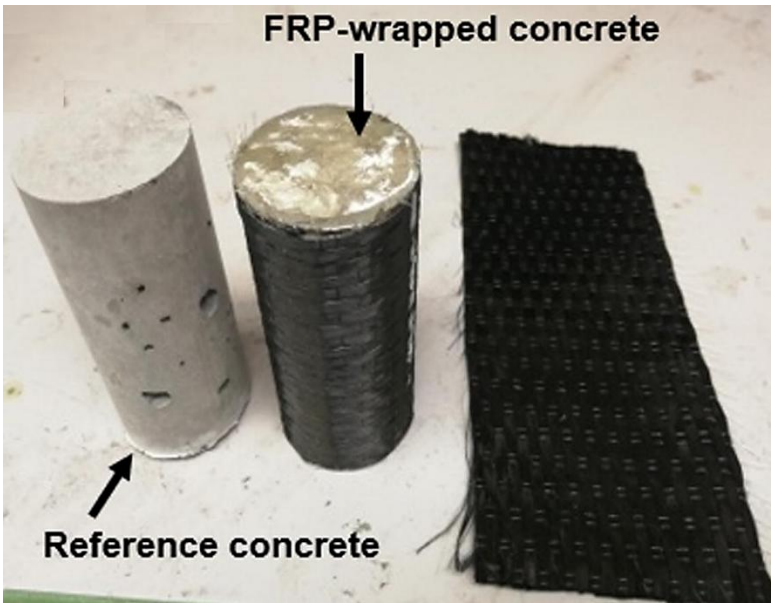

Figure. 8. CFRP-wrapped concrete cylinders.

3.2.5. FRP-wrapped pre-aged concrete

Pre-aged cylinders were first cleaned of loose paste and aggregates with a steel brush and compressed air. A thin mortar layer (sand : cement : water = 2:2:1) was applied to level irregularities and fill pits. After 24 h of hardening, the epoxy adhesive was applied and the specimens were wrapped with one layer of CFRP fabric. These specimens (FRP-A) were cured for 14 days before testing.

Figure. 9. Cement mortar-repaired pre-aged concrete cylinders.

3.2.6. Nano-modified FRP-wrapped concrete

Concrete cylinders were wrapped following the FRP procedure, except that the epoxy adhesive was modified with nanomaterials (nC, nS, or GO) at designated dosages. After uniform dispersion of nanoparticles into the resin, the adhesive was applied and fabric wrapping performed as above. These specimens (nFRP) were cured for 7 days.

3.2.7. Nano-modified FRP-wrapped pre-aged concrete

Pre-aged cylinders were surface-prepared and leveled with mortar, as described for FRP-A. The epoxy used for wrapping was modified with nanomaterials, dispersed at specified dosages, before application with CFRP fabric. These specimens (nFRP-A) were cured for 14 days.

3.3. Exposure Protocols

To evaluate the durability of CFRP-concrete systems under environmental conditions representative of cold-region infrastructure, a set of controlled exposure protocols was implemented to simulate both pre-existing substrate deterioration and in-service environmental actions affecting bonded FRP systems. The conditioning regimes were designed to isolate the effects of moisture ingress, temperature, chloride exposure, and F/T cycling on interfacial bond performance, transport behavior, and mechanical response. Specifically, HTA was applied to CFRP-strengthened specimens to represent service-level and accelerated hot–wet exposure, while a chloride-assisted F/T protocol was used to generate pre-aged concrete substrates with a controlled level of deterioration prior to FRP application. In addition, extended F/T cycling in saline solution was employed to assess the long-term performance of unwrapped and CFRP-confined concrete under coupled environmental loading. The exposure conditions, durations, and evaluation criteria adopted in this study are detailed in the following subsections.

3.3.1. Hydrothermal aging

Hydrothermal aging of the CFRP-concrete specimens in this study was performed using a two-condition immersion protocol designed to represent both service-level moisture exposure and accelerated hot–wet degradation. Following curing, specimens were assigned to one of two HTA regimes:

3.3.1.1. Room-temperature immersion (RT-28d)

Specimens were fully submerged in deionized water maintained at 23°C for 28 days. This conditioning stage represents long-term moisture exposure under typical service temperatures. Specimens were supported on non-reactive racks and spaced to ensure uniform wetting on all sides.

3.3.1.2. Elevated-temperature immersion (60℃-14d)

Specimens were fully submerged in deionized water maintained at 60 ℃ for 14 days. This condition provides an accelerated hydrothermal environment intended to promote enhanced moisture diffusion, polymer plasticization, and early interfacial deterioration. Temperature was continuously monitored and controlled within the specified tolerance.

For both conditioning regimes, specimens were removed at the end of the designated immersion period, lightly surface-dried to a saturated-surface-dry state, and immediately tested (after cooling to room temperature in the case of the 60 ℃ exposure). Control specimens were stored in standard laboratory conditions at 23°C and 50% RH for the same total durations. This dual-condition HTA protocol captures the combined effects of moisture uptake, temperature-accelerated degradation, and interfacial weakening, enabling comparison of CFRP-concrete bond performance under service-like and accelerated hydrothermal environments.

3.3.2. Pre-aging procedure

Concrete cylinders were pre-aged through rapid F/T deterioration in a 5 wt% NaCl solution. Reference concrete specimens were subjected to cyclic F/T exposure following ASTM C666 until their mean compressive strength decreased to 85% of the original 28-day value. Preliminary trials showed that approximately 175 cycles were required to achieve this 15% reduction. During exposure, samples remained fully immersed in the NaCl solution, were rotated and flipped every 10 cycles to avoid positional bias, and were monitored using embedded thermocouples to confirm proper F/T temperature ranges and consistent thermal gradients within the cylinders. After reaching the target deterioration level, the cylinders were oven-dried at 50 °C for 24 h, mechanically cleaned to remove loose surface paste, and leveled with a thin 2:2:1 (sand:cement:water) mortar layer to ensure proper bonding prior to CFRP wrapping.

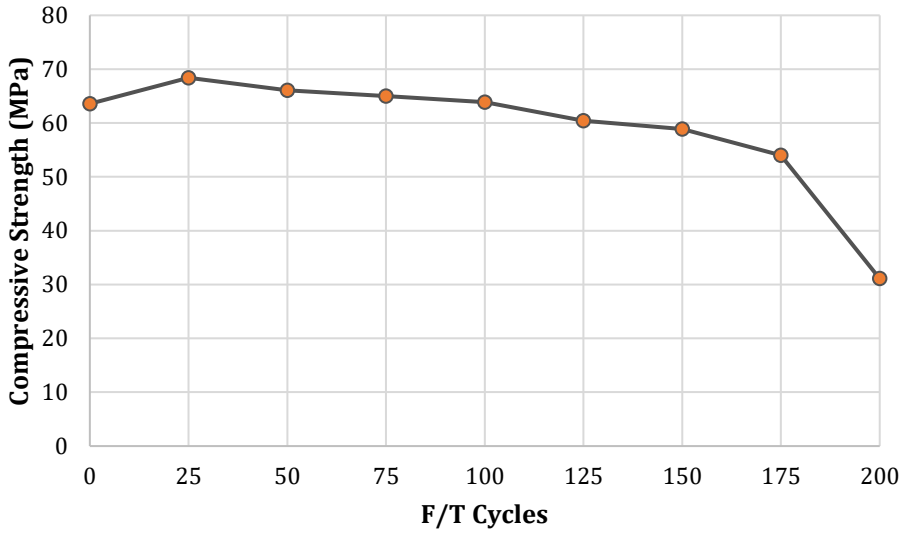

Figure 10. Compressive strength degradation of REF concrete under accelerated F/T-salt exposure.

Preliminary compressive strength measurements collected throughout the pre-aging process confirmed the progressive degradation expected under F/T-salt exposure. As shown in the accompanying figure, the REF exhibited an initial 28-day compressive strength of 63.6 MPa, followed by a modest strength gain during the early cycles (up to 68.4 MPa at 25 cycles), likely attributable to continued cement hydration. Strength gradually declined thereafter, with values decreasing to 63.9 MPa at 100 cycles and 58.9 MPa at 150 cycles. By 175 cycles, the compressive strength had fallen to 54.0 MPa, corresponding to approximately 85% of the original strength, marking the target threshold for defining the specimens as pre-aged. Beyond this point, the degradation accelerated sharply, reaching 31.1 MPa at 200 cycles, indicative of severe structural damage and confirming the suitability of the 175-cycle criterion for representing aged concrete conditions. These data validate the selected pre-aging protocol and provide a quantitative basis for comparing the performance of CFRP and nano-modified CFRP systems applied to both normal and pre-aged substrates.

3.3.3. Freezing and thawing cycles

Concrete specimens were first saturated in water for 24 h and brought to saturated-surface-dry condition. The initial SSD mass of each specimen was recorded. Afterwards, samples were fully immersed in a 10 wt.% NaCl solution and placed in a cyclic F/T chamber operating according to ASTM C666, with NaCl solution replacing water. Periodically throughout the cycling regime, the mass, compressive strength, MoE, and dimensions of the specimens were recorded as a function of the number of F/T cycles.

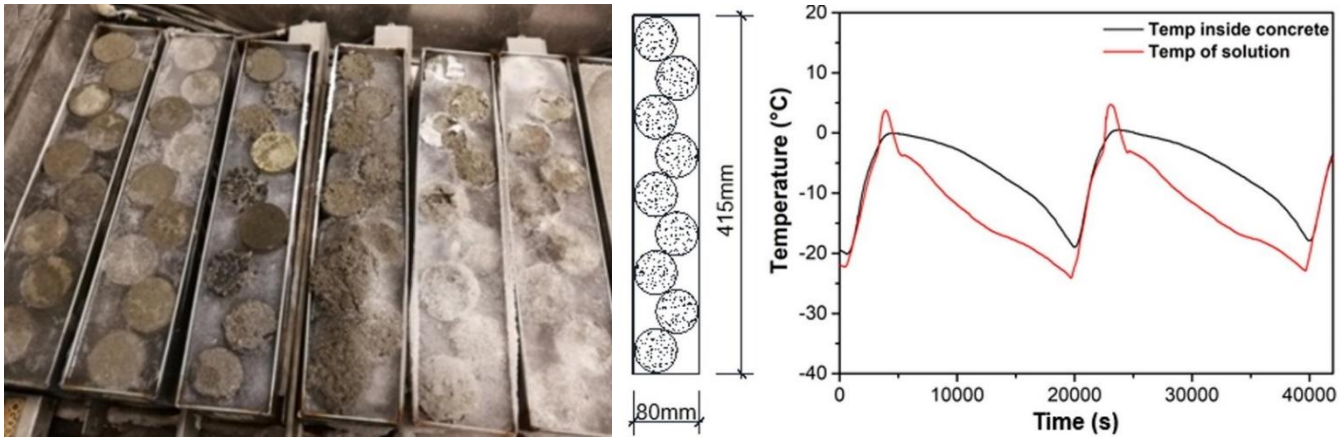

(a) digital photograph illustrating the arrangement of concrete specimens

(b) periodic temperature variation within the concrete specimens and soaking solution

Figure 11. Experimental setup and temperature monitoring during accelerated environmental conditioning of concrete specimens.

3.4. Test Methods

A multi-scale experimental program was implemented to quantify the interfacial, mechanical, transport, and material-level responses of concrete and CFRP-strengthened concrete subjected to the exposure protocols described in Section 3.3. The test methods were selected to capture degradation mechanisms governing the performance of externally bonded CFRP systems, with particular emphasis on bond strength as the primary durability-controlling parameter. Mechanical testing was conducted to assess interfacial bond capacity, compressive strength, stiffness degradation, failure modes, and F/T scaling resistance. Complementary transport measurements were used to evaluate moisture and gas ingress at the CFRP-concrete interface, while material characterization techniques were employed to investigate changes in epoxy surface wettability, microstructure, chemical interactions, and thermal stability resulting from nanomaterial modification. Together, these test methods provide an integrated framework for linking nanoscale modifications in the adhesive matrix to macroscopic durability and mechanical performance of CFRP-strengthened concrete systems under coupled environmental and mechanical loading.

3.4.1. Mechanical testing

3.4.1.1. Bond strength

Bond strength between the externally bonded CFRP laminate and the concrete substrate was evaluated using the pull-off test, which provides a direct and localized measure of the tensile capacity of the CFRP-epoxy-concrete interface. This parameter is critical for assessing the durability and effectiveness of externally bonded FRP systems, as interfacial degradation often governs premature failure under environmental exposure. The pull-off test induces a tensile stress normal to the bonded interface, allowing identification of the weakest failure plane within the composite system, including cohesive failure in the concrete substrate, adhesive failure at the epoxy-concrete or epoxy-CFRP interface, or mixed-mode failure. In this study, pull-off bond strength was used as the primary metric to quantify the effects of HTA, and nanomaterial modification of the epoxy adhesive on interfacial performance. The results from this test provide the basis for linking nanoscale modifications in the adhesive matrix to macroscopic durability and mechanical behavior of CFRP-strengthened concrete systems.

3.4.1.2. Compressive strength

Compressive strength of concrete and CFRP-confined cylinders was measured using an INSTRON 5900 Series Multi-Station testing system following ASTM C1231. A two-stage loading protocol was employed: specimens were loaded at 2 mm/min, then the rate was reduced to 0.5 mm/min once the load reached approximately 11.1 kN to improve accuracy near peak load. The peak compressive load, load-displacement response, and stress–strain curves were recorded for each specimen. For pre-aged or salt-scaled cylinders, the loading faces were leveled with a thin layer of gypsum paste to ensure uniform stress distribution and minimize eccentricity effects. This test was conducted on unconditioned specimens to establish baseline mechanical properties, and on conditioned specimens to evaluate residual strength following environmental exposures.

3.4.1.3. Modulus of elasticity

The static MoE was obtained from the linear portion of the stress–strain curve captured during the compressive strength test. This method provides a sensitive indicator of internal microcracking and stiffness degradation, especially under F/T and chloride exposures. The MoE was calculated from the initial linear slope before the onset of nonlinear deformation. Measurements were taken at pre-determined intervals of conditioning to quantify stiffness retention and to evaluate the contribution of CFRP confinement and nano-modified epoxy to the mitigation of degradation.

3.4.1.4. Failure mode assessment

During compressive testing, specimens were visually inspected to document characteristic failure modes. Unwrapped concrete typically exhibited crushing and asymmetric cracking, whereas CFRP-confined specimens showed constrained dilation, rupture of carbon fabric, or end debonding depending on substrate condition. These observations were used to support interpretation of mechanical test results and to assess how nano-modified epoxy influenced CFRP-concrete interaction.

3.4.1.5. Scaling resistance

Mass loss and dimensional changes (length, diameter, and L/D ratio) were monitored periodically throughout F/T exposure in salt solution to quantify salt-scaling deterioration. Following each designated F/T cycle interval, specimens were removed from the bath, brought to saturated-surface-dry (SSD) condition, and weighed to determine cumulative material loss. Dimensional measurements were collected using calipers to detect scaling-induced erosion and geometric distortion. This procedure provides a quantitative measure of F/T-salt damage progression and is essential for comparing deterioration in REF, CFRP-wrapped concrete, and nano-modified CFRP systems.

3.4.2. Transport testing

3.4.2.1. Water absorption

Water absorption behavior of FRP-wrapped and pre-aged FRP-wrapped specimens was evaluated using a modified procedure derived from ASTM C1585. Disk samples (30 mm height × 10 mm diameter) were cut from composite cylinders, oven-dried at 50 °C for 24 h, and sealed with a 2 mm hydrophobic coating on the top and bottom faces, leaving the FRP-epoxy interfacial perimeter exposed. Samples were immersed in deionized water, and mass gain was recorded at regular intervals to determine initial

sorptivity (capillary-controlled uptake) and secondary sorptivity (void-filling behavior). This method was used to assess transport resistance imparted by CFRP, epoxy modification, and environmental conditioning.

3.4.2.2. Gas permeability

Gas permeability at the FRP-concrete interface was evaluated using a modified method based on Alshamsi & Imran's setup. Disk specimens (10 mm thickness) were oven-dried and sealed on the top face with a 2 mm hydrophobic coating, exposing only the FRP-epoxy perimeter for vapor transmission. Samples were mounted in a sealed methanol vapor diffusion cell and placed in a 40 °C water bath, with mass loss recorded at fixed intervals (0, 2, 4, 6, 24, 48 h, etc.) until a linear steady-state rate was achieved. The rate of gas mass loss was used as an indicator of interfacial permeability and microstructural integrity

3.4.3. Material characterization

3.4.3.1. Water Contact Angle (WCA)

Hydrophobicity of unmodified and nano-modified epoxy adhesives was characterized using a VCA Optima contact angle goniometer following ASTM D7334. A water droplet was deposited on the cured epoxy surface, and the contact angle was measured 5 seconds after deposition. Increased WCA indicated reduced surface free energy and enhanced moisture resistance of the modified epoxy.

3.4.3.2. High-Resolution Optical Microscopy

Microstructural observations of concrete, epoxy, and CFRP-concrete interfaces were carried out using a Keyence VHX-7000 optical microscope (up to 2000× magnification). Imaging was performed before and after environmental conditioning to document interfacial cracking, epoxy morphology, and microstructural refinement associated with nanomaterial modification.

3.4.3.3. Fourier Transform Infrared Spectroscopy (FTIR)

FTIR spectra of unmodified and nano-modified epoxy adhesives were collected using a Nicolet Nexus 8700 FTIR spectrometer. Powdered epoxy samples were mixed with KBr (1:100 ratio) and scanned over 400–4000 cm^{-1} to identify chemical bonding changes, particularly those associated with siloxane groups and nanomaterial-epoxy interactions.

3.4.3.4. Thermogravimetric Analysis (TGA)

Thermal stability of cured epoxy systems was analyzed using a PYRIS 1 TGA analyzer from 50 °C to 800 °C at 10 °C/min. Residual mass at elevated temperatures was used to assess thermal degradation resistance and crosslink density improvements due to nanomaterial modification.

3.4.3.5. Differential Scanning Calorimetry (DSC)

Glass transition behavior of epoxy and nano-modified epoxy was measured using a TA Instruments Q2000 DSC system. Approximately 5-10 mg of sample was heated from –50 °C to 200 °C at 10 °C/min under nitrogen. Changes in Tg and endothermic response were used to characterize polymer mobility and crosslinking enhancements resulting from nanomaterial incorporation.

Chapter 4. Results and Discussion

4.1. Bond Durability

The bond durability of externally bonded CFRP systems governs their long-term effectiveness, particularly under moisture- and temperature-driven environmental exposures typical of chloride-affected concrete infrastructure. This subsection first evaluates the bond performance of control CFRP-concrete systems without nano-modification to establish a quantitative baseline against which the effects of HTA and subsequent nano-modification can be assessed. Figure 12 presents the pull-off bond strength results for under-saturated and fully saturated specimens reinforced with CCS11 and CCS22 fabrics under reference room-temperature dry conditions and two HTA regimes. By isolating unmodified epoxy systems, these results provide a clear benchmark for assessing interfacial degradation mechanisms prior to introducing nano-scale enhancements.

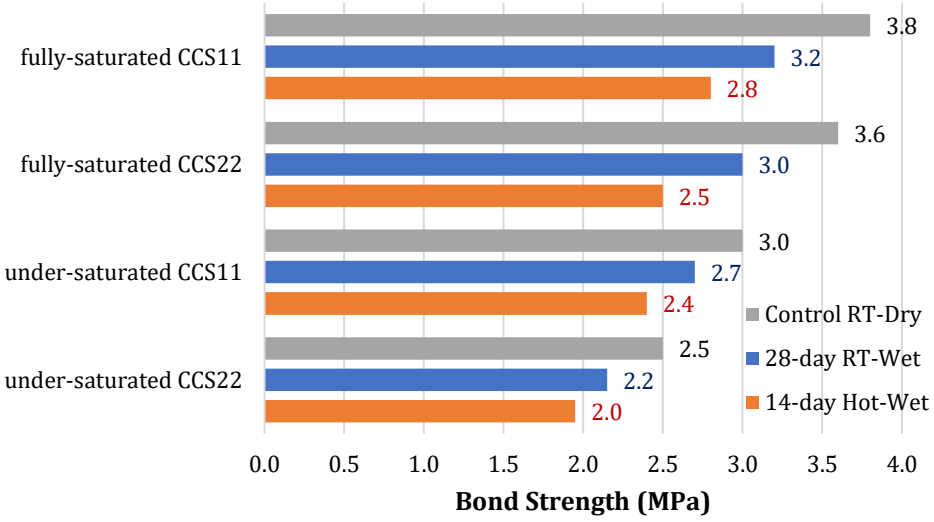

Figure 12. Bond strength of CFRP-to-concrete under HTA.

Under reference room-temperature dry conditions, the control specimens exhibited the highest bond strengths across all configurations, ranging from 2.5 to 3.8 MPa. Fully saturated CCS11 specimens achieved the maximum bond strength of 3.8 MPa, followed by fully saturated CCS22 at 3.6 MPa, under-saturated CCS11 at 3.0 MPa, and under-saturated CCS22 at 2.5 MPa. For both fabric types, full resin saturation resulted in a bond strength increase of approximately 20–25% compared to under-saturated conditions, indicating improved epoxy impregnation and more effective stress transfer at the CFRP-concrete interface. In addition, CCS11 consistently outperformed CCS22 under identical saturation conditions, with bond strength advantages of approximately 0.5 MPa (≈17–20%), reflecting the influence of fabric architecture and thickness on interfacial stress distribution in unmodified systems.

Hydrothermal aging led to a systematic and quantifiable reduction in bond strength for all control specimens, with degradation severity dependent on exposure temperature, saturation condition, and CFRP fabric type. After 28 days of room-temperature water immersion, bond strength decreased by

approximately 10–16% relative to the dry control values. Specifically, fully saturated CCS11 specimens decreased from 3.8 to 3.2 MPa (≈16% reduction), while fully saturated CCS22 decreased from 3.6 to 3.0 MPa (≈17%). Under-saturated CCS11 and CCS22 specimens showed smaller but still notable reductions, decreasing from 3.0 to 2.7 MPa (≈10%) and 2.5 to 2.2 MPa (≈12%), respectively.

More pronounced degradation was observed following 14 days of elevated-temperature (60 °C) water immersion, where bond strength losses reached approximately 25–30% relative to the dry controls. Fully saturated CCS11 specimens decreased to 2.8 MPa (≈26% reduction), and fully saturated CCS22 specimens decreased to 2.5 MPa (≈31%). Similarly, under-saturated CCS11 and CCS22 specimens exhibited bond strengths of 2.4 MPa and 2.0 MPa, corresponding to reductions of approximately 20% and 20%, respectively. Overall, elevated-temperature hydrothermal exposure consistently produced greater bond deterioration than room-temperature immersion, highlighting the combined effects of accelerated moisture diffusion, epoxy plasticization, and thermally activated interfacial weakening. These quantitative results demonstrate that while conventional CFRP systems maintain adequate bond capacity under dry conditions, their interfacial durability is significantly compromised under hydrothermal environments, thereby motivating the need for nano-modified epoxy systems examined in the subsequent sections.

4.1.1. Nano-modification

This subsection examines the influence of nano-modification of the epoxy adhesive on the bond strength of CFRP-concrete interfaces under control (unaged) conditions, prior to exposure to HTA. Three classes of nanomaterials, nS, GO, and nC, were investigated to represent distinct nano-scale modification mechanisms, including particle-based pore refinement, surface-chemistry-driven interfacial interaction, and layered silicate–induced rheological control. For each nano-modifier, bond strength was evaluated as a function of dosage, saturation state (under-saturated versus fully saturated), and CFRP fabric type (CCS22 versus CCS11). This systematic framework enables direct comparison of dosage-dependent performance trends and isolates the competing effects of interfacial enhancement at low nanomaterial contents and degradation associated with agglomeration, viscosity increase, or impaired resin impregnation at higher dosages. The following subsections present and discuss the control-condition bond responses for each nano-modifier, establishing a baseline for interpreting their durability performance under HTA in subsequent sections.

4.1.1.1. Nanosilica

Figure 13 illustrates the effect of nS dosage on the bond strength of CFRP-to-concrete joints under control (unaged) conditions, considering both saturation state (under-saturated vs. fully saturated) and CFRP fabric type (CCS22 vs. CCS11). Across all configurations, the incorporation of nS produced a nonlinear, dosage-dependent response, characterized by an initial increase in bond strength at low dosages followed by a gradual decline at higher dosages. This trend indicates the presence of an optimal nS content for enhancing interfacial performance in unaged systems.

For under-saturated CCS22 specimens (Figure 13a), the baseline bond strength of 2.5 MPa (0.0 wt%) increased to 2.9 MPa at 0.5 wt% nS, corresponding to an improvement of approximately 16%. A slightly lower value of 2.7 MPa was observed at 1.0 wt%, while further increases in nS dosage resulted in a reduction to 2.5 MPa and 2.4 MPa at 1.5 wt% and 2.0 wt%, respectively. A similar trend was observed for under-saturated CCS11 specimens (Figure 13b), where bond strength increased from 3.0 MPa at 0.0 wt% to a peak value of 3.3 MPa at 0.5–1.0 wt% nS (≈10% improvement), followed by a gradual decline

to 3.1 MPa and 2.9 MPa at higher dosages. These results suggest that, under under-saturated conditions, moderate nS addition enhances the epoxy-concrete interface, whereas excessive nS content may adversely affect resin continuity or dispersion efficiency.

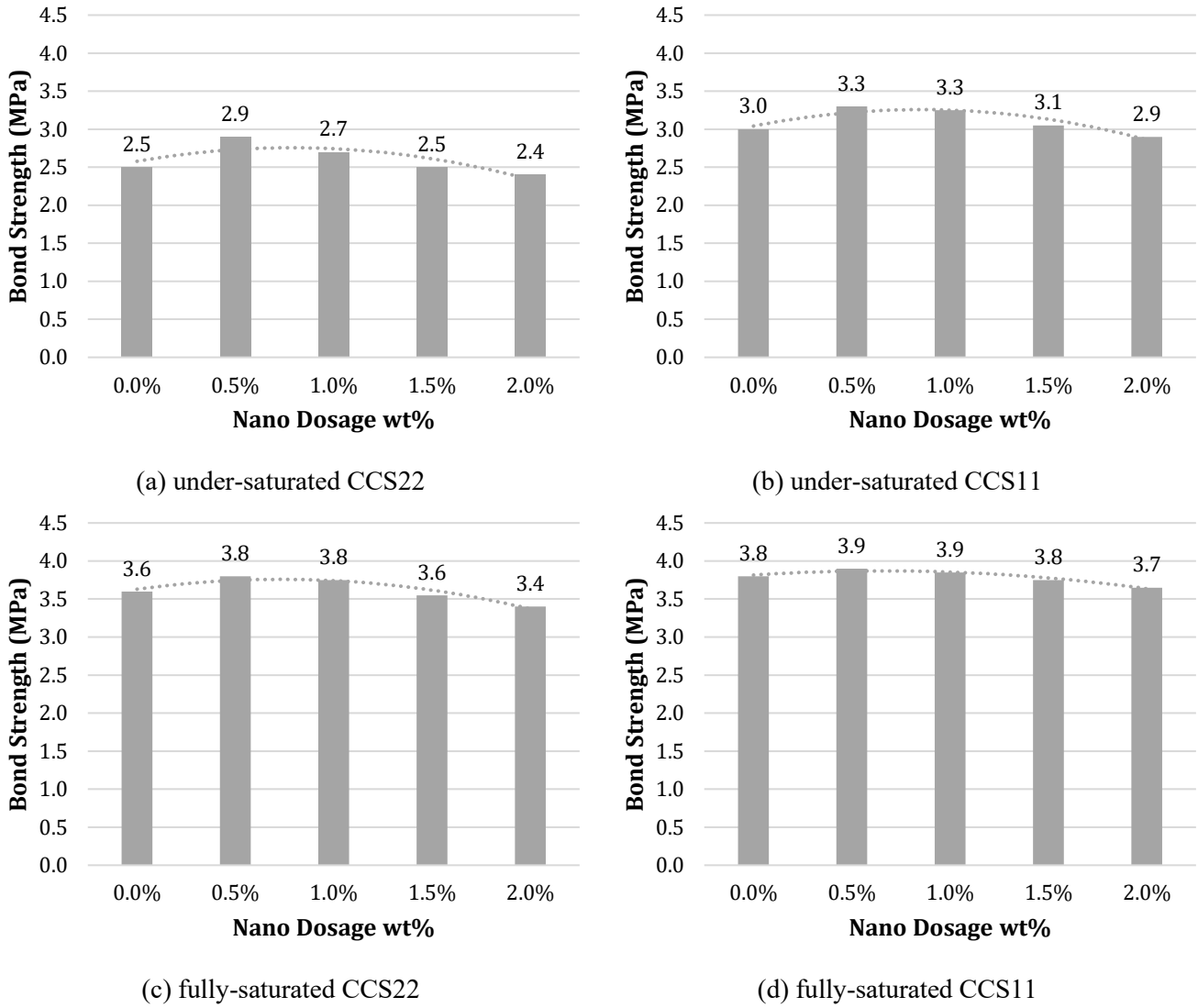

(a) under-saturated CCS22

(b) under-saturated CCS11

(c) fully-saturated CCS22

(d) fully-saturated CCS11

Figure 13. Effect of nS modification on CFRP-to-concrete bond strength.

For fully saturated specimens, higher absolute bond strengths were consistently achieved, and the beneficial effect of nS was more pronounced. In the case of fully saturated CCS22 (Figure 13c), bond strength increased from 3.6 MPa at 0.0 wt% to a maximum of 3.8 MPa at 0.5–1.0 wt% nS, representing an improvement of approximately 6%, before decreasing to 3.6 MPa and 3.4 MPa at 1.5 wt% and 2.0 wt%, respectively. The fully saturated CCS11 specimens (Figure 13d) exhibited the highest overall bond strengths, increasing from 3.8 MPa at 0.0 wt% to 3.9 MPa at 0.5–1.0 wt% nS, followed by a slight reduction to 3.8 MPa and 3.7 MPa at higher dosages. Although the relative percentage gains were smaller than those observed in under-saturated systems, the consistently higher bond strengths highlight the synergistic role of adequate resin saturation and nS modification in promoting effective stress transfer across the CFRP-concrete interface.

Overall, the control-condition results demonstrate that nS modification can enhance CFRP-concrete bond strength when applied at low to moderate dosages (approximately 0.5–1.0 wt%), regardless of fabric type or saturation state. The observed decline in bond strength at higher nS contents suggests the onset of adverse effects such as nanoparticle agglomeration, increased resin viscosity, or disruption of effective fiber impregnation. These baseline findings establish an optimal dosage window for nS in unaged systems and provide a critical reference for interpreting the durability performance of nS-modified CFRP joints under HTA conditions, as discussed in the following subsection.

4.1.1.2. Graphene Oxide

Graphene oxide was investigated as a nano-modifier for the epoxy adhesive to evaluate the role of surface chemistry and functional group density on the bond performance of CFRP-concrete interfaces under control (unaged) conditions. Two distinct GO types were examined: an acidic, oxygen-rich GO (GO^a) and a neutral, partially reduced GO (GO^n), allowing direct assessment of how oxygen-containing functional groups influence interfacial bonding. Bond strength results were analyzed as a function of GO dosage, saturation state (under-saturated versus fully saturated), and CFRP fabric type (CCS22 versus CCS11). This comparative framework isolates the contribution of GO chemistry from geometric and saturation effects, providing insight into the mechanisms by which graphene-based nanomaterials interact with the epoxy matrix and the concrete substrate. The following subsections separately discuss the performance trends observed for acidic and GO^n systems.

1. Acidic GO

Figure 14 summarizes the influence of GO^a dosage on the CFRP-concrete bond strength under control (unaged) conditions, considering saturation state and CFRP fabric type. In contrast to nS, GO^a produced a monotonic increase in bond strength up to an intermediate dosage, followed by a mild plateau or slight reduction at the highest dosage. This behavior was consistent across all configurations, indicating that low-to-moderate GO^a contents are effective in enhancing interfacial performance in unaged systems.
For under-saturated CCS22 specimens (Figure 14a), the baseline bond strength of 2.5 MPa increased progressively with GO^a dosage, reaching 2.7 MPa (0.02 wt%), 3.0 MPa (0.04 wt%), and a maximum of 3.3 MPa at 0.06 wt%, corresponding to an overall improvement of approximately 32% relative to the control. A slight decrease to 3.2 MPa was observed at 0.08 wt%, suggesting the onset of diminishing returns at higher GO^a contents. A similar trend was observed for under-saturated CCS11 specimens (Figure 14b), where bond strength increased from 3.0 MPa at 0.0 wt% to 3.7 MPa at 0.06 wt% (≈23% increase), followed by a marginal reduction to 3.5 MPa at 0.08 wt%. These results indicate that GO^a is particularly effective in improving bond strength under under-saturated conditions, where interfacial deficiencies are more pronounced.

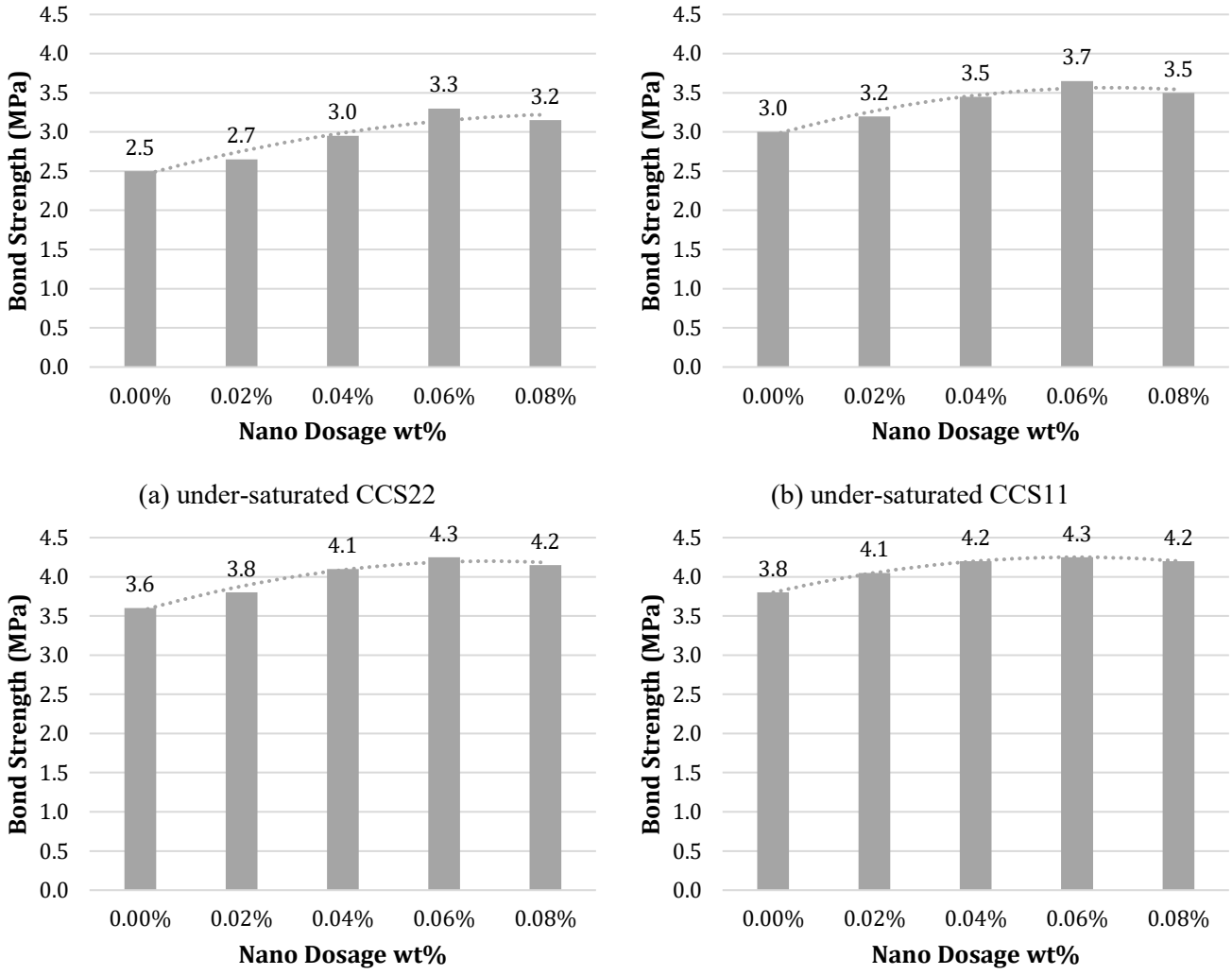

(a) under-saturated CCS22

(b) under-saturated CCS11

(c) fully-saturated CCS22

(d) fully-saturated CCS11

Figure 14. Effect of GO[a] modification on CFRP-to-concrete bond strength.

For fully saturated specimens, higher absolute bond strengths were achieved and the beneficial effect of GO[a] remained evident. In the case of fully saturated CCS22 (Figure 14c), bond strength increased from 3.6 MPa at 0.0 wt% to 4.3 MPa at 0.06 wt%, representing an enhancement of approximately 19%, before slightly decreasing to 4.2 MPa at 0.08 wt%. Similarly, fully saturated CCS11 specimens (Figure 14d) exhibited an increase from 3.8 MPa to 4.3 MPa at 0.06 wt% (≈13% improvement), followed by a minor reduction at higher dosage. Compared to under-saturated systems, the relative gains in fully saturated specimens were smaller, reflecting the already efficient resin impregnation and interfacial stress transfer in these configurations.

Overall, the control-condition results demonstrate that GO[a] is highly effective in enhancing CFRP-concrete bond strength at low dosages, with an optimal range centered around 0.04-0.06 wt%, regardless of fabric type or saturation state. The consistent improvement is attributed to the high surface area and abundant oxygen-containing functional groups of GO[a], which promote stronger interfacial interactions between the epoxy matrix and the concrete substrate. The slight reductions observed at 0.08 wt% suggest potential agglomeration or adverse effects on resin rheology at higher dosages. These baseline findings

establish a clear performance window for GO^{a} in unaged systems and form the reference point for evaluating its durability performance under HTA in subsequent sections.

2. Neutral GO

Figure 15 presents the effect of GO^{n} dosage on the CFRP-concrete bond strength under control (unaged) conditions, considering both saturation state and CFRP fabric type. In contrast to GO^{a}, GO^{n} exhibited a much narrower optimal dosage range and a more pronounced reduction in bond strength at higher dosages. This response indicates that while GO^{n} can provide modest interfacial benefits at very low contents, its effectiveness is limited compared to oxygen-rich GO under unaged conditions.

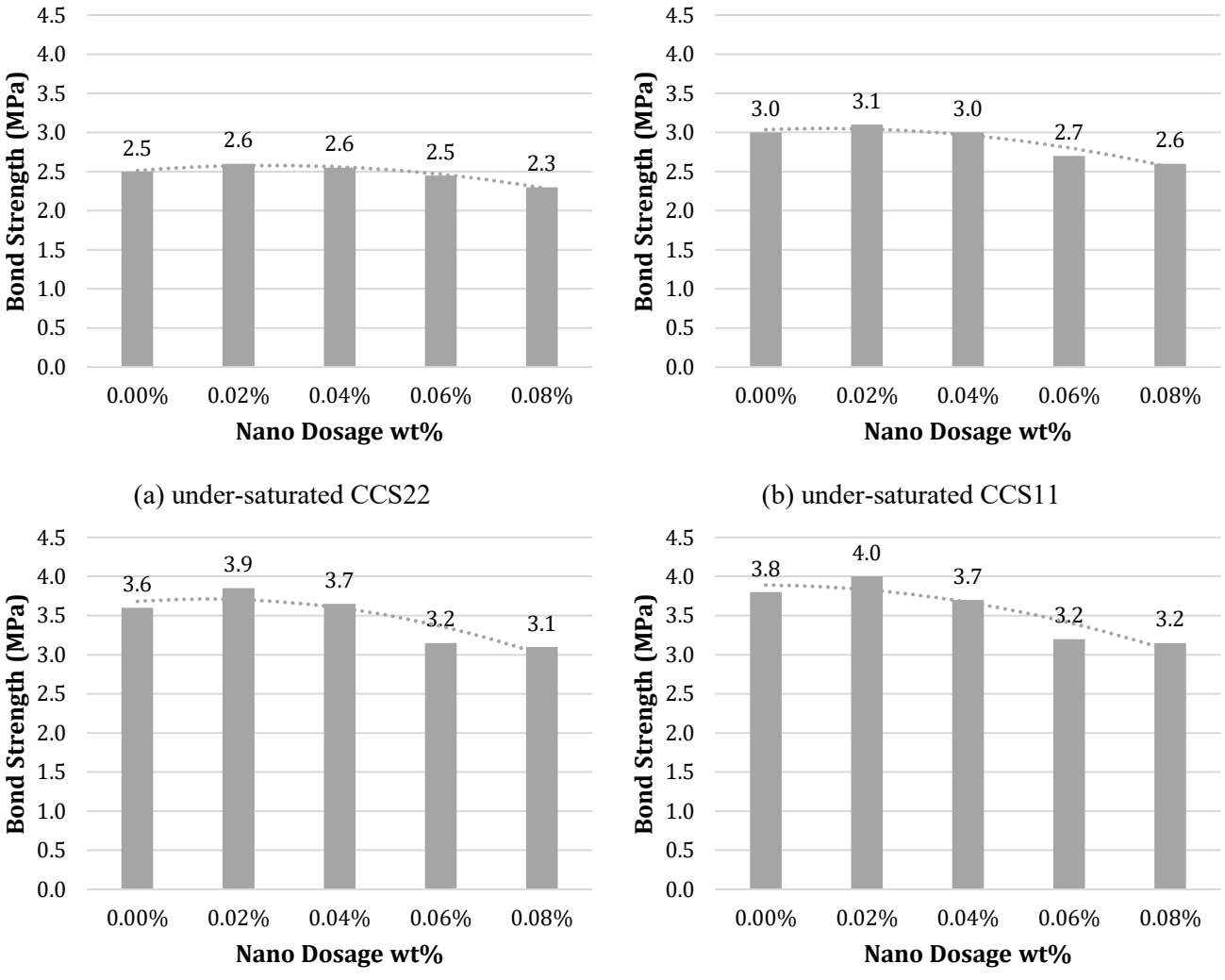

(a) under-saturated CCS22

(b) under-saturated CCS11

(c) fully-saturated CCS22

(d) fully-saturated CCS11

Figure 15. Effect of GO^{n} modification on CFRP-to-concrete bond strength.

For under-saturated CCS22 specimens (Figure 15a), the baseline bond strength of 2.5 MPa increased slightly to 2.6 MPa at 0.02–0.04 wt% GO^{n}, corresponding to a marginal improvement of approximately 4%. Beyond this dosage, bond strength declined to 2.5 MPa at 0.06 wt% and further to 2.3 MPa at 0.08 wt%, resulting in an overall reduction of approximately 8% relative to the control. A similar trend was

observed for under-saturated CCS11 specimens (Figure 15b), where bond strength increased modestly from 3.0 MPa to 3.1 MPa at 0.02 wt%, then decreased progressively to 2.7 MPa and 2.6 MPa at 0.06 wt% and 0.08 wt%, respectively. These results suggest that under under-saturated conditions, the beneficial effect of GO^n is minimal and highly sensitive to dosage.

For fully saturated specimens, higher absolute bond strengths were achieved, but the dosage-dependent trend remained consistent. In the case of fully saturated CCS22 (Figure 15c), bond strength increased from 3.6 MPa to 3.9 MPa at 0.02 wt%, followed by a decrease to 3.7 MPa, 3.2 MPa, and 3.1 MPa at 0.04 wt%, 0.06 wt%, and 0.08 wt%, respectively. Similarly, fully saturated CCS11 specimens (Figure 15d) exhibited a peak bond strength of 4.0 MPa at 0.02 wt%, compared to 3.8 MPa for the control, before declining to 3.7 MPa, 3.2 MPa, and 3.2 MPa at higher dosages. Even under optimal saturation, the maximum improvement achieved with GO^n was limited to approximately 5–8%, and bond strength decreased substantially once the dosage exceeded 0.02 wt%.

Overall, the control-condition results demonstrate that GO^n provides only marginal bond-strength enhancement at very low dosages (≈0.02 wt%), with performance deteriorating at higher contents regardless of saturation state or fabric type. Compared with GO^a, the reduced oxygen functional group density of GO^n appears to limit its ability to promote strong interfacial interactions within the epoxy-concrete system. Moreover, the rapid decline in bond strength at elevated dosages suggests adverse effects such as particle agglomeration, reduced epoxy wettability, or disruption of effective resin impregnation. These findings indicate that GO^n is less suitable than GO^a for interfacial enhancement in unaged CFRP-concrete systems and provide a critical reference for evaluating its durability performance under HTA conditions in subsequent sections.

The control-condition results clearly demonstrate that the bond performance of GO-modified CFRP systems is strongly governed by GO surface chemistry and functional group density. Acidic GO consistently provided substantial and systematic improvements in bond strength across all saturation states and fabric types, with peak enhancements observed at intermediate dosages (≈0.04-0.06 wt%), whereas GO^n produced only marginal benefits at very low dosage and exhibited pronounced performance degradation at higher contents. The superior performance of GO^a is attributed to its higher density of oxygen-containing functional groups, which promotes stronger physicochemical interactions with the epoxy matrix and the concrete substrate. In contrast, the reduced functionality of GO^n limits its interfacial contribution and increases sensitivity to dispersion-related deficiencies. Based on these findings, GO^a was selected for subsequent HTA evaluation, as it represents the most effective and robust graphene-based modification under control conditions. This selection enables focused assessment of the durability potential of GO in aggressive moisture–temperature environments, while avoiding confounding effects associated with suboptimal interfacial performance observed for GO^n.

4.1.1.3. Nanoclay

Nanoclay was investigated as an epoxy nano-modifier to evaluate the influence of layered silicate structure, surface chemistry, and rheological effects on the bond performance of CFRP-concrete interfaces under control (unaged) conditions. Three sodium montmorillonite nCs with distinct dispersion characteristics and thixotropic efficiencies, nC^B, nC^F, and nC^T, were examined to capture a representative range of nC behaviors. Bond strength results were analyzed as a function of nC dosage, saturation state (under-saturated versus fully saturated), and CFRP fabric type (CCS22 versus CCS11). This comparative framework enables direct assessment of the trade-off between microstructural refinement at low nC

contents and adverse effects associated with increased viscosity and particle agglomeration at higher dosages. The following subsections discuss the dosage-dependent bond performance of each nC and elucidate their distinct interfacial modification mechanisms in unaged CFRP-concrete systems.

1. Bentobrite® 770

Figure 16 illustrates the effect of nC^B sodium montmorillonite nC on the CFRP-concrete bond strength under control (unaged) conditions, considering saturation state and CFRP fabric type. In contrast to GO and nS, nC^B exhibited a distinctly different dosage–performance relationship, characterized by a narrow beneficial dosage window at low content followed by a pronounced deterioration in bond strength at higher dosages. This response highlights the strong sensitivity of the epoxy-CFRP-concrete interface to nC content and dispersion state.

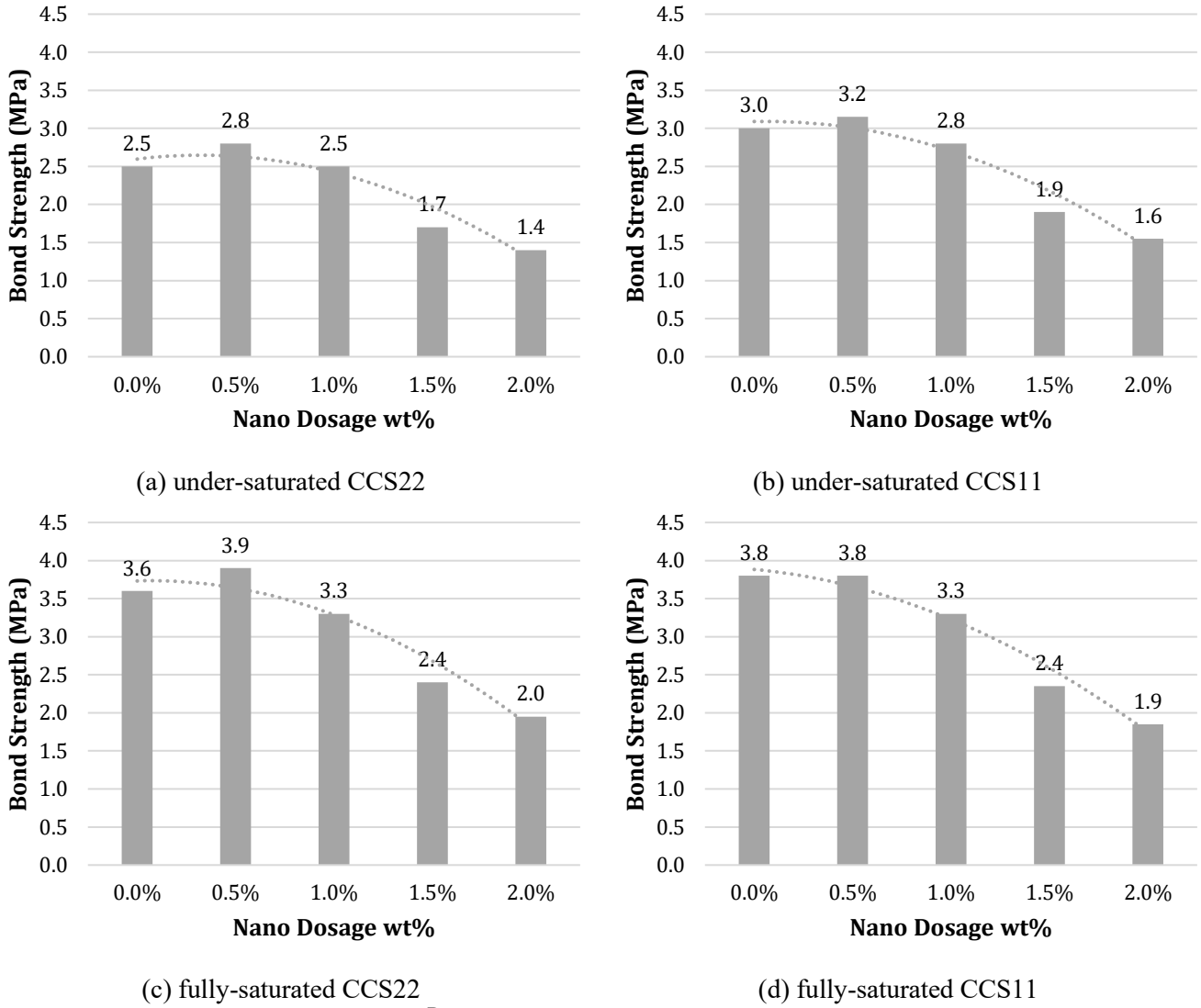

(a) under-saturated CCS22 (b) under-saturated CCS11

(c) fully-saturated CCS22 (d) fully-saturated CCS11

Figure 16. Effect of nC^B modification on CFRP-to-concrete bond strength.

For under-saturated CCS22 specimens (Figure 16a), the baseline bond strength of 2.5 MPa increased modestly to 2.8 MPa at 0.5 wt% nC, corresponding to an improvement of approximately 12%. However,

further increases in nC content led to a rapid decline in bond strength, decreasing to 2.5 MPa at 1.0 wt%, 1.7 MPa at 1.5 wt%, and 1.4 MPa at 2.0 wt%, representing a reduction of approximately 44% relative to the control. A similar but more pronounced trend was observed for under-saturated CCS11 specimens (Figure 16b), where bond strength peaked at 3.2 MPa at 0.5 wt% (≈7% increase) and then dropped sharply to 2.8 MPa, 1.9 MPa, and 1.6 MPa at 1.0 wt%, 1.5 wt%, and 2.0 wt%, respectively. These results indicate that under under-saturated conditions, excessive nC addition severely compromises interfacial integrity.

For fully saturated specimens, higher absolute bond strengths were achieved at low nC dosages; however, the same deterioration trend at elevated contents persisted. In the case of fully saturated CCS22 (Figure 16c), bond strength increased from 3.6 MPa to 3.9 MPa at 0.5 wt% (≈8% improvement), followed by a substantial decrease to 3.3 MPa, 2.4 MPa, and 2.0 MPa at 1.0 wt%, 1.5 wt%, and 2.0 wt%, respectively. Similarly, fully saturated CCS11 specimens (Figure 16d) exhibited a slight enhancement from 3.8 MPa to 3.8 MPa at 0.5 wt%, after which bond strength decreased progressively to 3.3 MPa, 2.4 MPa, and 1.9 MPa as nC dosage increased. Despite the initially higher performance of fully saturated systems, the magnitude of bond degradation at high nC contents remained substantial.

Overall, the control-condition results demonstrate that nC^{B} provides limited bond-strength enhancement only at low dosage (≈0.5 wt%), while higher nC contents are clearly detrimental to CFRP-concrete bond performance. The sharp decline in bond strength beyond the optimal dosage is attributed to the high surface area and strong interparticle attraction of sodium montmorillonite, which can significantly increase epoxy viscosity, hinder effective fiber impregnation, and promote nanoparticle agglomeration. These effects are particularly detrimental to interfacial stress transfer and override any potential microstructural refinement benefits at elevated dosages. The findings identify a narrow performance window for nC^{B} in unaged systems and establish a critical baseline for comparison with other nCs and with durability performance under HTA conditions discussed in subsequent subsections.

2. Polargel® NF

Figure 17 presents the effect of nC^{F} sodium montmorillonite nC on the CFRP-concrete bond strength under control (unaged) conditions, considering both saturation state and CFRP fabric type. Compared to nC^{B}, nC^{F} exhibited a stronger initial enhancement in bond strength at low dosages, followed by a progressive and substantial reduction at higher nC contents. This behavior reflects the high thixotropic efficiency and fine particle size of nC^{F}, which can be beneficial at low dosages but increasingly detrimental as dosage increases.

For under-saturated CCS22 specimens (Figure 17a), the bond strength increased markedly from 2.5 MPa at 0.0 wt% to 3.8 MPa at 0.5 wt%, corresponding to an improvement of approximately 52%. However, further increases in nC dosage led to a steady decline in bond strength, decreasing to 3.2 MPa at 1.0 wt%, 2.2 MPa at 1.5 wt%, and 1.7 MPa at 2.0 wt%, the latter representing a reduction of approximately 32% relative to the control. A similar trend was observed for under-saturated CCS11 specimens (Figure 17b), where bond strength increased from 3.0 MPa to 4.0 MPa at 0.5 wt% (≈33% improvement), followed by decreases to 3.4 MPa, 2.5 MPa, and 2.0 MPa as the dosage increased to 1.0 wt%, 1.5 wt%, and 2.0 wt%, respectively. These results indicate that nC^{F} is highly effective in improving bond performance at low dosages under under-saturated conditions but becomes increasingly detrimental beyond the optimal range.

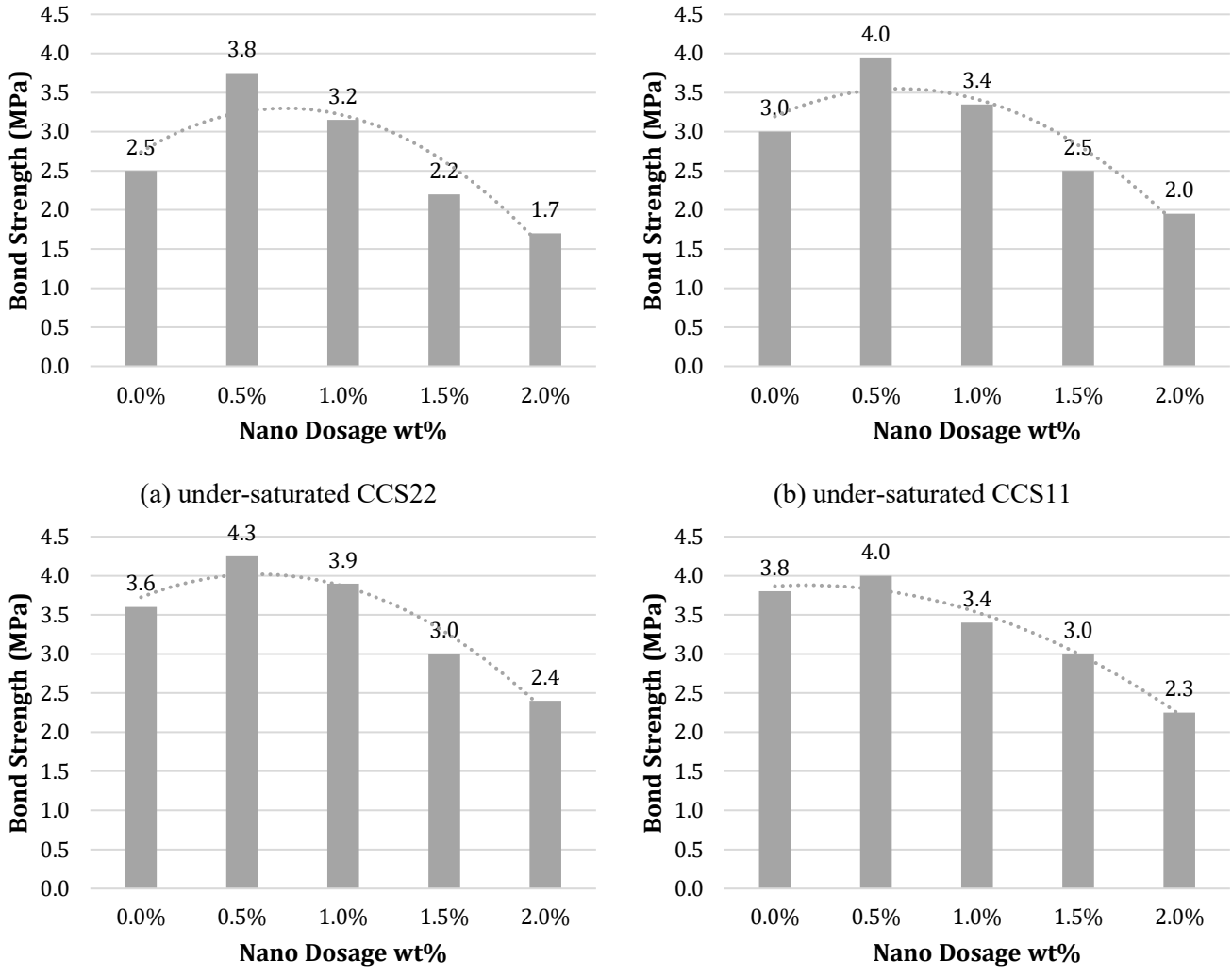

(a) under-saturated CCS22

(b) under-saturated CCS11

(c) fully-saturated CCS22

(d) fully-saturated CCS11

Figure 17. Effect of nC^F modification on CFRP-to-concrete bond strength.

For fully saturated specimens, higher absolute bond strengths were consistently achieved, and the beneficial effect of low nC dosage was further amplified. In the case of fully saturated CCS22 (Figure 17c), bond strength increased from 3.6 MPa at 0.0 wt% to 4.3 MPa at 0.5 wt%, corresponding to an improvement of approximately 19%, before decreasing to 3.9 MPa, 3.0 MPa, and 2.4 MPa at 1.0 wt%, 1.5 wt%, and 2.0 wt%, respectively. Similarly, fully saturated CCS11 specimens (Figure 17d) exhibited an increase from 3.8 MPa to 4.0 MPa at 0.5 wt%, followed by a progressive decline to 3.4 MPa, 3.0 MPa, and 2.3 MPa at higher dosages. Although full saturation mitigated the severity of bond degradation at elevated nC contents, the downward trend remained pronounced.

Overall, the control-condition results demonstrate that nC^F provides substantial bond-strength enhancement at low dosage (≈0.5 wt%), exceeding the improvements observed for nC^B and highlighting its strong interfacial modification capability. However, the rapid deterioration in bond strength beyond the optimal dosage underscores the sensitivity of the epoxy-CFRP-concrete interface to nC-induced increases in viscosity and thixotropy. At higher contents, nC^F likely hinders effective resin impregnation and promotes particle agglomeration, leading to impaired stress transfer and premature interfacial failure.

These findings establish a clear optimal dosage window for nC^F in unaged systems and provide a critical benchmark for comparison with other nCs and with durability performance under HTA conditions in subsequent sections.

3. Polargel® T

Figure 18 illustrates the effect of nC^T sodium montmorillonite nC on the CFRP-concrete bond strength under control (unaged) conditions, considering both saturation state and CFRP fabric type. Similar to the other nCs investigated, nC^T exhibited a nonlinear dosage-dependent response, with bond strength enhancement confined to a low-dosage range and pronounced degradation at higher contents. However, compared with nC^B and nC^F, nC^T showed a moderate enhancement magnitude and a relatively gradual post-peak decline, reflecting its distinct rheological and thixotropic characteristics.

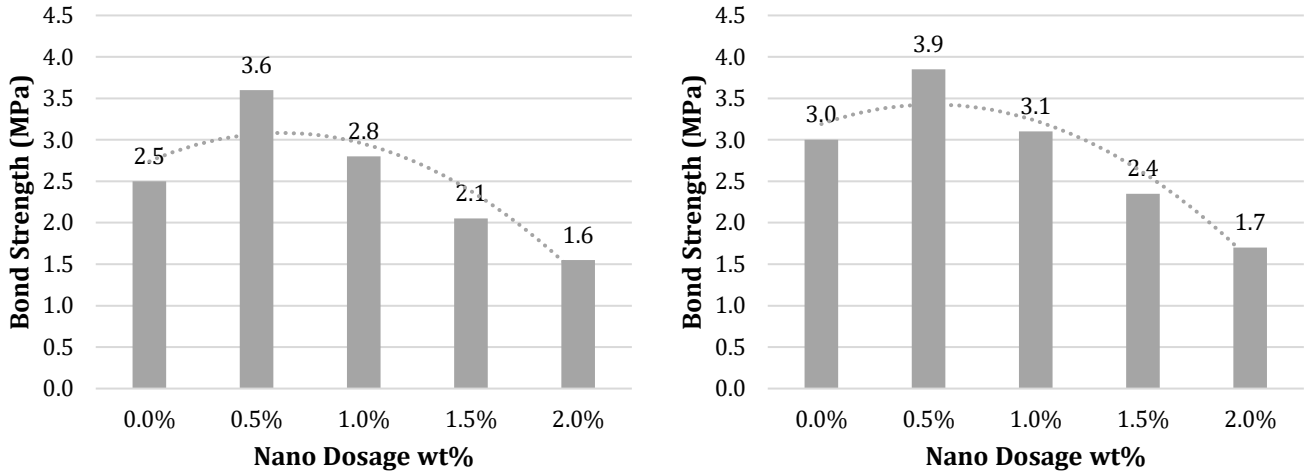

(a) under-saturated CCS22

(b) under-saturated CCS11

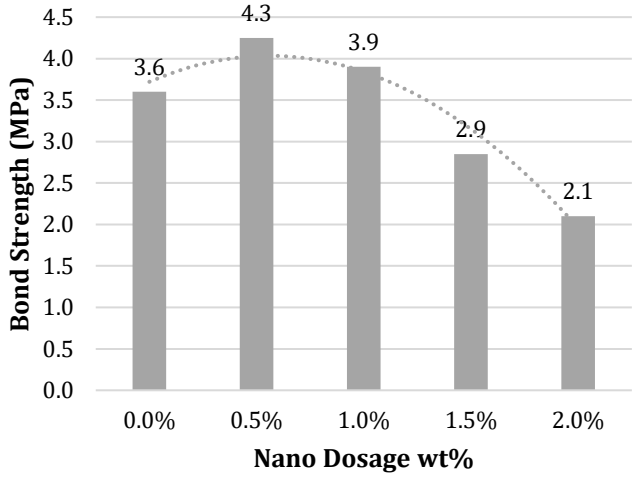

(c) fully-saturated CCS22

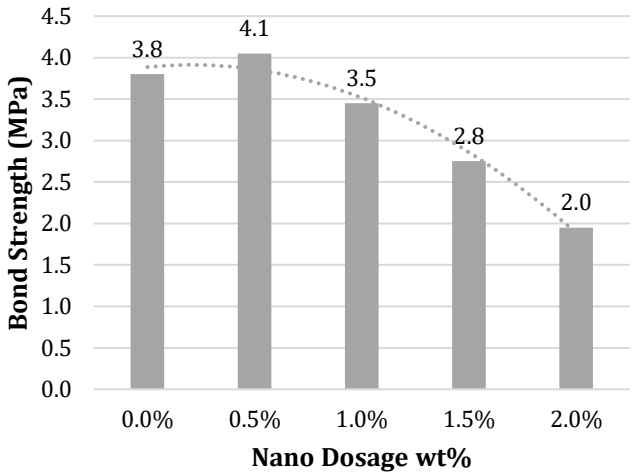

(d) fully-saturated CCS11

Figure 18. Effect of nC^T modification on CFRP-to-concrete bond strength.

For under-saturated CCS22 specimens (Figure 18a), the baseline bond strength of 2.5 MPa increased to 3.6 MPa at 0.5 wt%, corresponding to an improvement of approximately 44%. Beyond this dosage, bond

strength decreased to 2.8 MPa at 1.0 wt%, 2.1 MPa at 1.5 wt%, and 1.6 MPa at 2.0 wt%, representing a reduction of approximately 36% relative to the control. A similar trend was observed for under-saturated CCS11 specimens (Figure 18b), where bond strength increased from 3.0 MPa to 3.9 MPa at 0.5 wt% (≈30% improvement), followed by progressive decreases to 3.1 MPa, 2.4 MPa, and 1.7 MPa as nC dosage increased. These results indicate that, under under-saturated conditions, nC^T significantly improves bond performance at low dosage but rapidly impairs interfacial integrity when overdosed.

For fully saturated specimens, higher absolute bond strengths were achieved, and the beneficial effect of low nC^T content was clearly evident. In the case of fully saturated CCS22 (Figure 18c), bond strength increased from 3.6 MPa to 4.3 MPa at 0.5 wt%, corresponding to an enhancement of approximately 19%, before decreasing to 3.9 MPa, 2.9 MPa, and 2.1 MPa at 1.0 wt%, 1.5 wt%, and 2.0 wt%, respectively. Similarly, fully saturated CCS11 specimens (Figure 18d) exhibited an increase from 3.8 MPa to 4.1 MPa at 0.5 wt%, followed by a decline to 3.5 MPa, 2.8 MPa, and 2.0 MPa at higher dosages. While full saturation delayed the onset of severe degradation, the downward trend at elevated nC contents remained pronounced.

Overall, the control-condition results demonstrate that nC^T provides substantial bond-strength enhancement at low dosage (≈0.5 wt%), comparable to nC^F but with slightly reduced peak gains and a smoother post-peak decline. At higher dosages, however, the excessive thixotropic behavior and viscosity increase associated with nC^T likely hinder effective epoxy impregnation and promote nC agglomeration, leading to impaired stress transfer and premature bond failure. These findings confirm that nC^T, like other nCs, exhibits a narrow optimal dosage window in unaged CFRP-concrete systems and establish a critical baseline for evaluating its durability performance under HTA in subsequent sections.

The control-condition results indicate that the influence of nC on CFRP-concrete bond performance is highly dosage-sensitive and strongly dependent on nC type and rheological behavior. All three sodium montmorillonite nCs, nC^B, nC^F, and nC^T, exhibited measurable bond-strength enhancement at low dosage (≈0.5 wt%), followed by pronounced deterioration at higher contents due to increased epoxy viscosity, thixotropy, and particle agglomeration. Among the nCs evaluated, nC^F consistently provided the largest bond-strength gains under control conditions, achieving substantial improvements across both saturation states and CFRP fabric types, while maintaining higher absolute bond strength than nC^B and nC^T at comparable dosages. nC^B and nC^T, although effective at low dosage, showed either lower peak enhancement or more rapid post-peak degradation. Based on its superior and more consistent performance under control conditions, nC^F was selected for subsequent HTA evaluation. This targeted selection allows assessment of the durability potential of nC-modified epoxy systems while minimizing confounding effects associated with suboptimal rheology or dispersion observed in the other nCs.

4.1.2. Hydrothermal aging

This subsection examines the influence of HTA on the bond durability of nano-modified CFRP-concrete interfaces, focusing on the combined effects of moisture ingress and temperature elevation on interfacial degradation mechanisms. Two conditioning regimes were employed, 28-day room-temperature water immersion (RT-wet) and 14-day elevated-temperature water immersion (hot-wet), to represent service-level exposure and accelerated aging, respectively. Building on the control-condition results presented in Subsection 4.1.1, only the most effective nano-modifiers identified under unaged conditions were advanced to HTA evaluation, allowing targeted assessment of their durability potential. Bond strength responses are analyzed as a function of nano-modifier type and dosage, saturation state (under-saturated

versus fully saturated), and CFRP fabric type (CCS22 versus CCS11). This framework enables direct comparison of nano-modification strategies in mitigating hydrothermal degradation and clarifies the extent to which control-condition performance translates into long-term interfacial stability under aggressive moisture–temperature environments.

4.1.2.1. Nanosilica

Figure 19 presents the effect of nS modification on the CFRP-concrete bond strength after HTA, including 28 days of room-temperature water immersion (RT-wet) and 14 days of elevated-temperature water immersion (hot-wet). Results are shown for under-saturated and fully saturated specimens reinforced with CCS22 and CCS11 fabrics. Compared with the control (unaged) condition, HTA caused a systematic reduction in bond strength for all specimens; however, the dosage-dependent trends observed under control conditions were largely preserved, indicating that nS remained effective in mitigating interfacial degradation under moisture- and temperature-accelerated environments.

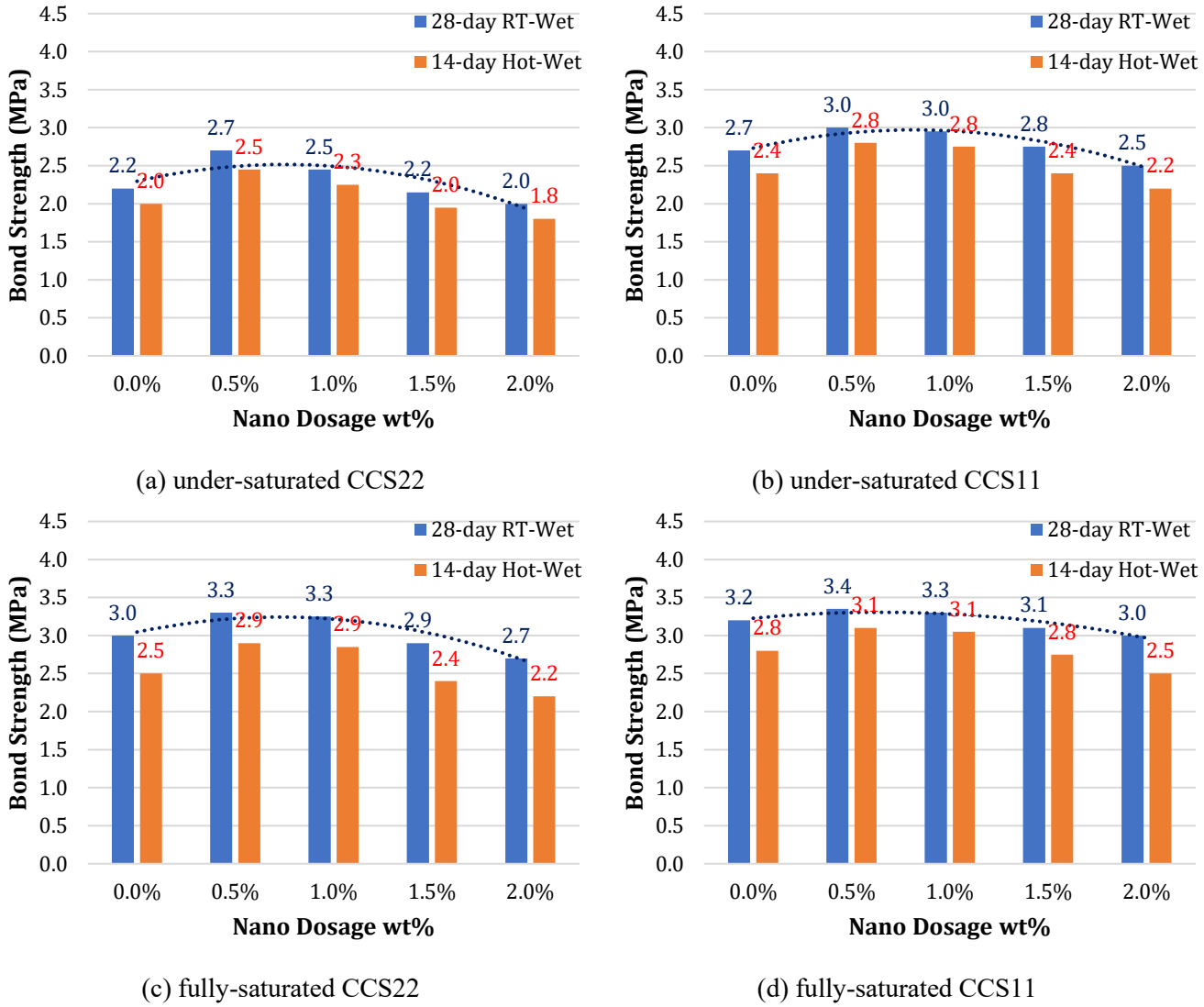

(a) under-saturated CCS22

(b) under-saturated CCS11

(c) fully-saturated CCS22

(d) fully-saturated CCS11

Figure 19. Effect of nS modification on bond strength under HTA.

For under-saturated CCS22 specimens (Figure 19a), the unmodified epoxy system exhibited bond strengths of 2.2 MPa after RT-wet exposure and 2.0 MPa after hot-wet exposure. Incorporation of nS increased bond strength to a maximum of 2.7 MPa (RT-wet) and 2.5 MPa (hot-wet) at 0.5 wt%, corresponding to improvements of approximately 23% and 25%, respectively. At 1.0 wt%, bond strength remained relatively high (2.5 MPa RT-wet; 2.3 MPa hot-wet), while higher dosages resulted in progressive reductions to 2.0 MPa (RT-wet) and 1.8 MPa (hot-wet) at 2.0 wt%. These results demonstrate that nS effectively compensates for HTA-induced degradation at low dosages but becomes less beneficial at elevated contents.

A similar response was observed for under-saturated CCS11 specimens (Figure 19b). The baseline bond strength increased from 2.7 MPa (RT-wet) and 2.4 MPa (hot-wet) to peak values of 3.0 MPa (RT-wet) and 2.8 MPa (hot-wet) at 0.5–1.0 wt% nS, representing improvements of approximately 10–15%. Beyond this dosage range, bond strength declined to 2.5 MPa (RT-wet) and 2.2 MPa (hot-wet) at 2.0 wt%, indicating a diminishing benefit of nS at higher contents under HTA.

For fully saturated specimens, higher absolute bond strengths were consistently achieved, and the beneficial effect of nS under HTA was more pronounced. In the case of fully saturated CCS22 (Figure 19c), bond strength increased from 3.0 MPa (RT-wet) and 2.5 MPa (hot-wet) at 0.0 wt% to 3.3 MPa (RT-wet) and 2.9 MPa (hot-wet) at 0.5–1.0 wt%, corresponding to improvements of approximately 10% and 16%, respectively. Similarly, fully saturated CCS11 specimens (Figure 19d) exhibited peak bond strengths of 3.4 MPa (RT-wet) and 3.1 MPa (hot-wet) at 0.5–1.0 wt% nS, compared to 3.2 MPa and 2.8 MPa for the unmodified system. Although bond strength decreased slightly at higher dosages, nS-modified specimens consistently outperformed the unmodified epoxy system under both HTA regimes.

Overall, the HTA results confirm that nS modification enhances the resistance of the CFRP-concrete interface to hydrothermal degradation, particularly at low to moderate dosages (≈0.5–1.0 wt%). While elevated-temperature immersion caused greater bond deterioration than room-temperature exposure for all specimens, the relative performance ranking among nS dosages remained consistent. These findings indicate that nS contributes to improved interfacial stability under coupled moisture–temperature exposure, likely through microstructural refinement and reduced moisture-induced softening of the epoxy matrix. The effectiveness of nS under HTA provides a critical benchmark for comparison with GO and nC systems discussed in the following subsections.

4.1.2.2. Graphene Oxide

Figure 20 presents the bond strength of GO[a]-modified CFRP-concrete systems after HTA, including 28 days of room-temperature water immersion (RT-wet) and 14 days of elevated-temperature water immersion (hot-wet). Results are shown for under-saturated and fully saturated specimens reinforced with CCS22 and CCS11 fabrics. Relative to the unmodified epoxy systems, GO[a] modification consistently mitigated HTA-induced bond degradation, with performance strongly dependent on dosage and saturation state. Across all configurations, the beneficial dosage window identified under control conditions (≈0.04-0.06 wt%) was preserved under HTA, indicating robust interfacial stabilization by GO[a].

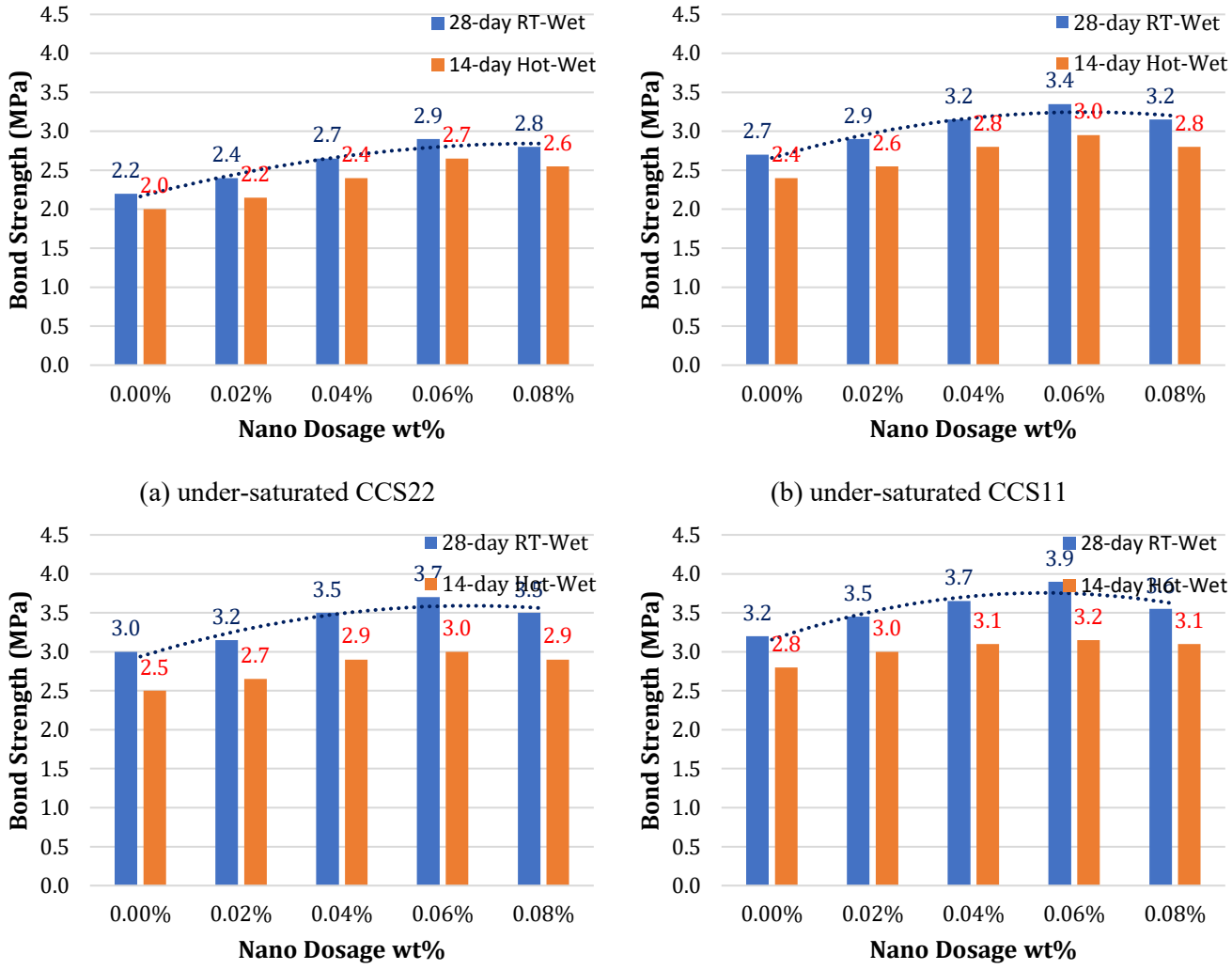

(a) under-saturated CCS22

(b) under-saturated CCS11

(c) fully-saturated CCS22

(d) fully-saturated CCS11

Figure 20. Effect of GO modification on bond strength under HTA.

For under-saturated CCS22 specimens (Figure 20a), the unmodified system exhibited bond strengths of 2.2 MPa (RT-wet) and 2.0 MPa (hot-wet). With increasing GO[a] dosage, bond strength increased monotonically, reaching 2.9 MPa (RT-wet) and 2.7 MPa (hot-wet) at 0.06 wt%, corresponding to improvements of approximately 32% and 35%, respectively. A slight reduction was observed at 0.08 wt%, although bond strength remained higher than that of the unmodified control. Similar trends were observed for under-saturated CCS11 specimens (Figure 20b), where bond strength increased from 2.7 MPa (RT-wet) and 2.4 MPa (hot-wet) at 0.0 wt% to peak values of 3.4 MPa (RT-wet) and 3.0 MPa (hot-wet) at 0.06 wt%, representing improvements of approximately 26% and 25%, respectively.

For fully saturated specimens, higher absolute bond strengths were achieved and the stabilizing effect of GO[a] under HTA was even more pronounced. In the case of fully saturated CCS22 (Figure 20c), bond strength increased from 3.0 MPa (RT-wet) and 2.5 MPa (hot-wet) at 0.0 wt% to 3.7 MPa (RT-wet) and 3.0 MPa (hot-wet) at 0.06 wt%, corresponding to enhancements of approximately 23% and 20%, respectively. Similarly, fully saturated CCS11 specimens (Figure 20d) exhibited increases from 3.2 MPa (RT-wet) and 2.8 MPa (hot-wet) to 3.9 MPa (RT-wet) and 3.2 MPa (hot-wet) at 0.06 wt%, representing

improvements of approximately 22% and 14%. In all cases, elevated-temperature immersion caused greater bond deterioration than room-temperature exposure; however, GO^a-modified systems consistently retained higher bond strength than the unmodified epoxy systems.

Overall, the HTA results confirm that GO^a provides effective and durable enhancement of CFRP-concrete bond performance under coupled moisture–temperature exposure, with an optimal dosage centered around 0.04-0.06 wt%. The preservation of the optimal dosage range under HTA, together with the substantial mitigation of bond degradation relative to unmodified systems, highlights the strong resistance of GO^a-modified interfaces to hydrothermal damage. These findings demonstrate the potential of GO^a as a robust nano-modifier for improving the long-term durability of externally bonded CFRP systems in aggressive service environments and provide a direct comparison point for nS- and nC-modified systems discussed in adjacent subsections.

4.1.2.3. Nanoclay

Figure 21 presents the bond strength of nC^F-modified CFRP-concrete systems after HTA, including 28 days of room-temperature water immersion (RT-wet) and 14 days of elevated-temperature water immersion (hot-wet). Results are shown for under-saturated and fully saturated specimens reinforced with CCS22 and CCS11 fabrics. Relative to the unmodified epoxy system, nC^F provided partial mitigation of HTA-induced bond degradation at low dosage, while higher nC contents led to accelerated performance loss, consistent with the strong rheological sensitivity observed under control conditions.

For under-saturated CCS22 specimens (Figure 21a), the unmodified system exhibited bond strengths of 2.2 MPa (RT-wet) and 2.0 MPa (hot-wet). Incorporation of 0.5 wt% nC^F increased bond strength to 3.4 MPa (RT-wet) and 3.1 MPa (hot-wet), corresponding to improvements of approximately 55% and 55%, respectively. However, further increases in nC dosage resulted in progressive degradation, with bond strength decreasing to 2.8 MPa / 2.6 MPa at 1.0 wt%, 2.0 MPa / 1.8 MPa at 1.5 wt%, and 1.5 MPa / 1.4 MPa at 2.0 wt% (RT-wet / hot-wet). This sharp decline highlights the sensitivity of under-saturated interfaces to excessive nC content under hydrothermal exposure.

A similar trend was observed for under-saturated CCS11 specimens (Figure 21b). Bond strength increased from 2.7 MPa (RT-wet) and 2.4 MPa (hot-wet) at 0.0 wt% to peak values of 3.6 MPa (RT-wet) and 3.2 MPa (hot-wet) at 0.5 wt%, representing improvements of approximately 33%. Beyond this dosage, bond strength decreased steadily to 3.1 MPa / 2.7 MPa at 1.0 wt%, 2.3 MPa / 2.0 MPa at 1.5 wt%, and 1.8 MPa / 1.6 MPa at 2.0 wt%, indicating diminishing durability at elevated nC contents.

For fully saturated specimens, higher absolute bond strengths were achieved, and the beneficial effect of low nC^F dosage was retained under HTA. In the case of fully saturated CCS22 (Figure 21c), bond strength increased from 3.0 MPa (RT-wet) and 2.5 MPa (hot-wet) to 3.7 MPa (RT-wet) and 3.1 MPa (hot-wet) at 0.5 wt%, corresponding to improvements of approximately 23% and 24%, respectively. However, at higher dosages, bond strength declined to 3.6 MPa / 3.0 MPa at 1.0 wt%, 2.5 MPa / 2.1 MPa at 1.5 wt%, and 2.0 MPa / 1.7 MPa at 2.0 wt%. A comparable response was observed for fully saturated CCS11 specimens (Figure 21d), where bond strength peaked at 3.4 MPa (RT-wet) and 3.0 MPa (hot-wet) at 0.5 wt%, before decreasing to 2.9 MPa / 2.5 MPa, 2.5 MPa / 2.2 MPa, and 2.0 MPa / 1.7 MPa with increasing nC dosage.

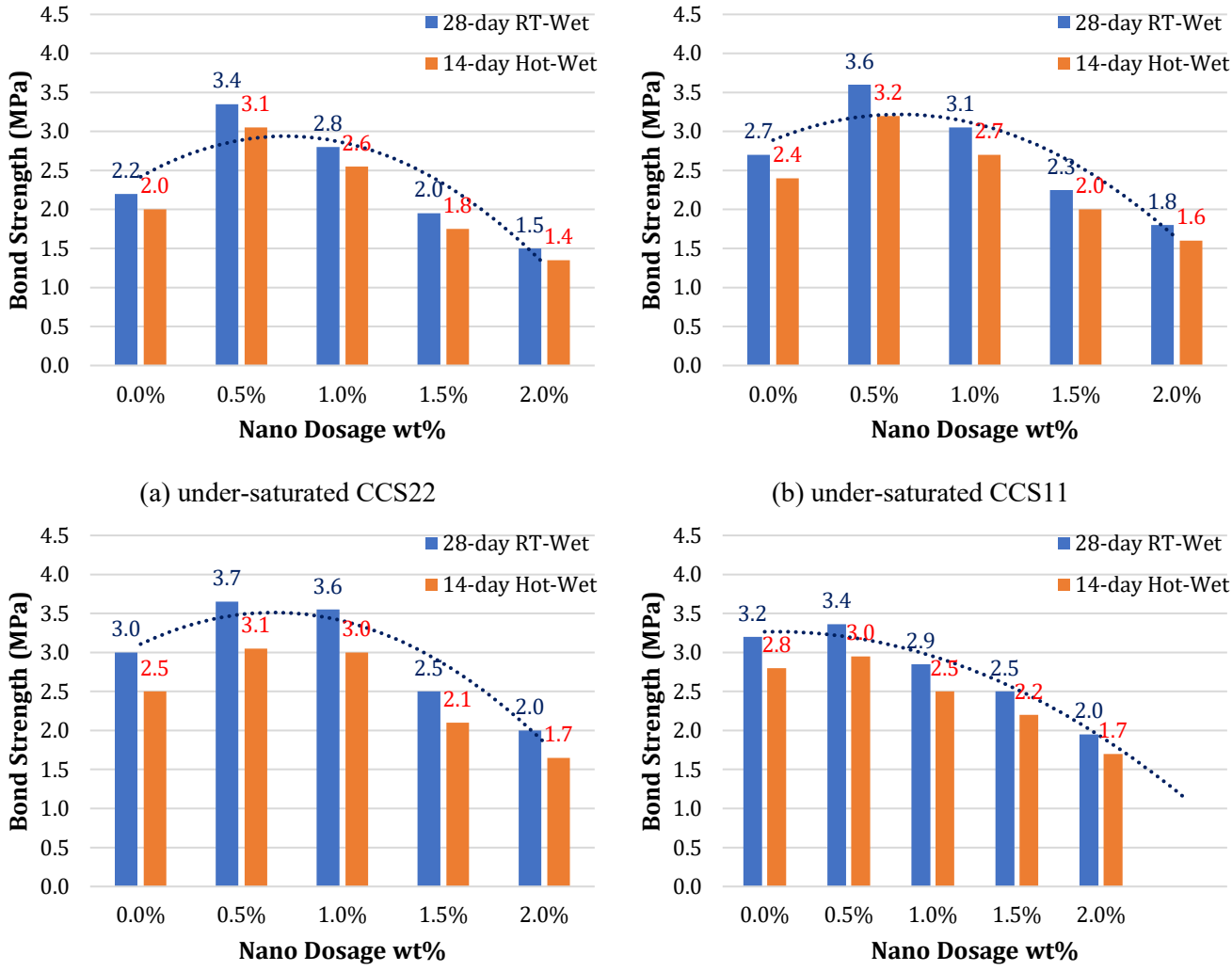

(a) under-saturated CCS22

(b) under-saturated CCS11

(c) fully-saturated CCS22

(d) fully-saturated CCS11

Figure 21. Effect of nC modification on bond strength under HTA.

Overall, the HTA results indicate that nC^F provides effective mitigation of hydrothermal bond degradation only within a narrow low-dosage window (≈0.5 wt%), beyond which bond performance deteriorates rapidly. While nC^F significantly enhances bond strength at optimal dosage—even under elevated-temperature water immersion—the pronounced loss at higher contents underscores the dominant role of nC-induced viscosity increase, thixotropy, and dispersion instability under moisture–temperature coupling. Compared with nS and GO^a, the durability window for nC modification under HTA is considerably narrower, highlighting the need for careful dosage control when nCs are employed for long-term durability enhancement of CFRP-concrete interfaces.

The results presented in Subsections 4.1.1 and 4.1.2 demonstrate that nano-modification of the epoxy adhesive can substantially improve CFRP-concrete bond durability, provided that the nano-modifier type and dosage are carefully optimized. Under control conditions, nS, GO, and nC each exhibited distinct dosage-dependent trends, with bond-strength enhancement confined to a narrow optimal range and deterioration occurring at higher contents due to agglomeration, increased viscosity, or impaired resin impregnation. When subjected to HTA, bond degradation was observed for all systems, particularly under

elevated-temperature immersion, yet selected nano-modified configurations retained superior bond performance relative to the unmodified epoxy. Among all nano-modifiers evaluated, nC-modified systems, particularly the best-performing nC at its optimal dosage, exhibited the most consistent bond-strength enhancement and retention across saturation states and HTA conditions. Based on this superior and robust bond-durability performance, nC was selected as the sole nano-modification strategy for subsequent evaluation of compressive performance in Section 4.2, enabling focused investigation of how enhanced interfacial stability influences the mechanical behavior of CFRP-confined concrete under structural loading.

4.2. Compressive Performance

This section evaluates the compressive behavior and damage evolution of concrete specimens subjected to F/T cycling in a 3 wt% NaCl solution, with emphasis on the influence of CFRP confinement and nC-modified epoxy adhesives. Compressive strength, MoE, failure modes, and associated changes in mass, geometry, and transport-related properties were examined for unwrapped, CFRP-wrapped, and nC-modified CFRP-confined concrete, including both normal and pre-aged substrates. By integrating mechanical performance with transport behavior and microstructural characterization, this section provides a comprehensive assessment of how interfacial modification and confinement efficiency govern the resistance of concrete to coupled environmental and mechanical deterioration.

4.2.1. Mechanical properties and failure mode

This subsection examines the evolution of the mechanical response and damage characteristics of the concrete specimens subjected to F/T cycling in a 3 wt% NaCl solution. The compressive strength, MoE (derived from the linear portion of the stress–strain response), failure modes, and changes in mass and specimen geometry were evaluated for unwrapped, CFRP-wrapped, and nC-modified CFRP-wrapped concrete, including both normal and pre-aged substrates. By jointly analyzing strength degradation, stiffness loss, surface deterioration, and failure mechanisms, this section provides an integrated assessment of how CFRP confinement and nano-modification influence the mechanical integrity and damage progression of concrete under coupled environmental and mechanical loading. The results presented in the following subsections elucidate the relationships between interfacial durability, confinement efficiency, and macroscopic mechanical performance.

4.2.1.1. Strength enhancement and degradation

Figure 22 presents the evolution of compressive strength of the different concrete specimens as a function of F/T cycles in a 3 wt% NaCl solution. The unwrapped REF exhibited a short-term increase in compressive strength during the early stages of exposure, rising from 61.9 MPa to 71.1 MPa within the first 15 F/T cycles. This initial strength gain is commonly attributed to continued cement hydration and pore refinement under intermittent moisture exposure. However, beyond this early stage, the REF specimens experienced a steady deterioration in compressive strength as F/T cycling progressed. A 20% strength loss was reached at approximately 175 cycles, followed by rapid structural degradation, such that the specimens were unable to sustain compressive load beyond 200 cycles, accompanied by more than 50% mass loss. Similar early-age strength gains followed by progressive degradation have been reported in the literature; for example, Fan et al. (2015) observed a 50% strength loss at approximately 125 F/T cycles, with differences attributed to variations in concrete composition, freezing rate, and cycle duration.

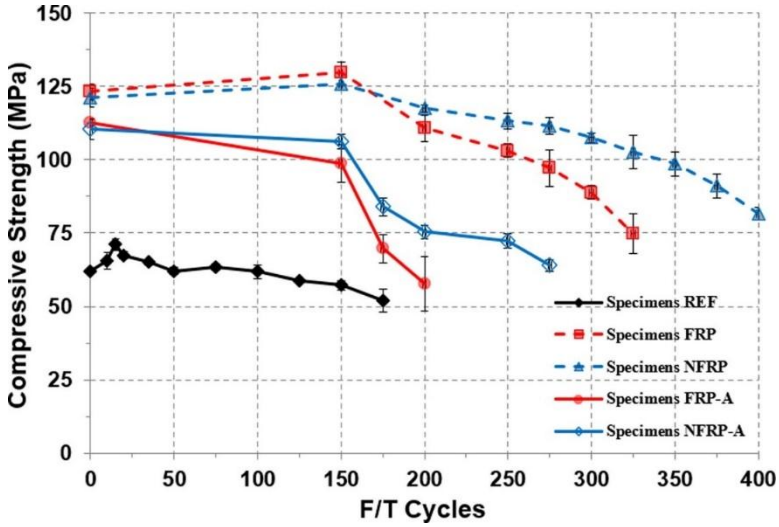

Figure 22. Compression strength of different samples at selected F/T cycles.

CFRP confinement substantially altered the degradation behavior of both normal and pre-aged concrete. Prior to any F/T or salt exposure, CFRP wrapping increased the compressive strength of normal concrete from 61.9 MPa to 123.2 MPa, corresponding to a 99% enhancement, while pre-aged concrete increased to 112.5 MPa, an 82% improvement relative to the unwrapped reference. This marked strengthening effect is attributed to the confinement provided by the externally bonded CFRP, which restrains lateral dilation of the concrete core and delays crack propagation. The high tensile strength (4600 MPa) and MoE (260 GPa) of the carbon fabric enable effective mobilization of confining stresses, resulting in significant strength enhancement (Spoelstra Marijn & Monti, 1999).

Under prolonged F/T exposure in NaCl solution, CFRP-confined specimens exhibited a much slower rate of compressive strength degradation compared with the REF concrete. Moreover, incorporation of 1.5 wt% montmorillonite nC into the epoxy adhesive further improved the durability of the CFRP-concrete composite. After 200 F/T cycles, nC-modified FRP-confined concrete (nFRP) exhibited compressive strengths that were approximately 6% higher for normal concrete and 39% higher for pre-aged concrete compared with their unmodified FRPC counterparts. This beneficial effect became increasingly pronounced with continued cycling: from 200 to 325 F/T cycles, the compressive strength of nC-modified FRPC specimens decreased by only ~13%, whereas unmodified FRPC specimens exhibited a reduction of approximately 32% over the same interval.

The enhanced compressive performance of nC-modified systems is attributed to improved interfacial integrity and epoxy microstructure. Previous studies have shown that nanomodification of polymer matrices can significantly enhance bond strength at the FRP-epoxy-concrete interface, thereby delaying interfacial debonding and improving load transfer efficiency under cyclic environmental loading (Irshidat & Al-Saleh, 2016). In the present study, optical microscopy (Figure 23) reveals that the nC-modified epoxy exhibits a more homogeneous and refined microstructure with reduced microcrack density, whereas the unmodified epoxy displays a network of interconnected microcracks. These microcracks act as preferential pathways for moisture ingress and stress concentration during F/T cycling. The refined microstructure of the nC-modified epoxy enhances adhesive stiffness, crack-bridging capacity, and stress transfer efficiency at the FRP-concrete interface, providing direct mechanistic support for the superior compressive strength retention of nC-modified FRP-confined concrete observed in Figure 22 (Lau et al., 2006).

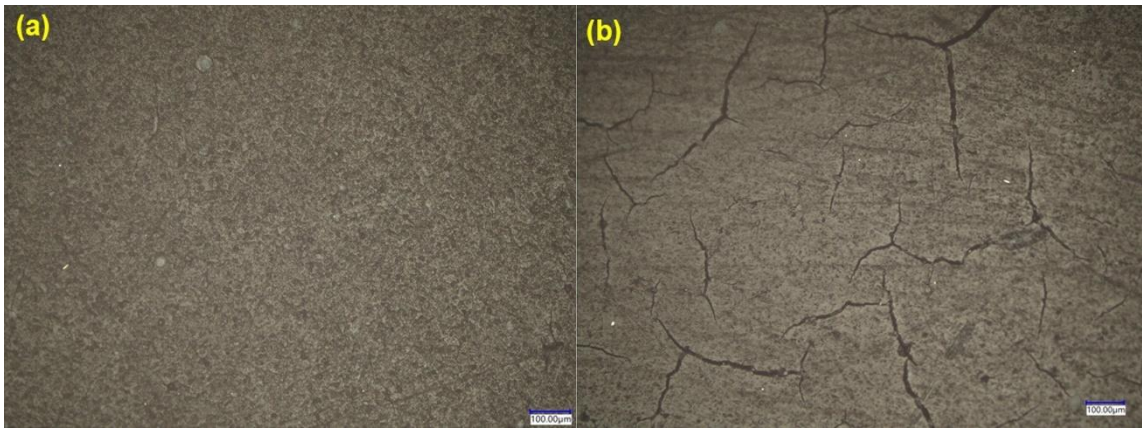

(a) nano-modified epoxy resin (b) unmodified (original) epoxy resin

Figure 23. Optical microscopy characterization of epoxy resin microstructure.

4.2.1.2. Failure modes

Figure 24 illustrates the representative failure modes observed for the different concrete specimens following compressive strength testing. For the unwrapped REF, the dominant failure mechanism was concrete crushing, characterized by longitudinal splitting and surface spalling along the height of the cylinder (Figure 24a). In several REF specimens, eccentric compression behavior was also observed, where localized crushing occurred on one side of the cylinder while tensile cracking developed on the opposite side (Figure 24b). This asymmetric failure pattern is attributed to nonuniform internal damage induced by F/T cycling in the NaCl environment, which can lead to heterogeneous stiffness degradation due to the random distribution of air voids and coarse aggregates within the concrete matrix. Such nonuniformity promotes uneven stress distribution under axial loading and facilitates eccentric failure.

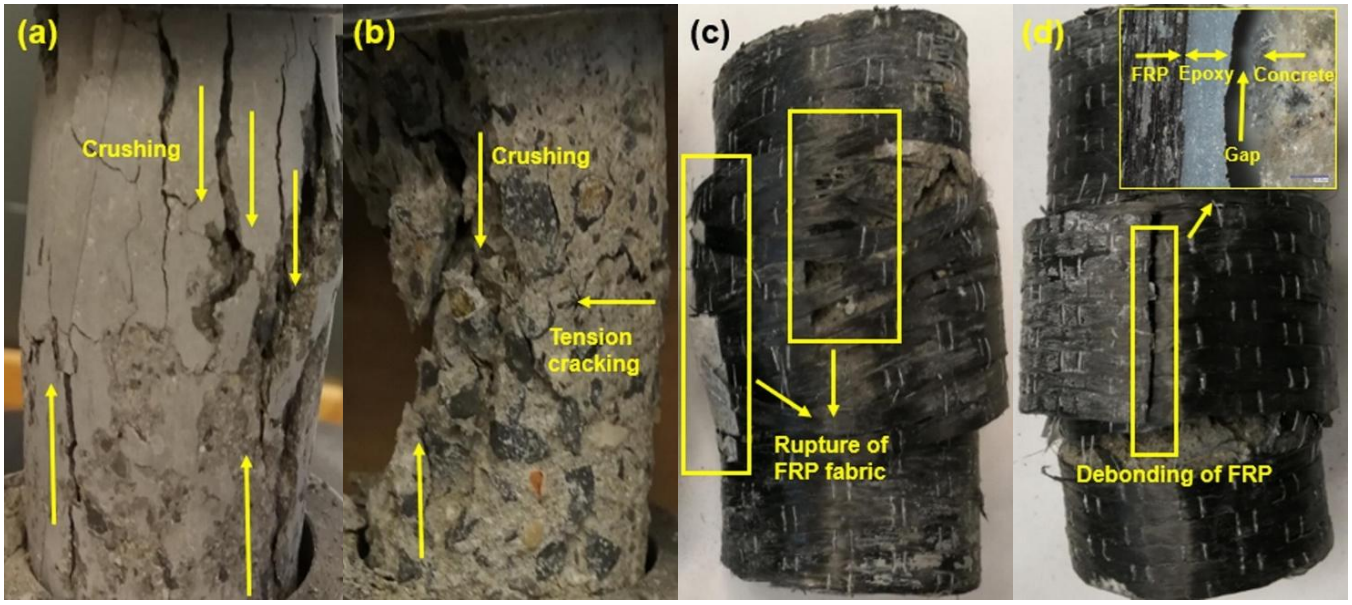

(a) concrete crushing (b) eccentric compression of concrete (c) rupture of carbon fiber fabric (d) debonding of carbon fiber fabric

Figure 24. Representative failure modes observed during mechanical testing.

CFRP confinement significantly altered the failure characteristics of the concrete cylinders. In addition to concrete crushing, two CFRP-related failure modes were identified: rupture of the carbon fiber fabric (Figure 24c) and interfacial debonding of the CFRP laminate, particularly at the overlap region (Figure 24d). These failures were often accompanied by a sudden release of stored elastic energy, manifested as an audible explosive sound at peak load. Compared with the REF specimens, CFRP-wrapped cylinders exhibited more severe crushing of the concrete core, indicating that the externally bonded CFRP effectively restrained lateral dilation and enabled the concrete to sustain higher compressive stresses prior to failure. In this confined state, the concrete and CFRP acted compositely, allowing the CFRP to carry tensile stresses generated by concrete dilation until either fiber rupture or interfacial debonding occurred. Distinct differences were observed between CFRP-wrapped normal concrete and CFRP-wrapped pre-aged concrete (FRP-A). While fiber rupture was commonly observed in CFRP-confined normal concrete, end debonding became the dominant failure mode for FRP-A specimens after prolonged F/T exposure, particularly beyond 200 cycles in 3 wt% NaCl solution. This behavior is attributed to the reduced mechanical integrity of the pre-aged concrete substrate, which is more susceptible to localized crushing and cracking under compressive load. Once local damage initiates near the specimen ends—where CFRP confinement is inherently less effective—the stress concentration accelerates interfacial separation between the CFRP, epoxy adhesive, and concrete substrate. These observations are consistent with the compressive strength results presented in Figure 22 and highlight the critical role of substrate condition and interfacial integrity in governing the failure mechanisms of CFRP-confined concrete under combined environmental and mechanical loading.

4.2.1.3. Mass and dimensional changes

In addition to the compressive strength enhancement discussed in Subsection 4.2.1.1 (Figure 22), the protective role of CFRP confinement is further evidenced by the temporal evolution of mass loss and geometric changes of the concrete cylinders subjected to F/T cycling in a 3 wt% NaCl solution (Figure 25). As F/T exposure progressed, all specimens exhibited increasing mass loss (Figure 25a) and changes in the L/D ratio (Figure 25b), primarily due to progressive cracking, surface scaling, and detachment of paste and aggregate. These degradation mechanisms are attributed to the combined effects of internal damage induced by F/T cycling (Farnam et al., 2014) and chemical attack associated with chloride exposure (Xie et al., 2017).

The unwrapped REF experienced the most severe deterioration. Its mass loss increased rapidly with the number of F/T cycles, reaching approximately 4.9 kg/m² (≈20%), 7.7 kg/m² (≈30%), and 13.9 kg/m² (≈55%) after 150, 175, and 200 cycles, respectively. The extensive surface scaling and material loss observed for the REF specimens are illustrated in Figure 25c. Similar trends have been reported in the literature; for example, Liu and Hansen documented mass losses of 2.8 kg/m², 3.6 kg/m², and a predicted 4.4 kg/m² after 150, 175, and 200 F/T cycles in a 3% NaCl solution, respectively (Liu & Hansen, 2016). The higher mass loss observed in the present study is likely attributable to differences in concrete mix design and strength level, as well as variations in F/T cycling parameters.

In contrast, CFRP confinement substantially mitigated surface deterioration and material loss. For all CFRP-wrapped specimens, the maximum mass loss remained below 20%, even at advanced stages of F/T exposure, and visible scaling was largely confined to localized regions near the specimen ends (Figure 25d). When the REF specimens failed at approximately 200 cycles, the mass loss of CFRP-wrapped cylinders was typically an order of magnitude lower (≈10% or less) than that of the unwrapped concrete.

Incorporation of nC into the epoxy adhesive provided a modest additional reduction in mass loss and L/D variation for the wrapped specimens, although these differences were not always statistically significant. Nevertheless, the overall trend indicates that nano-modified CFRP systems offered slightly improved resistance to surface degradation under coupled F/T-salt exposure.

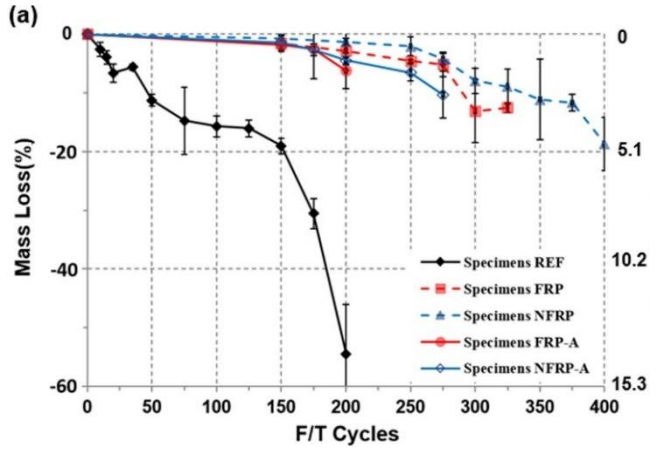

(a) mass loss of different samples at selected F/T cycles

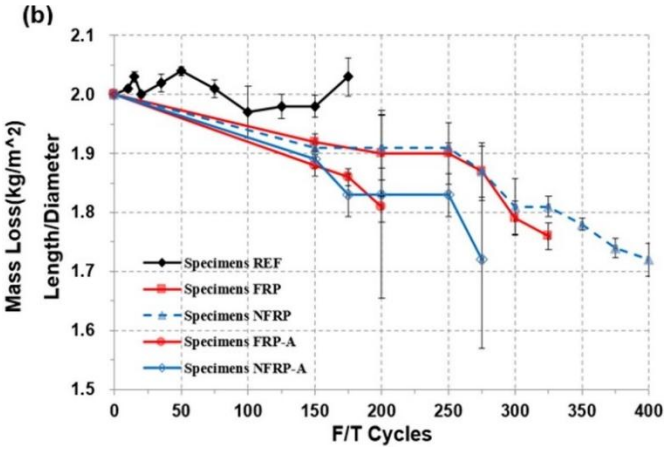

(b) L/D ratio of different samples at selected F/T cycles

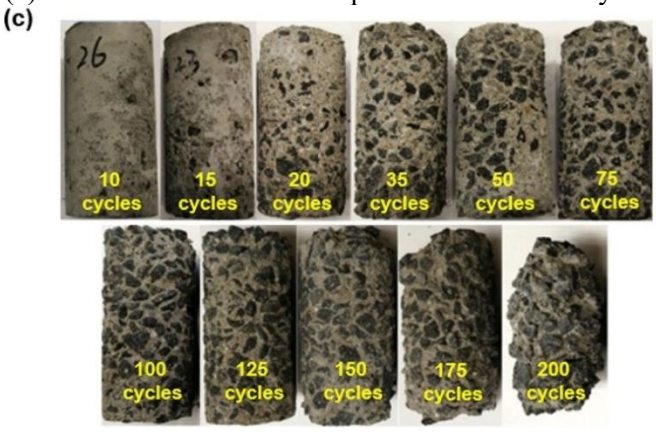

(c) representative REF specimens at selected F/T cycles

(d) surface scaling of CFRP-concrete composites induced by F/T-NaCl exposure

Figure 25. F/T-induced deterioration of concrete and CFRP-concrete composite specimens.

Changes in specimen geometry further highlight the distinct degradation mechanisms between unwrapped and CFRP-confined concrete. The L/D ratio of REF specimens exhibited relatively minor variation throughout F/T cycling (Figure 25b), as both length and diameter decreased proportionally due to uniform surface scaling. In contrast, CFRP-wrapped specimens showed more noticeable changes in L/D ratio, primarily driven by axial shortening associated with end damage and localized crushing, while the diameter remained largely unchanged due to the restraining effect of the CFRP jacket. These observations confirm that CFRP confinement effectively suppresses radial scaling and lateral expansion, thereby altering the damage pattern from uniform surface loss to more localized end-region deterioration.

Overall, the mass-loss and dimensional-change results provide complementary evidence to the compressive strength data, demonstrating that CFRP confinement, particularly when combined with nC-modified epoxy, significantly reduces F/T- and chloride-induced surface deterioration. This reduction in material loss and geometric instability contributes directly to the improved mechanical performance and durability of CFRP-confined concrete under aggressive environmental conditions.

4.2.1.4. Elastic modulus evolution

In addition to the improvements in compressive strength (Figure 22) and the reduction in surface scaling and mass loss (Figure 25), the effectiveness of CFRP confinement is further demonstrated by the evolution of the MoE of the concrete cylinders subjected to F/T cycling in a 3 wt% NaCl solution (Figure 26). With increasing F/T cycles, all specimens exhibited a progressive reduction in MoE, reflecting the accumulation of internal microcracking, stiffness degradation, and surface damage induced by the aggressive environment. Compared with compressive strength and mass loss, the MoE proved to be a more sensitive indicator of material deterioration, responding earlier and more sharply to F/T-induced damage.

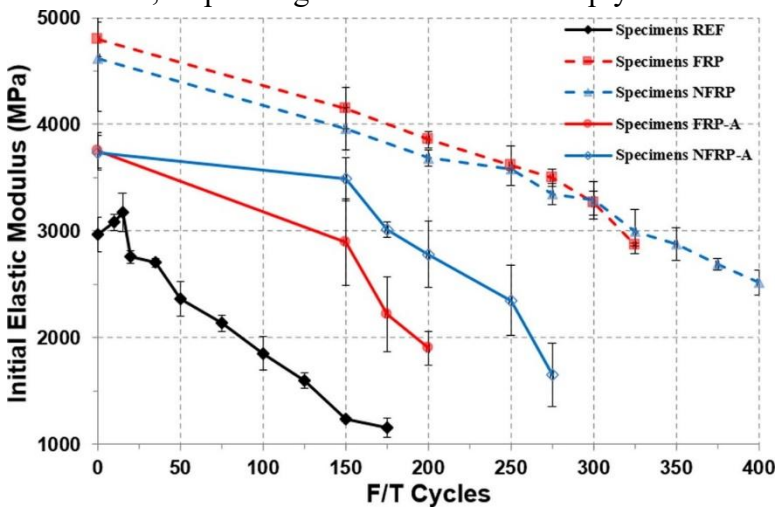

Figure 26. MoE of different samples after selected of F/T cycles.

For the unwrapped REF, a slight increase in MoE of approximately 7.0% was observed during the first 15 F/T cycles, which is attributed to continued cement hydration and short-term densification of the microstructure under intermittent moisture exposure. Beyond this initial stage, the MoE decreased rapidly and almost linearly with continued cycling. After 150 F/T cycles, the MoE of the REF specimens had declined by approximately 60%, in good agreement with the F/T-induced MoE degradation model proposed by Zhang et al. (2017), who reported a predicted MoE reduction of 56.2% after 175 cycles. The minor discrepancy between the two studies is likely associated with differences in concrete mix design, strength level, and F/T cycling parameters.

CFRP confinement markedly mitigated stiffness degradation for both normal and pre-aged concrete. After 150 F/T cycles, the MoE loss was limited to approximately 13.5% for FRP, 14.3% for nFRP, 22.9% for FRP-A, and only 6.6% for nFRP-A, highlighting the protective role of the CFRP jacket. The epoxy adhesive and carbon fabric acted as an effective barrier to water and chloride ingress, thereby reducing internal damage and preserving stiffness of the concrete core. These results corroborate the mass-loss and strength-retention trends discussed earlier, confirming that CFRP confinement significantly delays F/T- and salt-induced deterioration.

As F/T exposure progressed beyond 150 cycles, differences between normal and pre-aged concrete became more pronounced. At 200 F/T cycles, the MoE of FRP-confined normal concrete degraded more slowly than that of FRP-A specimens, indicating that pre-existing damage in the aged substrate accelerates stiffness loss under cyclic environmental loading. Notably, the MoE of FRP-A specimens decreased by approximately 50% at 200 cycles, whereas the corresponding reduction for nC-modified FRP-A (nFRP-A) specimens was limited to about 26%. This substantial contrast demonstrates that nC modification of

the epoxy adhesive significantly enhances stiffness retention in CFRP-confined pre-aged concrete, likely by improving interfacial integrity and reducing microcrack propagation under repeated F/T action. In comparison, the differences between FRP and nFRP specimens for normal concrete were less pronounced, suggesting that nano-modification plays a more critical role when the substrate is already damaged.
Overall, the MoE results provide strong complementary evidence to the compressive strength and mass-loss data, illustrating that CFRP confinement, particularly when combined with nC-modified epoxy, effectively preserves the stiffness of concrete under severe F/T-salt exposure. The pronounced sensitivity of MoE to environmental damage further underscores its value as a key parameter for evaluating the durability and long-term performance of FRP-strengthened concrete systems.

4.2.2. Transport and correlation analyses

This subsection examines the evolution of transport properties of CFRP-confined concrete subjected to F/T cycling in a 3 wt% NaCl solution and explores their quantitative relationship with mechanical performance degradation. Gas permeability and water absorption behavior were evaluated to characterize the development of transport pathways associated with microcracking, interfacial deterioration, and surface scaling. In addition, regression-based correlation analyses were performed using normalized parameters to elucidate the coupling between transport properties and mechanical indicators, including compressive strength and MoE. By integrating transport measurements with mechanical response, this subsection provides mechanistic insight into how environmental damage progression governs both durability-related transport behavior and structural performance of CFRP-strengthened concrete systems.

4.2.2.1. Changes in gas permeability

Figure 27 presents the gas permeability behavior of the different concrete specimens at selected numbers of F/T cycles, expressed in terms of the rate of gas mass loss, which serves as an effective indicator of interfacial transport properties for gaseous phases. Prior to F/T exposure, all CFRP-wrapped specimens exhibited substantially lower gas permeability than the unwrapped REF. This reduction reflects the barrier effect provided by the epoxy adhesive and carbon fabric, which limit the ingress of gases such as oxygen, carbon dioxide, and moisture, thereby contributing to improved durability and extended service life of the concrete substrate.

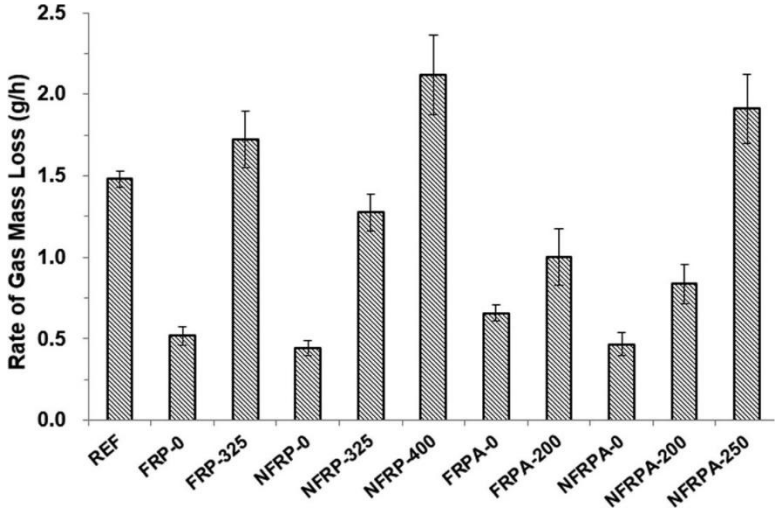

Figure 27. Rate of gas mass loss of different samples after selected number of F/T cycles.

With increasing numbers of F/T cycles in the 3 wt% NaCl solution, the gas permeability of all specimens increased progressively (Figure 27). This trend is attributed to the accumulation of damage at the CFRP-concrete interface, including microcracking, coarsening of the interfacial microstructure, and partial debonding, which create preferential pathways for gas transport. These damage mechanisms are consistent with the microstructural observations discussed in later sections and align with the deterioration trends observed in compressive strength, MoE, and mass loss.

Nano-modification of the epoxy adhesive significantly mitigated gas transport for both normal and pre-aged concrete specimens. Before F/T cycling, the nC-modified CFRP specimens (nFRP-0) exhibited gas permeability rates approximately 15% lower than those of the unmodified CFRP specimens (FRP-0). A more pronounced reduction of approximately 29% was observed for the pre-aged nC-modified specimens (nFRP-A-0) compared with their unmodified counterparts (FRP-A-0), highlighting the enhanced sealing effect of nano-modification on damaged substrates. After F/T exposure, the same beneficial trend persisted. For the nFRP-A specimens, the gas mass loss rate was approximately 16% lower than that of FRP-A after 200 F/T cycles, and this reduction increased to approximately 26% after 325 cycles, demonstrating the increasing effectiveness of nC modification as interfacial damage accumulates.

The observed reduction in gas permeability due to nC modification is consistent with findings reported in the literature. Guo et al. (2021) showed that admixing nano-additives (TiO_2 and graphene) into epoxy coatings slightly reduced gas permeability, which was attributed to densification of the polymer microstructure. Similarly, Li et al. (2018) reported a substantial decrease in gas permeability of a siloxane-treated cement paste after incorporation of nS, ascribed to refinement and densification of the surface layer. In the present study, the reduced gas transport in nC-modified systems is attributed to improved epoxy microstructure, reduced microcrack connectivity, and enhanced interfacial integrity, all of which restrict gas diffusion pathways.

Overall, the gas permeability results complement the mechanical and mass-loss data, demonstrating that CFRP confinement, particularly when combined with nC-modified epoxy, effectively limits interfacial transport degradation under coupled F/T-salt exposure. Reduced gas permeability not only delays chemical and moisture ingress but also supports the improved mechanical performance and durability observed in CFRP-confined concrete systems.

4.2.2.2. Water absorption behavior

Figure 28 presents the cumulative water absorption of the different concrete specimens as a function of time following exposure to selected numbers of F/T cycles in a 3 wt% NaCl solution. The unwrapped REF consistently exhibited the highest water uptake over the entire testing duration (Figures 28a and 28c), indicating a high susceptibility to moisture ingress. In contrast, all CFRP-wrapped specimens absorbed substantially less water, confirming the protective role of the externally bonded CFRP system in limiting water penetration into the concrete substrate.

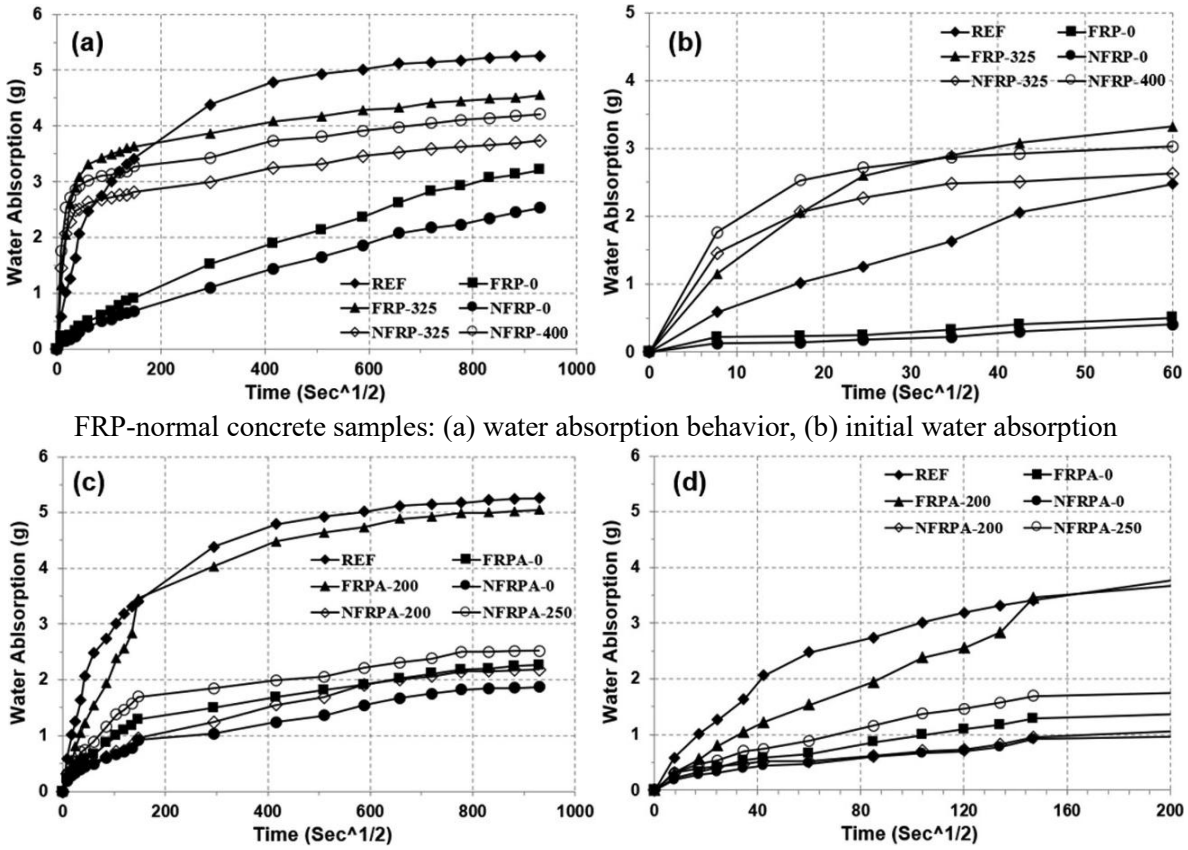

FRP-normal concrete samples: (a) water absorption behavior, (b) initial water absorption

FRP-aged concrete samples: (c) water absorption behavior, (d) initial water absorption

Figure 28. Water absorption characteristics of FRP-concrete composite specimens.

For most specimens, the water absorption curves exhibited a characteristic two-stage behavior. During the initial stage (approximately the first 6 h), the cumulative absorbed water increased rapidly, corresponding to initial water sorptivity, which is governed primarily by capillary suction through microcracks and fine pores. This was followed by a second stage, where the absorption rate slowed and gradually approached a plateau (after approximately 24 h), corresponding to secondary water sorptivity, associated with the filling of larger air voids and disconnected pore spaces. An exception was observed for the unconditioned CFRP-wrapped specimens (FRP-0 and nFRP-0), which showed little distinction between the two stages (Figure 28a), suggesting a highly intact CFRP–concrete interface that significantly delayed the onset of bulk pore filling.

After exposure to F/T-NaCl cycling, the CFRP-confined specimens, regardless of nano-modification, exhibited notably higher initial water sorptivity compared with the unexposed FRP-0 and nFRP-0 specimens (Figures 28b and 28d, and Figure 29a). This increase reflects the development of microcracks and interfacial defects induced by the combined physicochemical attack of F/T cycling and chloride exposure, which accelerate early-stage water ingress. In contrast, the differences in secondary water sorptivity among the CFRP-wrapped specimens were relatively small (Figure 29b), indicating that once capillary-controlled transport pathways were saturated, the rate of filling of larger voids was less sensitive to specimen type. This observation suggests that nano-modification and F/T damage primarily affect microcrack-controlled transport, rather than macropore filling at the CFRP-concrete interface (Mora et al., 2019).

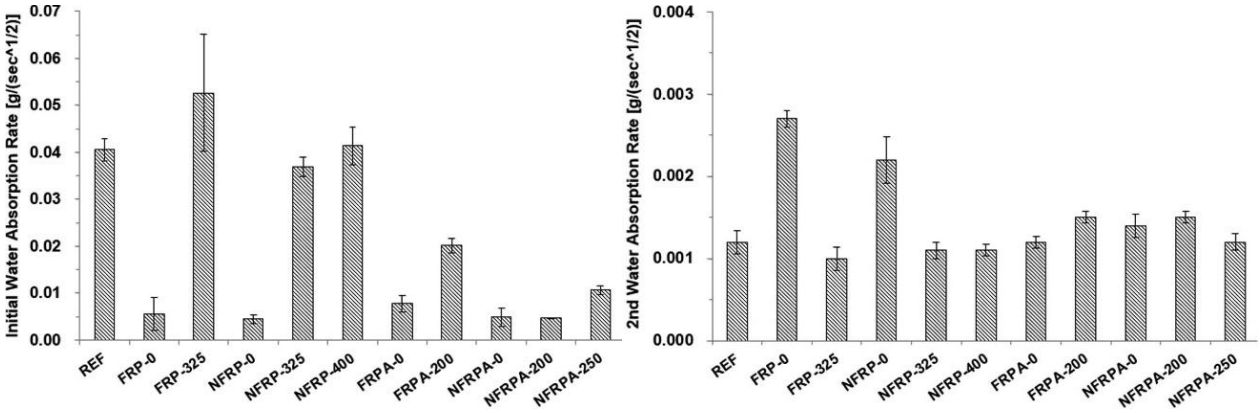

(a) initial water sorptivity (b) secondary water sorptivity

Figure 29. Water sorptivity characteristics of various concrete cylinders.

Nano-modification of the epoxy adhesive significantly reduced water absorption, particularly during the initial sorptivity stage, for both normal and pre-aged concrete. Prior to F/T exposure, the initial water sorptivity of nFRP-0 and nFRP-A-0 specimens was approximately 20% and 38% lower, respectively, than that of their unmodified counterparts (FRP-0 and FRP-A-0). After F/T cycling, the same beneficial trend persisted. For example, the initial water sorptivity of nFRP-A-200 was 0.0046 $g \cdot s^{-1/2}$, which is approximately 77% lower than that of the FRP-A-200 specimen. Similarly, the initial water sorptivity of nFRP-325 reached 0.0369 $g \cdot s^{-1/2}$, representing a reduction of approximately 30% relative to FRP-325. These results demonstrate that nano-modification remains effective in mitigating early-stage water ingress even after substantial environmental degradation.

The improved water resistance of nano-modified CFRP systems can be attributed to multiple synergistic mechanisms, including microstructural refinement of the epoxy matrix, reduced microcrack connectivity (as evidenced in Figure 23), and lower surface hydrophilicity, which is discussed in the subsequent section. Similar reductions in water absorption due to nano-modification have been reported in the literature. Guo et al. (2021) observed a reduction of approximately 33% in the water absorption coefficient of epoxy-coated concrete after incorporation of TiO_2 and graphene nanoparticles, attributed to densification of the polymer matrix. Li et al. (2018) reported a 50% reduction in water absorption of a siloxane-treated paste modified with nS, associated with both microstructural refinement and reduced hydrophilicity of the coating. In addition to pore structure, the intrinsic wettability of the material matrix plays a critical role in governing water transport in composite systems (Mora et al., 2019; Rahman et al., 2018).

Overall, the water absorption results complement the gas permeability and mechanical performance data, demonstrating that CFRP confinement, particularly when combined with nano-modified epoxy, effectively restricts moisture ingress under F/T-salt exposure. The pronounced reduction in initial water sorptivity highlights the importance of nano-modification in controlling early-stage transport through microcracks, which is critical for preserving long-term durability of CFRP-strengthened concrete systems in aggressive environments.

4.2.2.3. Interconnection of performance parameters

Figure 30 summarizes the interrelationships among the key performance parameters measured in this study, including compressive strength, MoE, water absorption, and gas permeability. To enable direct comparison and reduce scale effects, all variables were normalized prior to regression analysis, and several

outlier data points were excluded to avoid overfitting. The resulting regression models provide quantitative insight into how mechanical performance is coupled with transport behavior in CFRP-confined concrete systems under F/T exposure.

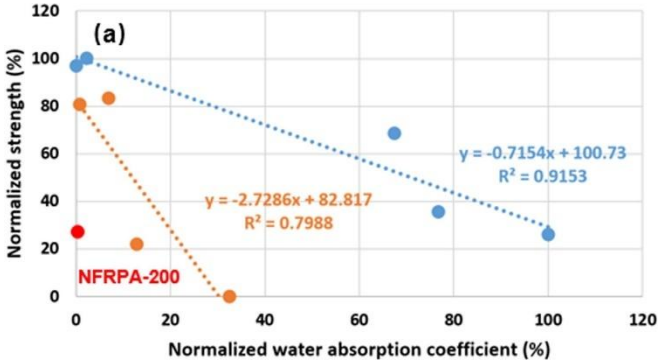

(a) normalized water absorption coefficient versus normalized strength

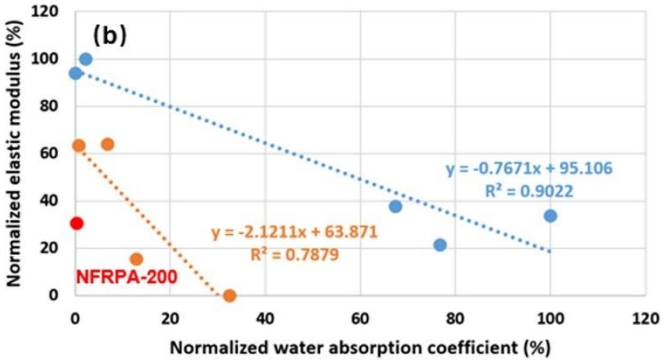

(b) normalized water absorption coefficient versus normalized MoE

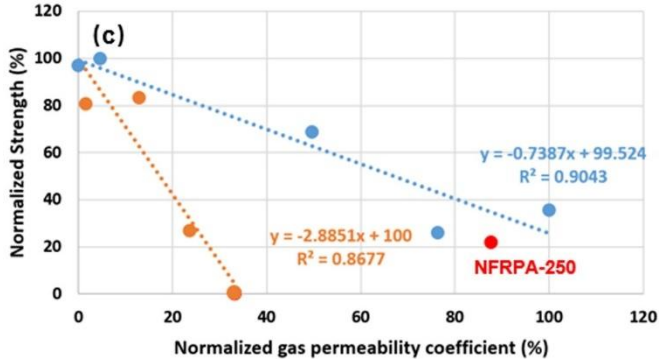

(c) normalized gas permeability coefficient versus normalized strength

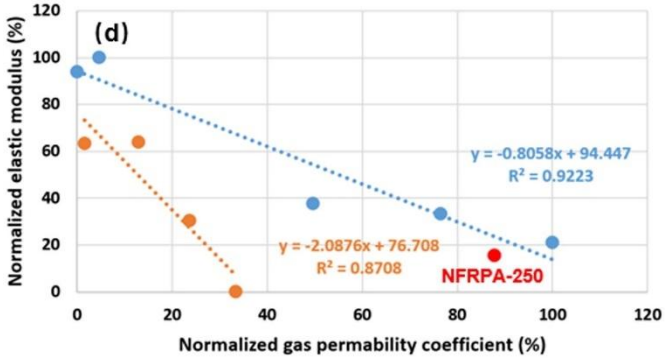

(d) normalized gas permeability coefficient versus normalized MoE

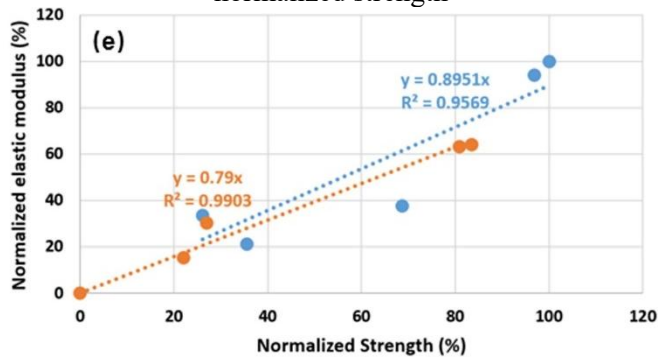

(e) normalized strength versus normalized MoE

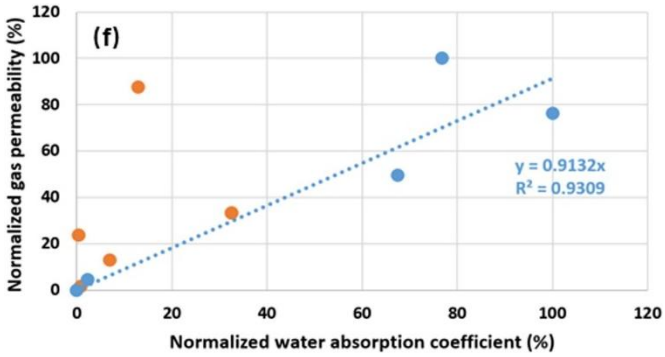

(f) normalized water absorption coefficient versus normalized gas permeability coefficient

Figure 30. Correlations among normalized experimental parameters.

Figures 30a and 30b illustrate the relationships between the normalized water absorption coefficient (NW) and the normalized compressive strength (NS) and normalized MoE (NE), respectively. For normal (non-aged) specimens, strong negative linear correlations were obtained, with coefficients of determination of $R^2 = 0.9153$ for NW–NS and $R^2 = 0.9022$ for NW–NE. These results indicate that increased water ingress is strongly associated with reductions in both strength and stiffness, reflecting the dominant role of microstructural damage and crack development in governing mechanical degradation. In contrast, the

corresponding data for pre-aged specimens were more scattered, and one notable outlier (nFRP-A-200) was identified. Similar trends were observed for the relationships between the normalized gas permeability coefficient (NG) and NS and NE (Figures 30c and 30d), where the outlier was nFRP-A-250. The increased scatter and steeper regression slopes observed for the aged specimens suggest that mechanical properties of pre-aged concrete are more sensitive to changes in transport properties, likely due to the presence of pre-existing cracks generated during the pre-aging process and the variability introduced by the application of a surface repair mortar.

Figure 30e presents the relationship between NS and NE, revealing a very strong positive correlation for both normal and aged specimens, with R^2 values of 0.9569 and 0.9903, respectively. This strong coupling confirms that compressive strength and MoE respond in a similar manner to F/T deterioration, as both parameters are governed by the integrity and continuity of the concrete microstructure. The result further supports the use of MoE as a sensitive indicator of internal damage, consistent with the observations discussed in Subsection 4.2.1.4.

Finally, Figure 30f illustrates the relationship between NW and NG. A strong linear correlation was observed for normal specimens, indicating that water absorption and gas permeability are both primarily controlled by pore connectivity and microcrack development in intact concrete. In contrast, this correlation was significantly weaker for aged specimens. This divergence suggests that water absorption is influenced not only by pore structure but also by surface wettability and hydrophilicity, whereas gas permeability is governed mainly by pore continuity and crack connectivity. The presence of pre-existing cracks and the variability associated with surface repair further decouple these transport mechanisms in aged concrete.

Overall, the regression analyses presented in Figure 30 demonstrate that mechanical degradation, moisture ingress, and gas transport are strongly interconnected in CFRP-confined concrete systems, particularly for non-aged substrates. The steeper sensitivity of mechanical properties to transport parameters in aged specimens highlights the critical role of initial damage state in durability performance. While the proposed relationships provide valuable quantitative insight into damage coupling mechanisms, additional data are required to further refine these models and improve their predictive reliability for long-term durability assessment.

4.2.3. Microscopic investigations

This subsection presents a multi-scale microscopic and physicochemical characterization of the epoxy adhesive and CFRP-concrete interface to elucidate the mechanisms underlying the mechanical and transport performance trends observed in Section 4.2. Contact angle measurements, high-resolution optical microscopy, FTIR, and thermal analyses (DSC/TGA) were employed to investigate changes in surface wettability, microcrack development, chemical interactions, and polymer network structure induced by nC modification. By linking microstructural refinement and molecular-level interactions to reductions in water and gas transport, improved stiffness retention, and enhanced compressive performance, this subsection provides mechanistic validation for the durability benefits of nC-modified CFRP systems under F/T and chloride exposure.

4.2.3.1. Water contact angle

Figure 31 presents the WCA measurements for the unmodified epoxy adhesive and the nC-modified epoxy adhesive after curing, providing direct insight into changes in surface wettability induced by nano-modification. The unmodified epoxy exhibited an average contact angle of approximately 43°, with left

and right measurements of 46° and 40°, indicating a relatively hydrophilic surface. In contrast, incorporation of 1.5 wt% nC into the epoxy hardener increased the average contact angle to approximately 54° (L: 50.7°, R: 58.4°), reflecting a clear reduction in surface wettability.

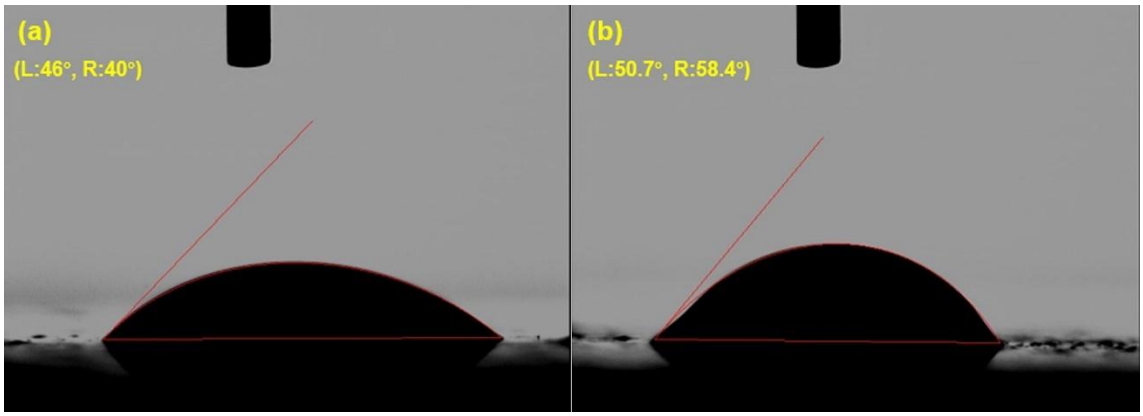

(a) original epoxy (b) nano-modified epoxy

Figure 31. WCA measurements of epoxy surfaces.

The observed increase in contact angle is consistent with previously reported trends for nC-modified polymer systems. For example, Rahman reported an increase in WCA from 47° to 65° for an epoxy resin modified with 10 wt% nC, attributing the change to altered surface chemistry and microstructure (Rahman et al., 2018). From a thermodynamic perspective, the higher contact angle measured in the present study corresponds to a reduction in surface free energy, which lowers the tendency of the epoxy surface to interact with and absorb water or aqueous solutions (Du et al., 2017). This reduction in hydrophilicity provides a mechanistic explanation for the significant decrease in initial water sorptivity observed for nC-modified CFRP-concrete systems (Subsection 4.2.2.2 and Figure 29).

The improved water resistance of the nC-modified epoxy is further supported by microstructural observations. As discussed in Subsection 4.2.1.1 (Figure 23), nC modification resulted in a more homogeneous and refined epoxy microstructure with reduced microcrack density. The combined effects of reduced surface wettability and diminished microcrack connectivity limit the availability of preferential pathways for moisture ingress, thereby enhancing the durability of the CFRP-concrete interface under F/T and chloride exposure. It is also noted that at higher nC dosages, where dispersion may become less uniform, additional hydrophobic effects could arise from the formation of hierarchical nano-/micro-scale surface roughness, as reported in the literature (Shi et al., 2012). However, within the optimized dosage employed in this study, the primary contribution of nC modification is attributed to controlled microstructural refinement and moderate reduction in epoxy surface hydrophilicity.

4.2.5.3. High-resolution optical microscope

High-resolution optical microscopy was employed to examine the microstructural characteristics of the CFRP-epoxy-concrete interface before and after F/T exposure in a 3 wt% NaCl solution, and the representative observations are presented in Figure 32. At the initial, unexposed stage, no discernible differences were observed between the FRP and nC-modified FRP (nFRP) specimens (Figures 32a and 32d), indicating comparable epoxy impregnation quality and interfacial integrity prior to environmental conditioning. The epoxy layer appeared continuous and well bonded to the concrete substrate, with no visible interfacial separation or cracking.

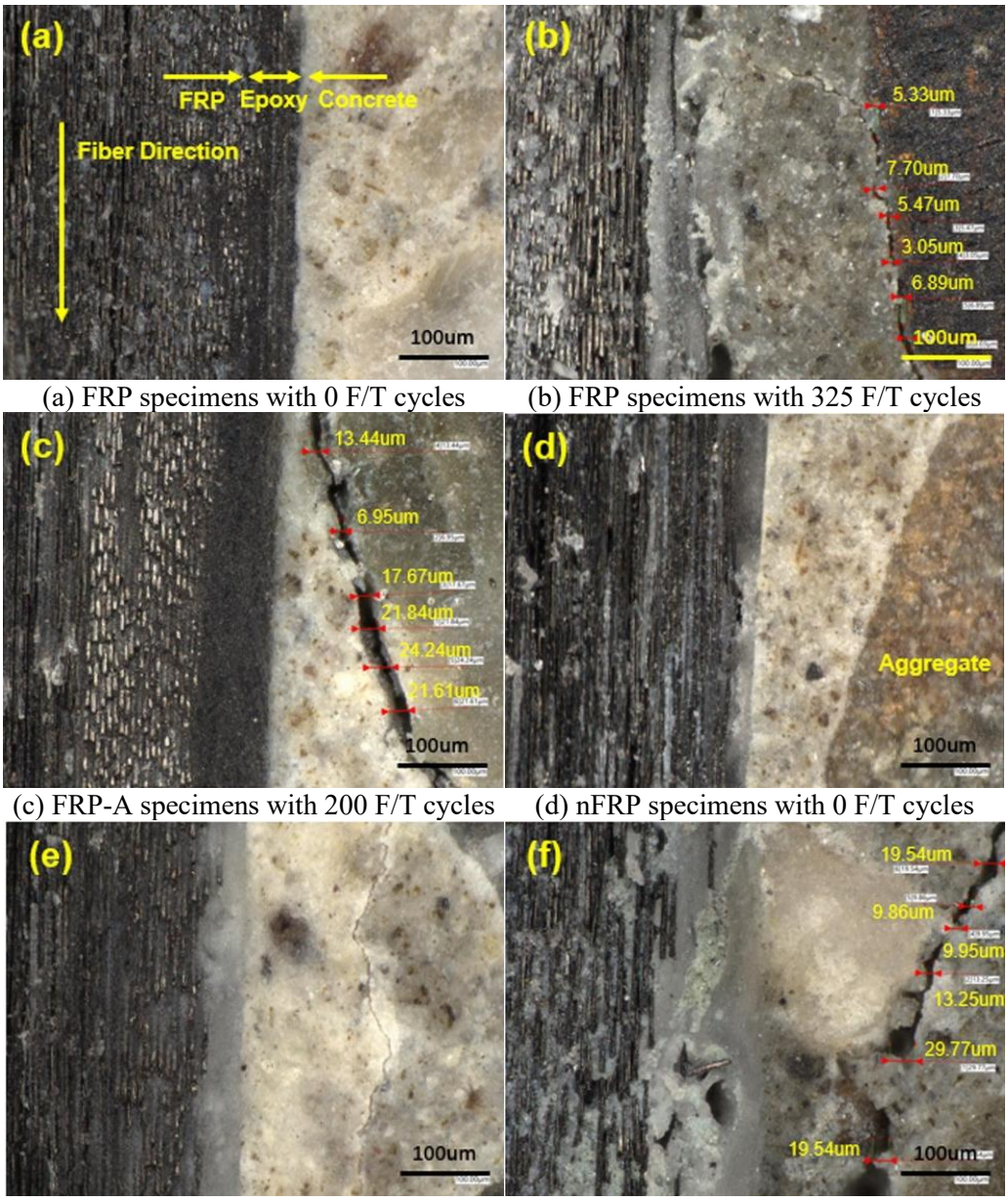

(a) FRP specimens with 0 F/T cycles (b) FRP specimens with 325 F/T cycles

(c) FRP-A specimens with 200 F/T cycles (d) nFRP specimens with 0 F/T cycles

(e) nFRP specimens with 325 F/T cycles (f) nFRP-A specimens with 200 F/T cycles

Figure 32. Microstructural characteristics of selected FRP-based specimens under F/T exposure.

With progressive F/T-salt exposure, distinct differences emerged between unmodified and nC-modified systems. After 325 F/T cycles, the unmodified FRP specimens exhibited pronounced interfacial cracking and crack coalescence at the epoxy-concrete interface (Figure 32b). The cracks were continuous and readily measurable, indicating advanced interfacial deterioration induced by salt scaling and repeated thermal stresses. In contrast, the corresponding nFRP specimens (Figure 32e) showed significantly reduced crack development; the cracks were sparse, discontinuous, and in many locations too narrow to be accurately quantified at the applied magnification. This observation confirms that nC modification effectively suppresses crack initiation and propagation within the epoxy layer and at the interface, consistent with the reduced gas permeability and water sorptivity reported in Subsections 4.2.2.1 and 4.2.2.2.

For pre-aged concrete specimens, the beneficial effect of nC modification on crack-width reduction was less pronounced. After 200 F/T cycles, the average crack width measured in the FRP-A specimens was approximately 17.6 μm (Figure 32c), while the corresponding value for nFRP-A specimens was approximately 17.0 μm (Figure 32f). Although nC modification still resulted in slightly narrower cracks, the difference between the two systems was relatively small compared with that observed in normal concrete. This reduced effectiveness is likely associated with the heterogeneity introduced by the surface repair mortar layer applied to the pre-aged concrete prior to CFRP wrapping. Variability in mortar thickness, bonding quality, and microcrack distribution can obscure the intrinsic crack-mitigating effect of the nC-modified epoxy.

Overall, the optical microscopy results provide direct microstructural evidence supporting the mechanical and transport performance trends observed in this study. The markedly reduced crack density and crack width in nC-modified FRP systems for normal concrete explain the enhanced compressive strength retention, lower gas permeability, and reduced water sorptivity under severe F/T-salt exposure. For pre-aged concrete, while nC modification still offers some benefit, the presence of pre-existing damage and repair-induced variability limits the extent of crack-width control, highlighting the need for further optimization of surface preparation and repair strategies when strengthening deteriorated substrates.

4.2.3.3. Fourier transform infrared spectroscopy

The FTIR spectra of the epoxy adhesive with and without nC modification are presented in Figure 33, covering the full spectral range of 4000-400 cm^{-1} (Figure 33a) with an emphasized low-wavenumber region of 1400-400 cm^{-1} (Figure 33b). In both spectra, a broad absorption band in the range of 3600-3200 cm^{-1} is observed and attributed to N-H stretching vibrations, arising from the amine-based curing agent used in the epoxy system. Peaks associated with C-H stretching and deformation vibrations are also evident in the 3000-2800 cm^{-1} region, including asymmetric C-H stretching and CH_3 deformation, which are characteristic of the epoxy resin backbone.

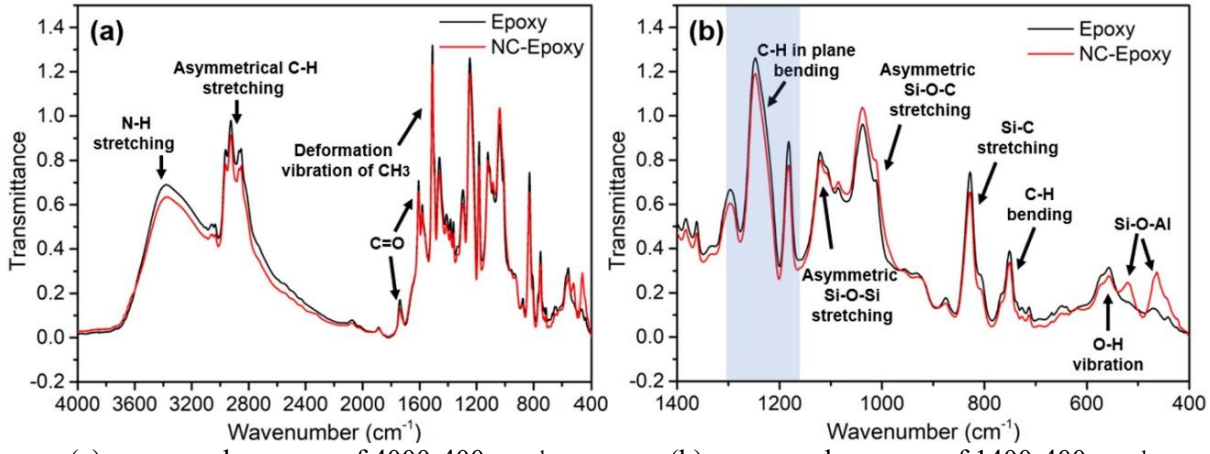

(a) wavenumber range of 4000-400 cm^{-1} (b) wavenumber range of 1400-400 cm^{-1}

Figure 33. FTIR spectra of epoxy resin and nC-modified epoxy resin.

A dominant feature common to both unmodified and nC-modified epoxy is the intense broadband in the 1100-1000 cm^{-1} region, which can be assigned to Si-O-R stretching, particularly asymmetric Si-O-C vibrations, with a pronounced peak at approximately 1124 cm^{-1} corresponding to asymmetric Si-O-Si stretching. These peaks confirm that the epoxy adhesive employed in this study is a siloxane-modified

epoxy system. Although characteristic epoxy functional group vibrations, such as asymmetric aliphatic C-O stretching near 1184 cm^{-1} and epoxide ring vibrations at approximately 970, 914, and 862 cm^{-1}, are present, they are partially obscured or attenuated due to overlap with siloxane-related bands. In addition, absorption peaks near 1580 cm^{-1} and 1650 cm^{-1} are indicative of C=O stretching, while a peak near 830 cm^{-1} can be assigned to Si-C stretching, further supporting the hybrid siloxane-epoxy nature of the adhesive (Chan et al., 2011).

Notable differences between the unmodified and nC-modified epoxy spectra are observed in the low-wavenumber region. Specifically, additional absorption features appearing at approximately 520 cm^{-1} and 460 cm^{-1} in the nC-modified epoxy are attributed to Si-O-Al vibrations associated with the aluminosilicate structure of montmorillonite nC (Djebbar et al., 2012). These peaks are absent in the unmodified epoxy and indicate the incorporation of clay-derived functional groups into the polymer matrix. Although most spectral features of the two systems overlap, the emergence and intensity variation of the Si-O-Al bands suggest chemical interaction between the nC and the siloxane-modified epoxy, rather than simple physical dispersion.

The FTIR results provide direct chemical evidence supporting the enhanced performance of the nC-modified epoxy observed in earlier sections. The formation of clay-epoxy interactions is expected to improve crosslink density and interfacial bonding within the adhesive matrix, contributing to the refined microstructure, reduced microcrack development, and improved resistance to moisture and gas transport reported in Subsections 4.2.1 and 4.2.2. Thus, the FTIR analysis complements the mechanical, transport, and microscopic observations by confirming that nC modification alters the epoxy at the molecular level, underpinning the improved durability of the CFRP-concrete system.

4.2.3.4. Thermal properties analysis

Figure 34 presents the DSC and TGA results of the siloxane epoxy adhesive with and without nC modification, providing insight into the influence of nC on the thermal transitions and thermal stability of the cured adhesive. As shown in Figure 34a, the DSC curves indicate that incorporation of nC led to a slight but measurable increase in the glass transition temperature (Tg), from approximately 48.5 °C for the unmodified epoxy to about 50 °C for the nC-modified epoxy. This increase in Tg suggests restricted molecular mobility within the polymer network due to nC incorporation. Similar trends have been reported in the literature; for example, Shanmugharaj and Ryu (2012) observed an increase in Tg from 30.8 °C to 32 °C for an epoxy resin modified with 2 wt% nC at a lower heating rate. Using dynamic mechanical analysis (DMA), Zainuddin et al. (2010) further demonstrated that Tg increased progressively with nC content, rising from 99 °C (unmodified epoxy) to 105 °C, 115 °C, and 110 °C for 1, 2, and 3 wt% nC, respectively.

Quantitative analysis of the DSC heat flow data further supports the effect of nC on the epoxy network structure. Based on the recorded heat flow, heating rate, and sample mass, the endothermic energy associated with the glass transition was calculated to be approximately 0.294 J $(g\ °C)^{-1}$ for the unmodified epoxy and 0.248 J $(g\ °C)^{-1}$ for the nC-modified epoxy. The lower endothermic energy of the nC-modified system is indicative of a higher crosslinking density, as fewer polymer chain segments are available to participate in the transition (Yi-qiu et al., 2012). Increased crosslinking density and stronger polymer–filler interactions restrict segmental motion of the epoxy chains, thereby requiring higher thermal energy to initiate the glass transition (Nguyen et al., 2016). This mechanism provides a direct explanation for the observed increase in Tg upon nC modification.

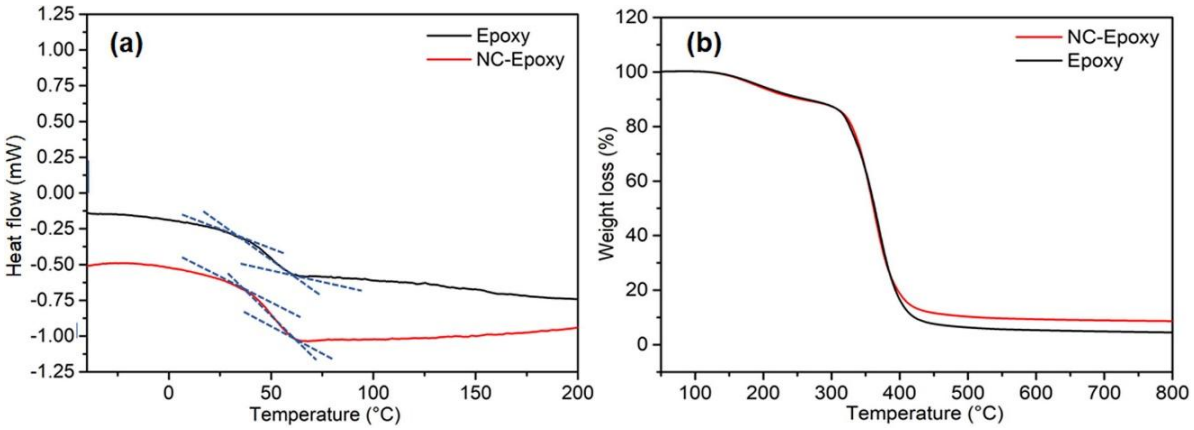

(a) DSC analysis (b) TGA analysis

Figure 34. Thermal characterization of the hardened epoxy adhesive.

The TGA results shown in Figure 34b reveal that nC modification also enhanced the thermal stability of the cured epoxy adhesive. Both systems exhibited a major mass-loss event associated with polymer decomposition; however, at temperatures exceeding approximately 450 °C, the nC-modified epoxy retained a residual mass about 2.5% higher than that of the unmodified epoxy. This increase in char residue is significantly greater than the nC content itself (1.5% by mass of the epoxy adhesive), indicating that the improvement cannot be attributed solely to the inorganic filler fraction. Instead, the higher residual mass reflects improved thermal resistance of the polymer network, consistent with enhanced crosslinking density and reduced chain mobility induced by nC incorporation. Similar improvements in epoxy thermal stability due to nC addition have been reported by Zainuddin et al. (2010), who attributed the effect to strengthened polymer-clay interactions and increased crosslink density.

Overall, the DSC and TGA results provide strong thermal evidence that nC modification alters the epoxy adhesive at the molecular level by increasing crosslink density, restricting polymer chain motion, and enhancing thermal stability. These thermal improvements are consistent with the refined microstructure, reduced crack development, lower transport coefficients, and improved mechanical performance observed for nC-modified CFRP-concrete systems in earlier sections. Together, the thermal analysis results support the conclusion that nC modification contributes to improved durability and performance of the epoxy adhesive under coupled mechanical and environmental loading.

Chapter 5. Summary and Conclusions

In this study, a comprehensive experimental program was conducted to evaluate the feasibility and effectiveness of using montmorillonite nC-modified epoxy adhesives to enhance the durability and mechanical performance of CFRP-wrapped concrete exposed to F/T cycling and chloride environments representative of cold-region infrastructure. The investigation systematically examined bond durability, transport properties, compressive performance, and microstructural and molecular-level mechanisms, with particular emphasis on distinguishing the behavior of normal and pre-aged concrete substrates.

The major findings of this work are summarized as follows:

1. Bond durability was identified as the governing performance criterion for nano-modified CFRP-concrete systems under hydrothermal and chloride exposure. Among the nano-modifiers investigated (nS, GO, and nC), each exhibited a distinct dosage-dependent response, with bond-strength enhancement confined to a narrow optimal range and degradation occurring at higher contents due to agglomeration, increased viscosity, or impaired resin impregnation. Hydrothermal aging caused systematic bond degradation for all systems; however, selected nano-modified configurations retained significantly higher bond strength than the unmodified epoxy under both room-temperature and elevated-temperature immersion.

2. Montmorillonite nC–modified epoxy, particularly at the optimal dosage, exhibited the most robust and consistent bond-durability performance across saturation states and HTA conditions. Compared with nS and GO systems, nC modification provided superior resistance to interfacial degradation and maintained bond integrity under coupled moisture–temperature exposure. Based on this performance, nC was selected as the sole nano-modification strategy for subsequent evaluation of compressive behavior.

3. Nanoclay modification significantly enhanced the mechanical performance of CFRP-wrapped concrete, especially for pre-aged substrates. CFRP confinement increased the compressive strength of normal and pre-aged concrete by approximately 99% and 82%, respectively, prior to environmental exposure. Under prolonged F/T cycling in a 3 wt% NaCl solution, nC-modified CFRP-confined concrete exhibited markedly improved strength retention, reduced stiffness degradation, and delayed failure compared with unmodified CFRP systems. The beneficial effect of nC became increasingly pronounced with higher numbers of F/T cycles and was particularly significant for pre-aged concrete.

4. Transport properties were strongly coupled with mechanical degradation, and nC modification effectively reduced both gas permeability and water absorption, especially during the initial sorptivity stage controlled by microcrack connectivity. The nC-modified epoxy reduced gas mass loss and initial water sorptivity for both normal and pre-aged concrete, even after extensive F/T exposure. Regression analyses revealed strong quantitative relationships between transport parameters and mechanical indicators, highlighting the critical role of moisture and gas ingress in driving stiffness and strength degradation.

5. Microscopic and physicochemical analyses provided mechanistic validation for the observed macroscopic performance improvements. Optical microscopy revealed reduced crack density and

narrower interfacial cracks in nC-modified systems, while WCA measurements demonstrated reduced epoxy hydrophilicity. FTIR analysis confirmed chemical interactions between nC and the siloxane-modified epoxy, and DSC/TGA results indicated increased glass transition temperature, higher crosslink density, and improved thermal stability. Together, these findings demonstrate that nC modification alters the epoxy adhesive at the microstructural and molecular levels, underpinning the enhanced durability of the CFRP-concrete system.

Overall, this work demonstrates that montmorillonite nC is an effective nano-modifier for improving the durability, transport resistance, and mechanical performance of CFRP-wrapped concrete in cold, chloride-laden environments, particularly for deteriorated substrates. The study further establishes bond durability as a critical screening metric for selecting nano-modification strategies prior to structural performance evaluation.

Although this research focused on the synergistic effects of F/T cycling and chloride exposure, CFRP-wrapped concrete structures in service may be subjected to additional degradation mechanisms, including sulfate attack, acid exposure, microbial activity, ultraviolet aging, and wet–dry cycling. Future research will investigate the combined effects of these environmental stressors under laboratory and field conditions. In addition, further studies are warranted to explore alternative nanomaterials, non-epoxy polymer matrices, and the co-incorporation of multiple nanomaterials to simultaneously enhance barrier performance, toughness, and impact resistance of polymeric adhesives. Such efforts will support the broader application of nano-modified FRP systems for durable protection and strengthening of concrete infrastructure.

References

ACI Committee 440. (2023). ACI PRC-440.2-23: Design and Construction of Externally Bonded Fiber-Reinforced Polymer (FRP) Systems for Strengthening Concrete Structures—Guide. In.

Al-Saadi, N. T. K., Mohammed, A., Al-Mahaidi, R., & Sanjayan, J. (2019). A state-of-the-art review: Near-surface mounted FRP composites for reinforced concrete structures. *Construction and Building Materials*, *209*, 748-769. https://doi.org/https://doi.org/10.1016/j.conbuildmat.2019.03.121

Bai, J., Yang, Y., Huang, P., Guo, X., Chen, Z., Wan-Wendner, R., & Li, W. (2024). Durability of CFRP strengthened RC beam after six years exposure to natural hygrothermal environment with sustained loads. *International Journal of Fatigue*, *181*, 108126. https://doi.org/https://doi.org/10.1016/j.ijfatigue.2023.108126

Brandtner-Hafner, M. (2024). Evaluating the bonding effectiveness of CFRP patches in strengthening concrete structures. *Construction and Building Materials*, *436*, 136966. https://doi.org/https://doi.org/10.1016/j.conbuildmat.2024.136966

Carbas, R. J. C., Marques, E. A. S., da Silva, L. F. M., & Lopes, A. M. (2014). Effect of Cure Temperature on the Glass Transition Temperature and Mechanical Properties of Epoxy Adhesives. *The Journal of Adhesion*, *90*(1), 104-119. https://doi.org/10.1080/00218464.2013.779559

Chan, M.-l., Lau, K.-t., Wong, T. T., & Cardona, F. (2011). Interfacial bonding characteristic of nanoclay/polymer composites. *Applied Surface Science*, *258*(2), 860-864. https://doi.org/https://doi.org/10.1016/j.apsusc.2011.09.016

Dai, J.-G., Yokota, H., Iwanami, M., & Kato, E. (2010). Experimental Investigation of the Influence of Moisture on the Bond Behavior of FRP to Concrete Interfaces. *Journal of Composites for Construction*, *14*(6), 834-844. https://doi.org/10.1061/(ASCE)CC.1943-5614.0000142

Dalfi, H. K., Alomarah, A., Jan, K., Al-Obaidi, A. J., Selver, E., Samaka, H., & Ruan, D. (2025). Enhancement of mechanical, physical, and electrical performances of epoxy composites by inclusion nano-particles: A review. *Journal of Composite Materials*, *59*(29), 3321-3351. https://doi.org/10.1177/00219983251350432

Djebbar, M., Djafri, F., Bouchekara, M., & Djafri, A. (2012). Adsorption of phenol on natural clay. *Applied Water Science*, *2*(2), 77-86. https://doi.org/10.1007/s13201-012-0031-8

Du, S., Zhao, H., Ge, Y., Yang, Z., & Shi, X. (2017). Laboratory Investigation into the Modification of Transport Properties of High-Volume Fly Ash Mortar by Chemical Admixtures. *Journal of Materials in Civil Engineering*, *29*(10), 04017184. https://doi.org/10.1061/(ASCE)MT.1943-5533.0002025

Evans, A. G., Hutchinson, J. W., & Wei, Y. (1999). Interface adhesion: effects of plasticity and segregation. *Acta Materialia*, *47*(15), 4093-4113. https://doi.org/https://doi.org/10.1016/S1359-6454(99)00269-4

Fan, Y., Zhang, S., Wang, Q., & Shah, S. P. (2015). Effects of nano-kaolinite clay on the freeze–thaw resistance of concrete. *Cement and Concrete Composites*, *62*, 1-12. https://doi.org/https://doi.org/10.1016/j.cemconcomp.2015.05.001

Farnam, Y., Bentz, D., Sakulich, A., Flynn, D., & Weiss, J. (2014). Measuring Freeze and Thaw Damage in Mortars Containing Deicing Salt Using a Low-Temperature Longitudinal Guarded Comparative Calorimeter and Acoustic Emission. *Advances in Civil Engineering Materials*, *3*(1), 316-337. https://doi.org/10.1520/ACEM20130095

Fazli, H., Yassin, A. Y. M., Shafiq, N., & Teo, W. (2018). Pull-off testing as an interfacial bond strength assessment of CFRP-concrete interface exposed to a marine environment. *International Journal of*

Adhesion and Adhesives, *84*, 335-342. https://doi.org/https://doi.org/10.1016/j.ijadhadh.2018.04.015
Frigione, M., & Lettieri, M. (2018). Durability Issues and Challenges for Material Advancements in FRP Employed in the Construction Industry. *Polymers*, *10*(3), 247.
Ghazy, A., & Bassuoni, M. T. (2018). Response of concrete to cyclic environments and chloride-based salts. *Magazine of Concrete Research*, *71*(10), 533-547. https://doi.org/10.1680/jmacr.17.00454
Gholami, M., Sam, A. R. M., Yatim, J. M., & Tahir, M. M. (2013). A review on steel/CFRP strengthening systems focusing environmental performance. *Construction and Building Materials*, *47*, 301-310. https://doi.org/https://doi.org/10.1016/j.conbuildmat.2013.04.049
Goda, I., Padayodi, E., & Raoelison, R. N. (2024). Computational analysis of the interfacial debonding in polymer composites: research progress and challenges. *Advanced Composites and Hybrid Materials*, *7*(6), 231. https://doi.org/10.1007/s42114-024-01038-7
Gonçalves, F. A. M. M., Santos, M., Cernadas, T., Alves, P., & Ferreira, P. (2022). Influence of fillers on epoxy resins properties: a review. *Journal of Materials Science*, *57*(32), 15183-15212. https://doi.org/10.1007/s10853-022-07573-2
Guo, J., Sun, W., Xu, Y., Lin, W., & Jing, W. (2022). Damage Mechanism and Modeling of Concrete in Freeze–Thaw Cycles: A Review. *Buildings*, *12*(9), 1317.
Guo, L., Chen, Z., Han, H., Liu, G., Luo, M., Cui, N., Dong, H., & Li, M.-Z. (2023). Advances and outlook in modified graphene oxide (GO)/epoxy composites for mechanical applications. *Applied Nanoscience*, *13*(5), 3273-3287. https://doi.org/10.1007/s13204-022-02653-w
Guo, S.-Y., Luo, H.-H., Tan, Z., Chen, J.-Z., Zhang, L., & Ren, J. (2021). Impermeability and interfacial bonding strength of TiO2-graphene modified epoxy resin coated OPC concrete. *Progress in Organic Coatings*, *151*, 106029. https://doi.org/https://doi.org/10.1016/j.porgcoat.2020.106029
Han, X., Jin, Y., Zhang, W., Hou, W., & Yu, Y. (2018). Characterisation of moisture diffusion and strength degradation in an epoxy-based structural adhesive considering a post-curing process. *Journal of Adhesion Science and Technology*, *32*(15), 1643-1657. https://doi.org/10.1080/01694243.2018.1436876
Hao, Z.-H., Zeng, J.-J., Chen, G.-M., Dai, J.-G., & Chen, J.-F. (2024). Durability of FRP-to-concrete bonded joints subjected to 110 months accelerated laboratory and field exposure. *Engineering Structures*, *305*, 117681. https://doi.org/https://doi.org/10.1016/j.engstruct.2024.117681
Harle, S. M. (2024). Durability and long-term performance of fiber reinforced polymer (FRP) composites: A review. *Structures*, *60*, 105881. https://doi.org/https://doi.org/10.1016/j.istruc.2024.105881
Hoque, M. A., & Yao, C.-W. (2025). Nanoscale Characterization of Nanomaterial-Based Systems: Mechanisms, Experimental Methods, and Challenges in Probing Corrosion, Mechanical, and Tribological Properties. *Nanomaterials*, *15*(23), 1824.
Irshidat, M. R., & Al-Saleh, M. H. (2016). Effect of using carbon nanotube modified epoxy on bond–slip behavior between concrete and FRP sheets. *Construction and Building Materials*, *105*, 511-518. https://doi.org/https://doi.org/10.1016/j.conbuildmat.2015.12.183
Jiang, F., Yang, Q., Wang, Y., Wang, P., Hou, D., & Jin, Z. (2021). Insights on the adhesive properties and debonding mechanism of CFRP/concrete interface under sulfate environment: From experiments to molecular dynamics. *Construction and Building Materials*, *269*, 121247. https://doi.org/https://doi.org/10.1016/j.conbuildmat.2020.121247
Karbhari, V. M. (2022). Long-term hydrothermal aging of Carbon-Epoxy materials for rehabilitation of civil infrastructure. *Composites Part A: Applied Science and Manufacturing*, *153*, 106705. https://doi.org/https://doi.org/10.1016/j.compositesa.2021.106705
Karimi, H., Khoramishad, H., & Fatolahi, A. R. (2023). The effect of aligning graphene-oxide nanoplatelets on moisture absorption and thermal stability of polymeric nanocomposites. *Journal of*

Applied Polymer Science, *140*(30), e54100. https://doi.org/https://doi.org/10.1002/app.54100
Korkees, F. (2023). Moisture absorption behavior and diffusion characteristics of continuous carbon fiber reinforced epoxy composites: a review. *Polymer-Plastics Technology and Materials*, *62*(14), 1789-1822. https://doi.org/10.1080/25740881.2023.2234461
Lau, K.-t., Gu, C., & Hui, D. (2006). A critical review on nanotube and nanotube/nanoclay related polymer composite materials. *Composites Part B: Engineering*, *37*(6), 425-436. https://doi.org/https://doi.org/10.1016/j.compositesb.2006.02.020
Lei, Z., Li, Z., Zhang, X., & Shi, X. (2021). Durability of CFRP-wrapped concrete in cold regions: A laboratory evaluation of montmorillonite nanoclay-modified siloxane epoxy adhesive. *Construction and Building Materials*, *290*, 123253. https://doi.org/https://doi.org/10.1016/j.conbuildmat.2021.123253
Lei, Z., Ran, H., Li, Z., & Shi, X. (2025). Synergistic Effect of Nano-TiO2 and Organic Montmorillonite Modification of Epoxy Resin on the Characteristics of the CFRP–Concrete Interface. *Journal of Composites for Construction*, *29*(4), 04025032. https://doi.org/10.1061/JCCOF2.CCENG-4918
Li, P.-D., Zhao, Y., Wu, Y.-F., & Lin, J.-P. (2023). Effect of defects in adhesive layer on the interfacial bond behaviors of externally bonded CFRP-to-concrete joints. *Engineering Structures*, *278*, 115495. https://doi.org/https://doi.org/10.1016/j.engstruct.2022.115495
Li, R., Hou, P., Xie, N., Ye, Z., Cheng, X., & Shah, S. P. (2018). Design of SiO2/PMHS hybrid nanocomposite for surface treatment of cement-based materials. *Cement and Concrete Composites*, *87*, 89-97. https://doi.org/https://doi.org/10.1016/j.cemconcomp.2017.12.008
Liu, S., Pan, Y., Li, H., & Xian, G. (2019). Durability of the Bond between CFRP and Concrete Exposed to Thermal Cycles. *Materials*, *12*(3), 515.
Liu, Z., & Hansen, W. (2016). Freeze–thaw durability of high strength concrete under deicer salt exposure. *Construction and Building Materials*, *102*, 478-485. https://doi.org/https://doi.org/10.1016/j.conbuildmat.2015.10.194
Luo, D., Li, F., & Niu, D. (2024). Study on the deterioration of concrete performance in saline soil area under the combined effect of high low temperatures, chloride and sulfate salts. *Cement and Concrete Composites*, *150*, 105531. https://doi.org/https://doi.org/10.1016/j.cemconcomp.2024.105531
Mariam, M., Afendi, M., Abdul Majid, M. S., Ridzuan, M. J. M., Azmi, A. I., & Sultan, M. T. H. (2019). Influence of hydrothermal ageing on the mechanical properties of an adhesively bonded joint with different adherends. *Composites Part B: Engineering*, *165*, 572-585. https://doi.org/https://doi.org/10.1016/j.compositesb.2019.02.032
Mhanna, H. H., Hawileh, R. A., & Abdalla, J. A. (2019). Shear Strengthening of Reinforced Concrete Beams Using CFRP Wraps. *Procedia Structural Integrity*, *17*, 214-221. https://doi.org/https://doi.org/10.1016/j.prostr.2019.08.029
Mora, E., González, G., Romero, P., & Castellón, E. (2019). Control of water absorption in concrete materials by modification with hybrid hydrophobic silica particles. *Construction and Building Materials*, *221*, 210-218. https://doi.org/https://doi.org/10.1016/j.conbuildmat.2019.06.086
Nguyen, T. A., Nguyen, T. H., Nguyen, T. V., Thai, H., & Shi, X. (2016). Effect of Nanoparticles on the Thermal and Mechanical Properties of Epoxy Coatings. *Journal of Nanoscience and Nanotechnology*, *16*(9), 9874-9881. https://doi.org/10.1166/jnn.2016.12162
Ortiz, J. D., Khedmatgozar Dolati, S. S., Malla, P., Nanni, A., & Mehrabi, A. (2023). FRP-Reinforced/Strengthened Concrete: State-of-the-Art Review on Durability and Mechanical Effects. *Materials*, *16*(5), 1990.
Pang, B., Zhang, Y., Liu, G., & She, W. (2018). Interface Properties of Nanosilica-Modified Waterborne Epoxy Cement Repairing System. *ACS Applied Materials & Interfaces*, *10*(25), 21696-21711. https://doi.org/10.1021/acsami.8b04092

Rahman, A. S., Mathur, V., & Asmatulu, R. (2018). Effect of nanoclay and graphene inclusions on the low-velocity impact resistance of Kevlar-epoxy laminated composites. *Composite Structures*, *187*, 481-488. https://doi.org/https://doi.org/10.1016/j.compstruct.2017.12.054
Raja Othman, R. N., Subramaniam, D. K., Abdullah, M. F., & Ku Ahmad, K. Z. (2025). Synergistic fracture toughening in epoxy composites with hybrid micro- and nano-silica: a new dual-mechanism model approach. *Journal of Materials Science*, *60*(44), 22064-22086. https://doi.org/10.1007/s10853-025-11705-9
Rajani, B., & Kleiner, Y. (2001). Comprehensive review of structural deterioration of water mains: physically based models. *Urban Water*, *3*(3), 151-164. https://doi.org/https://doi.org/10.1016/S1462-0758(01)00032-2
Rusnak, C. R. (2025). Sustainable Strategies for Concrete Infrastructure Preservation: A Comprehensive Review and Perspective. *Infrastructures*, *10*(4), 99.
Sen, R. (2015). Developments in the durability of FRP-concrete bond. *Construction and Building Materials*, *78*, 112-125. https://doi.org/https://doi.org/10.1016/j.conbuildmat.2014.12.106
Shadlou, S., Ahmadi-Moghadam, B., & Taheri, F. (2015). Nano-Enhanced Adhesives. In *Progress in Adhesion and Adhesives* (pp. 357-396). https://doi.org/https://doi.org/10.1002/9781119162346.ch10
Shanmugharaj, A. M., & Ryu, S. H. (2012). Study on the effect of aminosilane functionalized nanoclay on the curing kinetics of epoxy nanocomposites. *Thermochimica Acta*, *546*, 16-23. https://doi.org/https://doi.org/10.1016/j.tca.2012.07.026
Shelly, D., Singhal, V., Singh, S., Nanda, T., Mehta, R., Lee, S.-Y., & Park, S.-J. (2024). Exploring the Impact of Nanoclay on Epoxy Nanocomposites: A Comprehensive Review. *Journal of Composites Science*, *8*(12), 506.
Shi, X., Nguyen, T. A., Suo, Z., Wu, J., Gong, J., & Avci, R. (2012). Electrochemical and mechanical properties of superhydrophobic aluminum substrates modified with nano-silica and fluorosilane. *Surface and Coatings Technology*, *206*(17), 3700-3713. https://doi.org/https://doi.org/10.1016/j.surfcoat.2012.02.058
Shrestha, J., Ueda, T., & Zhang, D. (2015). Durability of FRP Concrete Bonds and Its Constituent Properties under the Influence of Moisture Conditions. *Journal of Materials in Civil Engineering*, *27*(2), A4014009. https://doi.org/10.1061/(ASCE)MT.1943-5533.0001093
Shrestha, J., Zhang, D., & Ueda, T. (2016). Durability Performances of Carbon Fiber–Reinforced Polymer and Concrete-Bonded Systems under Moisture Conditions. *Journal of Composites for Construction*, *20*(5), 04016023. https://doi.org/10.1061/(ASCE)CC.1943-5614.0000674
Spoelstra Marijn, R., & Monti, G. (1999). FRP-Confined Concrete Model. *Journal of Composites for Construction*, *3*(3), 143-150. https://doi.org/10.1061/(ASCE)1090-0268(1999)3:3(143)
Subash, S., & Subash, S. (2024). Scaling in Concrete – Causes, Prevention, and Repair. In *Industrial Scale Inhibition* (pp. 341-356). https://doi.org/https://doi.org/10.1002/9781394191208.ch17
Sun, Y., & Dang, Y. (2025). Multidimensional FRP connection technologies: Engineering performance, debonding resistance, and sustainable durability: A critical review. *Journal of Reinforced Plastics and Composites*, 07316844251382965. https://doi.org/10.1177/07316844251382965
Taheri, F. (2020). Improvement of the Performance of Structural Adhesive Joints with Nanoparticles and Numerical Prediction of Their Response. In *Structural Adhesive Joints* (pp. 35-78). https://doi.org/https://doi.org/10.1002/9781119737322.ch2
Ueda, T., & Dai, J. (2005). Interface bond between FRP sheets and concrete substrates: properties, numerical modeling and roles in member behaviour. *Progress in Structural Engineering and Materials*, *7*(1), 27-43. https://doi.org/https://doi.org/10.1002/pse.187
Uniyal, P., Gaur, P., Yadav, J., Bhalla, N. A., Khan, T., Junaedi, H., & Sebaey, T. A. (2025). A

Comprehensive Review on the Role of Nanosilica as a Toughening Agent for Enhanced Epoxy Composites for Aerospace Applications. *ACS Omega*, *10*(16), 15810-15839. https://doi.org/10.1021/acsomega.4c10073
Viana, G., Costa, M., Banea, M., & da Silva, L. (2016). A review on the temperature and moisture degradation of adhesive joints. *Proceedings of the Institution of Mechanical Engineers, Part L: Journal of Materials: Design and Applications*, *231*(5), 488-501. https://doi.org/10.1177/1464420716671503
Wang, K., Nelsen, D. E., & Nixon, W. A. (2006). Damaging effects of deicing chemicals on concrete materials. *Cement and Concrete Composites*, *28*(2), 173-188. https://doi.org/https://doi.org/10.1016/j.cemconcomp.2005.07.006
Wu, Q., Li, Y., Liu, Q., Jin, D., Lei, Y., Yao, R., Zhang, Y., Wang, H., & Zhu, J. (2025). Investigation the effects of further oxidative evolution of graphene oxide on carbon fiber strength and interfacial performances of epoxy composites. *Chemical Engineering Journal*, *516*, 164158. https://doi.org/https://doi.org/10.1016/j.cej.2025.164158
Xie, N., Shi, X., & Zhang, Y. (2017). Impacts of Potassium Acetate and Sodium-Chloride Deicers on Concrete. *Journal of Materials in Civil Engineering*, *29*(3), 04016229. https://doi.org/10.1061/(ASCE)MT.1943-5533.0001754
Xie, Z., Xie, J., Guo, Y., & Huang, Y. (2018). Durability of CFRP-Wrapped Concrete Exposed to Hydrothermal Environment. *International Journal of Civil Engineering*, *16*(5), 527-541. https://doi.org/10.1007/s40999-017-0159-x
Yang, J., Zhao, J.-J., Han, C.-R., & Duan, J.-F. (2014). Keys to enhancing mechanical properties of silica nanoparticle composites hydrogels: The role of network structure and interfacial interactions. *Composites Science and Technology*, *95*, 1-7. https://doi.org/https://doi.org/10.1016/j.compscitech.2014.02.003
Yi-qiu, T., Lei, Z., & Xing-you, Z. (2012). Investigation of low-temperature properties of diatomite-modified asphalt mixtures. *Construction and Building Materials*, *36*, 787-795. https://doi.org/https://doi.org/10.1016/j.conbuildmat.2012.06.054
Zainuddin, S., Hosur, M. V., Zhou, Y., Narteh, A. T., Kumar, A., & Jeelani, S. (2010). Experimental and numerical investigations on flexural and thermal properties of nanoclay–epoxy nanocomposites. *Materials Science and Engineering: A*, *527*(29), 7920-7926. https://doi.org/https://doi.org/10.1016/j.msea.2010.08.078
Zaman, A., Gutub, S. A., & Wafa, M. A. (2013). A review on FRP composites applications and durability concerns in the construction sector. *Journal of Reinforced Plastics and Composites*, *32*(24), 1966-1988. https://doi.org/10.1177/0731684413492868
Zhang, F., Dai, J.-G., Wang, Z., Wang, M., Leng, Y., & Xu, Q. (2021). Bond durability of epoxy and cement- bonded CFRP reinforcement to concrete interfaces subject to water immersion. *Materials and Structures*, *54*(2), 53. https://doi.org/10.1617/s11527-021-01641-w
Zhang, P., Shang, J.-Q., Fan, J.-J., Chen, Q.-Z., Zhu, H., Gao, D.-Y., & Sheikh, S. A. (2022). Experimental study on the bond behavior of the CFRP plate-ECC-concrete composite interface under freeze–thaw cycles. *Construction and Building Materials*, *316*, 125822. https://doi.org/https://doi.org/10.1016/j.conbuildmat.2021.125822
Zhang, X., Wang, L., & Zhang, J. (2017). Mechanical behavior and chloride penetration of high strength concrete under freeze-thaw attack. *Cold Regions Science and Technology*, *142*, 17-24. https://doi.org/https://doi.org/10.1016/j.coldregions.2017.07.004
Zhou, Y., Fan, Z., Du, J., Sui, L., & Xing, F. (2015). Bond behavior of FRP-to-concrete interface under sulfate attack: An experimental study and modeling of bond degradation. *Construction and Building Materials*, *85*, 9-21. https://doi.org/https://doi.org/10.1016/j.conbuildmat.2015.03.031